Imperial College London

Computational study of self-heating ignition of Lithium-ion batteries during storage: effects of heat transfer and multi-step kinetics

A thesis submitted in partial fulfilment of the

requirements for the degree of

Doctor of Philosophy

in

Mechanical Engineering

by

Zhenwen Hu

2021

Supervised by

Prof. Guillermo Rein

Co-supervised by Dr Francesco Restuccia

Declaration of Originality

I declare that this thesis and the work described within have been completed solely by myself under the supervision of Prof. Guillermo Rein. Where others have contributed or other sources are quoted, full references are given.

Zhenwen Hu

2021

Copyright Declaration

To my beloved parents.

ABSTRACT

Computational study of self-heating ignition of Lithium-ion batteries during storage: effects of heat transfer and multi-step kinetics

by

Zhenwen Hu

Doctor of Philosophy in Mechanical Engineering
Imperial College London, 2021
Supervised by Prof. Guillermo Rein

Fire safety is a serious concern when storing a large number of Lithium-ion batteries (LIBs) stacked as an ensemble. Many such fires reported in recent years have caused severe damage to industrial facilities, public property, and even loss of life. It is crucial to understand the mechanisms and causes of these storage fires to provide insights for prevention. While previous studies mostly focused on the chemistry of LIBs and ignition while charging or discharging, this thesis explores the possibility of another fundamental cause of such fires driven by heat transfer, self-heating ignition. Three major challenges are identified for the modelling of self-heating ignition of LIB ensembles: large sizes, multi-dimensional heat transfer, and multiple chemical reactions. In this thesis, a typical $LiCoO_2$ (LCO) battery with four-step reaction kinetics is chosen for analysis and modelling the fundamentals of self-heating ignition. Four numerical models based on COMSOL Multiphysics are developed to deal with these challenges. The numerical results show that the critical ambient temperature triggering self-heating ignition decreases significantly with the size of the battery ensemble, from 155℃ for a single cell to 45℃ for a rack of cells. The spacing and packaging materials used to separate LIBs in storage can promote self-heating ignition further decreasing the critical temperature.

The increase in size and the presence of packaging materials result in slower internal heat transfer, which allows the cells to self-ignite at lower ambient temperatures. The heat from self-discharge, which is often neglected in the literature, is predicted to have minor effects on small LIB ensembles but to be dominating for a shelf of LIBs, indicating a substantial change in important chemical mechanism for different sizes. The differences resulting from different numerical models are investigated by a benchmarking analysis using two simulation tools: COMSOL and Gpyro. This thesis provides insights on the fundamental mechanism of self-heating ignition of LIBs during open-circuit storage and scientifically proves that self-heating ignition can be a cause of fires when LIBs are stacked to large sizes.

ACKNOWLEDGEMENTS

To start, I would like to thank my supervisor Prof. Guillermo Rein. Thank you so much for giving me the opportunity to be a member of Imperial Hazelab and this amazing PhD research journey. Thank you for always being so supportive of my entire PhD research. Your professional guidance, positive life attitude, and enthusiasm in research helped and encouraged me to go through all the difficulties. Thanks for your generous financial supports for me to attend conferences. Thank you, China Scholarship Council, for providing funding for my PhD research.

Special thanks to our battery term members, Xuanze and Francesco for being with me to explore this research area. Thank you for your generous help, inspiring discussions, and valuable contributions to my PhD research. Thank you, Greg, Monica, Yatish, Laura, and Jorge for the collaboration of the review paper and the supports for the knowledge about electrochemistry.

Thanks to all my Hazelab family for the joy and happiness you have brought to me during my PhD life. Thank you Xinyan, Nieves, Egle, Iza, Nils, Guoxiang, Yuqi, Fahid, Franz, Matt, Agung, Han, Eirik, Heidari, Ed, Ben, Wuquan, Dwi, Francesca, Harry, Simona, Tatenda, Rik, and Nik for the beautiful memories we had together both in the Hazelab office.

Thanks to Gang Xiong, Yi Wang, Dong Zeng, and FM Global for the generous help for the accommodation and wonderful food treat during the 11th FM Global fire modelling workshop in the USA. Had a great time and really enjoyed the workshop.

Thank you my friends in the UK, Yixin, Kuiyuan, Jiajie, Dapeng, Zhenzhen, Zhaoxu, Mingyang, Lu, Aijuan, Mei, and so on. Thanks for the warm Chinese fellow community and

the time being together. Thank you my friends in China, Weihao, Jiahong, Dong, Xing, Miaomiao, Lei, Bingxiao, Shengduo, Yuanbin, Meng, Mingyi, and so on for the sincere friendships and the days that we helped and encouraged each other.

Last but not least, a Big thank you to my beloved family: my parents, my grandma, my brother, my aunts and uncles, my cousins, Thanks for your consistent support, encouragement, selfless love and for always being there for me. I am extremely grateful to have you in my life.

Zhenwen Hu

London, UK

July 2021

TABLE OF CONTENTS

NOMENCLATURE

A	Frequency factor (s^{-1})
C	Battery capacity (Ah)
c	Dimensionless concentration
c_p	Heat capacity ($J\ kg^{-1}\ K^{-1}$)
D	Mass diffusivity ($m^2\ s^{-1}$)
E	Activation energy ($J\ mol^{-1}$)
f	Mass fraction function
ΔH	Specific heat release ($J\ kg^{-1}$)
h	Convective heat transfer coefficient ($W\ m^{-2}\ K^{-1}$)
$\bar{h}$	Specific enthalpy ($J\ kg^{-1}$)
k	Effective thermal conductivity ($W\ m^{-1}\ K^{-1}$)
L	Typical length (m)
l	Length of the battery ensemble (m)
$\dot{m}''$	Mass flux ($kg\ m^{-2}\ s^{-1}$)
n	Reaction order
p	Pressure, Pa
Q	Heating power (W)
q'''	Volumetric heat source ($W\ m^{-3}$)

q'' Heat flux (W m^{-2})

R Reaction rate (s^{-1})

S Surface area (m^2)

s Effective sensitive coefficient

T Temperature (K)

t Time s

$\bar{U}$ Nominal voltage of the battery

V Volume (m^3)

W Material content (kg m^{-3})

Y Mass fraction

z Dimensionless SEI thickness

Greek symbols

α Degree of conversion

ρ Average density (kg m^{-3})

δ Non-dimensional heat generation rate

η Heat generation ratio

ε Emissivity

κ Permeability (m^2)

v Viscosity/stoichiometry

χ Battery volume ratio

$\dot{\omega}'''$ Volumetric reaction rate (kg m^{-3} s^{-1})

ϕ Porosity

φ Self-discharge ratio

Φ Stored chemical energy that could transfer to output work

Subscript

L Left boundary

R Right boundary

T Top boundary

B Bottom boundary

0 Initial state

a Ambient

air Air

b Battery

box The battery box

conv Convective heat transfer

d destruction

f Formation

g Gas

s Boundary at free surface

rad Radiative heat transfer

max	Maximum
sei	Solid electrolyte interphase (SEI)
n	Negative electrode
p	Positive electrode
e	Electrolyte
tot	Total reactions
on	Onset state of a cell when thermal runway starts to take place
a, cr	Critical state of ambient that can trigger thermal runaway

PREFACE

This thesis contains 8 chapters with **Chapter 1** introducing the research background and motivation of the thesis. **Chapter 2** presents theoretical foundations for self-heating ignition of lithium-ion batteries, which is also the cornerstone for numerical models developed in **Chapters 3-7**. These 5 chapters are the key research content of the thesis, and they have been integrated either in published manuscript or submitted for publication, as shown below:

Chapter 3 is based on:

> Hu, Z., He, X., Restuccia, F., Yuan, H., & Rein, G. (2021). Numerical study of scale effects on self-heating ignition of lithium-ion batteries stored in boxes, shelves and racks. ***Applied Thermal Engineering***, *190*, 116780.

Chapter 4 is based on:

> Hu, Z., He, X., Restuccia, F., & Rein, G. (2020). Numerical study of self-heating ignition of a box of lithium-ion batteries during storage. ***Fire Technology***, *56*(6), 2603-2621.

Chapter 5 is based on:

> Hu, Z., He, X., Restuccia, F., & Rein, G. (2021). Anisotropic and homogeneous model of heat transfer for self-heating ignition of large ensembles of Lithium-ion batteries during storage. ***Applied Thermal Engineering***, 117301.

Chapter 6 is based on:

> Hu, Z., He, X., Restuccia, F., & Rein, G.. Effects of self-discharge on self-heating ignition of Lithium-ion batteries during storage (to be submitted).

Chapter 7 is based on:

> Hu, Z., He, X., Restuccia, F., & Rein, G.. Benchmarking between COMSOL and Gpyro models in predicting self-heating ignition of Lithium-ion batteries (to be submitted).

Other Publications

The following scholarly output has also been produced as an outcome of this research:

Journal paper:

- Diaz, L. B., He, X., Hu, Z., Restuccia, F., Marinescu, M., Barreras, J. V., ... & Rein, G. (2020). Meta-review of fire safety of Lithium-Ion batteries: industry challenges and research contributions. ***Journal of The Electrochemical Society***, *167*(9), 090559.
- He, X., Restuccia, F., Zhang, Y., Hu, Z., Huang, X., Fang, J., & Rein, G. (2020). Experimental study of self-heating ignition of lithium-ion batteries during storage: effect of the number of cells. ***Fire Technology***, *56*(6), 2649-2669.
- He, X., Hu, Z., Restuccia, F., Yuan, H., & Rein, G. (2021). Self-heating ignition of large ensembles of Lithium-ion batteries during storage with different states of charge and cathodes. ***Applied Thermal Engineering***, 117349.

Oral presentations and posters for Conferences

- Hu, Z., He, X., Restuccia, F., & Rein, G.. Benchmarking COMSOL and GPYRO in predicting self-heating ignition of Lithium-ion batteries. **2nd International Symposium on Lithium Battery Fire Safety**. 25-28 August, 2021. Hefei, China. (Accepted Oral)
- Hu, Z., He, X., Restuccia, F., & Rein, G.. Numerical study of self-heating ignition of a box of lithium-ion batteries during storage. **1st International Symposium on Lithium Battery Fire Safety**. 18-20 July, 2019. Hefei, China. (Peer-reviewed conference paper + Accepted Oral)
- Hu, Z., He, X., Restuccia, F., & Rein, G.. Self-heating ignition of lithium-ion batteries during storage. **11th FM Global Open Source CFD Fire Modelling Workshop**. 5-6 June, 2019. Norwood, USA. (Accepted Oral).
- Hu, Z., He, X., Restuccia, F., & Rein, G.. Self-heating ignition of lithium-ion batteries during storage. **The Great Fired-up of London Workshop**. 16-17 May, 2019. London, UK (Oral presentation).
- He, X., Hu, Z., Restuccia, F., & Rein, G.. Overview of self-heating ignition of lithium-ion batteries in closed and open circuits. **3rd European Symposium on Fire Safety Science**. 12-14 September, 2018. Nancy, France (Poster).

Chapter 1. Introduction to Self-heating ignition and lithium-ion battery fire safety

1.1 Background and motivation

Lithium-ion batteries (LIBs) are rechargeable batteries, which use lithium-ions as the media for electrical cycles[1]. Due to their high specific energy and power density, long cycle life, LIBs have received rapid development since their first commercialization in the 1990s and quickly dominated the market of commercial electronics. With such great success and fast growth of related technologies, LIBs were then applied on much larger scales, for example, electric vehicles (EVs)[2–4], which are expected to dominate automobiles in the near future to replace the traditional fossil fuel powered vehicles and help relieve carbon emissions[5]. LIBs have also been used as a grid-scale energy storage unit for smart grids, namely the battery energy storage system (BESS)[6]. The global LIB market is expected to rise to $87.5 billion by 2027[7].

With increasing demands from various industries, LIBs need to improve their energy and power density, which unfortunately brings some unwanted side effects, such as, safety concerns[8–10]. As an energy storage unit, the major components of LIBs: the active materials of the negative electrode (NE), the positive electrode (PE), the separator, and electrolyte are highly flammable and release a large amount of heat and toxic gases when ignited. Under the adiabatic condition, the energy stored in a 18650 type of LIB could heat itself up to 700°C[11]. Unlike most traditional flammable materials, which only ignite via a chemical path that requires them to be heated up to a certain high temperature and in a suitable window of oxygen concentration[12], LIBs could also follow an electrochemical path, namely short-circuits[13–15], which can easily initiate a fire at ambient temperature. When the PE and NE are externally

or internally connected by a conductor, the chemical energy stored in the battery can be rapidly released in the form of heat, namely Joule heat, and may initiate a fire[16–18]. Such short-circuits are much easier to trigger by incorrect operations of the battery, unexpected abuse, or manufacturing defects. Therefore, many studies[19–21] have been conducted to investigate LIB safety with safer materials and developed relative prevention techniques to control or cut down the short-circuit current. Such techniques [1,5,22] include: the positive temperature coefficient device (PTC), shutdown separators, flame retardant additives, etc. The safety of LIBs has massively improved compared to the old generation when LIBs were just entering the market.

LIB safety has improved from the material scale, with reports of fire incidents for single cells and applications for consumer electronics declining. However, the safety tensions of large-scale applications of LIB are still not relieved. Many fires[23,24] related to EVs and BESS, which contains thousands or millions of cells and can therefore be catastrophic, have been reported in the past decade. A few notable fires are summarized in Table 1-1. Surprisingly, a certain number of fires took place when LIBs were merely in open-circuit storage conditions. According to a report by the U.S. Federal Aviation Administration[25], 238 airport incidents related to LIB transport occurred from 1991 to 2018. In July 2018, an e-bike warehouse in the Netherlands storing 6000 LIBs caught fire, leading to 300 people being evacuated. One year prior to this fire, a LIB recycling plant in the UK storing 4 tonnes of waste LIBs caught fire due to, as reported, spontaneous ignition of the LIBs[26]. Owing to the potential occurrence of fires, LIBs are classified as dangerous goods for transportation purposes[27,28]. LIB manufacturers, recycling companies as well as storage and transportation industries have suffered great losses due to these fires, and are increasingly concerned about how to safely store and transport these highly reactive batteries.

Table 1-1

A few notable fires of Lithium-ion batteries in large scale applications in the past decade. [29]

Application	Company	Year	Incident description
Electric Vehicle	Chevrolet	2011	Chevy Volt on fire weeks after crash test.
	Tesla	2013	Model S on fire after hitting debris.
		2013	Model S on fire after crash.
		2016-19	Model S suddenly on fire while parked.
	Jaguar	2018	i-Pace suddenly on fire while parked.
Aerospace	Boeing	2013	Sudden failure in auxiliary units of Dreamliner 787.
Marine	Corvus Energy	2019	Hybrid-battery ferry on fire due to coolant leaking.
Stationary energy storage systems	Various	2017-19	Battery fires in large grid-connected systems

Unfortunately, the causes of these fires are poorly understood. During storage and shipping, these batteries are in open circuit condition, and usually do not have signs of electrical or mechanical abuse[5]. One possible cause proposed in [30] is unexpected internal short circuits due to manufacturing defects[31–33]. However, this kind of internal short circuit involve high uncertainty and are almost impossible to verify in real fires. Blaming the causes of all these unexpected fires on an event that cannot be confirmed may omit more general mechanisms, for which preventative solutions may exist. Current studies on LIB safety mainly focused on testing a single cell or small module[34–39] to study the contribution of the chemical reactions[40–46] However, another important factor often omitted is that within a large-size stack of reactants, the poor heat transfer condition could also play a crucial role or trigger ignition[29]. This phenomenon has seldom been discussed for battery fires.

In this thesis, I explore and discuss another fundamental cause of fires which is induced by heat transfer, self-heating ignition. Self-heating ignition[47] is a spontaneous ignition of a material resulting from its internal exothermic reactions. This phenomenon has been reported in many natural reactive materials such as coal, shale, and biomass[48,49] when stacked in large piles. Under this large-scale stacking condition, the internal heat is much difficult to dissipate to the environment, in which case the heat generated by low-temperature oxidation processes or side reactions may no longer be able to be balanced by environmental cooling and may accumulate inside causing self-heating. When the temperature reaches a critical level, the system goes into a special state, thermal runaway, where the reaction rate of an exothermic reaction increases due to an increase of temperature leading to a further temperature increase and a further increase of reaction rate[1]. This positive feedback raises the temperature rapidly and then triggers more violent reactions such as pyrolysis, smouldering, and finally flaming combustion. Driven by the poor heat transfer, large-stacked natural fuels could self-ignite at a normal ambient temperature.

Such self-heating ignition is also theoretically possible for LIBs when ensembled on a large scale with multiple exothermic side reactions that have been reported, as shown in Figure 1-1. For a single cell directly exposed to the environment, the heat generated inside by low-temperature oxidation processes or side reactions is easy to dissipate to the environment, in which case, the temperature keeps unchanged. However, when numbers of cells are stacked together as an ensemble, the heat generated in the centre of the bulk is much more difficult to dissipate, as it needs to diffuse through half of the ensemble to reach the free surface and finally dissipate to the environment. In this case, this weak heat generation may accumulate inside resulting in a non-negligible temperature increase and self-heating.

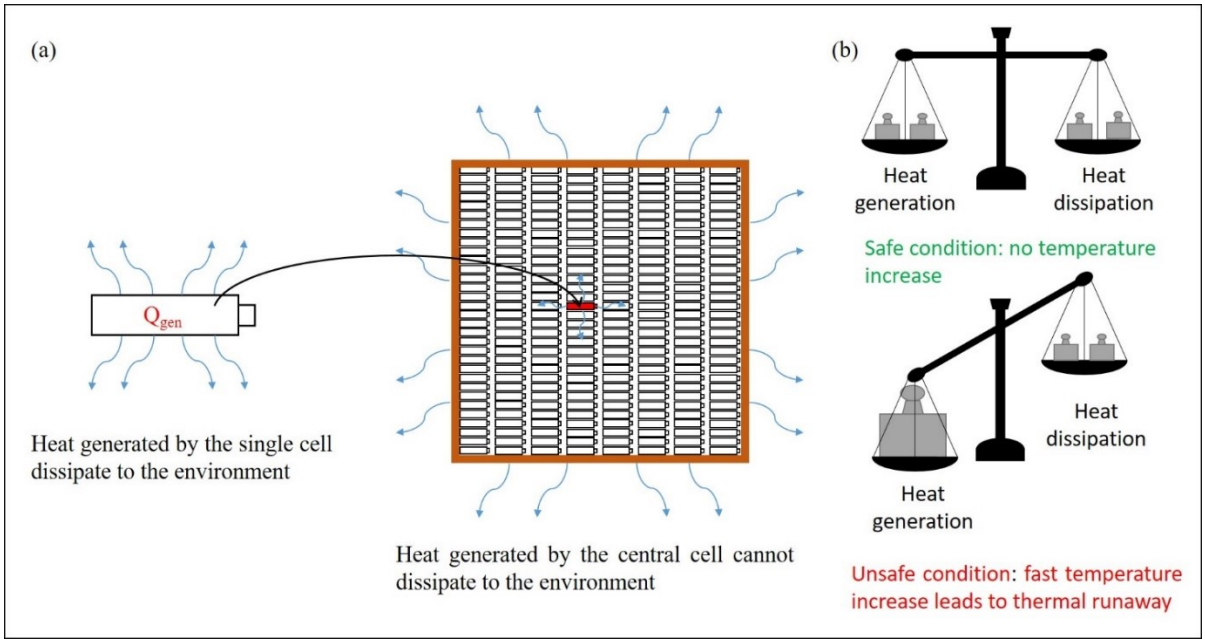

Figure 1-1. Diagram of self-heating of LIB. (a) For a single cell directly exposed to the environment, the heat generated by side reactions easily dissipates to the environment, so the heat balances result in no further temperature increase. However, for an ensemble of cells, the heat generated by the central cell is difficult to dissipate to the environment, resulting in self-heating and possibly (b) thermal runaway and ignition.

Unfortunately, this concept is barely discussed in the LIB community. The LIB community tended to take the temperature of self-ignition of LIB as a natural property, and use the critical self-ignition temperature obtained from single-cell testing as a criterion and apply to other scenarios for granted, failing to realize that the assembly of LIBs and the environment could significantly affect the self-heating behaviour of batteries. What was worse, self-heating ignition was often misunderstood and confused with another important research topic, thermal runaway propagation[36,50–53], which studies once a cell fails how the fire then propagates to the nearby cells. While self-heating ignition discusses when a large number of LIB cells are stacked, the weak heat transfer within the LIB ensemble might trigger a self-heating ignition. This confusion further blocked the understanding and scientific studies of self-heating behaviour of LIBs.

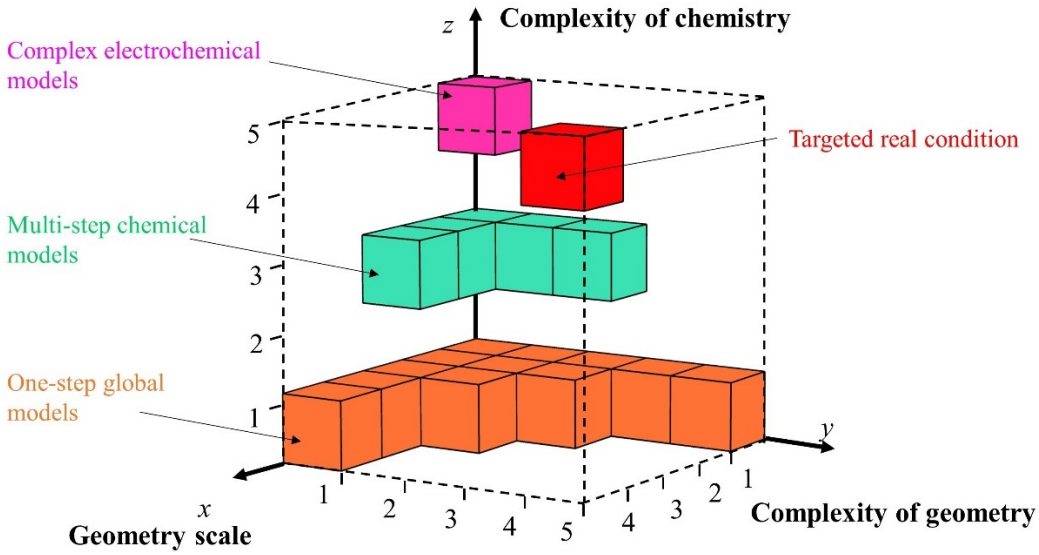

Figure 1-2. The 3-D diagram demonstrates three main challenges involved in modelling the thermal behaviour of large-scale LIB systems with the state of current models in the literature. Each challenge is divided into five levels. Depending on the kinetics used, models in the literature are classified into three types: complex electrochemical model (pink cube), multi-step chemical models (green cube), and one-step global models (orange cube). The red cube represents the real large-scale LIB storage.

Focusing on the safety of LIB ensembles at the warehouse-scale, which may contain thousands or millions of cells[54–57], self-heating ignition of LIBs contains a high level of complexity and is difficult to study by direct experiments due to the high costs and severe hazards. Current feasible approaches are through investigating the critical kinetics by lab-scale experiments[58–61] and then applying it to a self-heating theory or fundamental heat transfer model to make large-scale predictions[62]. However, simulating such a large-scale problem is still a challenge for the current state-of-the-art models in the literature. As Figure 1-2 shows, self-heating ignition of warehouse-scale storage of LIBs involves three independent challenges: the complexity of chemistry, the complexity of geometry, and the geometric scale, with the first challenge related to heat generation and the latter two related to heat transfer. If all three challenges are divided into 5 levels according to complexity, the real warehouse storage of LIBs lies in the red region, which involves high complexity of chemistry (complex reactions

when the battery is heated up), high complexity of geometry (the different materials used within battery cells, insulating materials between cells, and different 3D placements of battery packs), and large geometry size (several meters for a typical length). Depending on the kinetics used, current numerical models in the literature for analysing the thermal behaviour of LIBs could be roughly divided into three types: complex electrochemical models, multi-step chemical models, and one-step global models.

The complex electrochemical models (located in the pink cube in Figure 1-2) aim to understand the fundamental kinetics and dynamics of reactions within battery cells[42,45,63]. These models pursue extreme complexity of chemistry[64,65], to understand what exactly happens within battery cells and how reactions develop. These models usually have high requirements on accuracy and are often specified to be a very small size scale (usually component level, microscale) to eliminate the effects of heat transfer and purely focus on dynamics of reactions. The second type of model, multi-step chemical models (green cubes in Figure 1-2), commonly focus on the cell level (a single cell or several cells) and care more about the behaviour of whole-cell or pack of cells[11,66,67]. These models use several main chemical reactions[68,69] for the main components of LIBs to substitute all complex electrochemical reactions inside and simulate the thermal behaviour of the whole cell. This kind of simplification sacrifices a certain extent of accuracy, but greatly reduces computational costs and captures the global thermal characteristics. These models are widely used for simulating thermal runaway of single-cell or thermal runaway propagation[70,71] in arrays of cells. The third type of model is classed as the one-step global model (the orange cubes in Figure 1-2). When the size increases to that of real LIB storage (warehouse storage), numerical simulation on such a large-scale problem becomes challenging, as the computational costs of complex models for such a case are unaffordable. Current solutions used are classical self-

heating theories such as Semenov's theory or Frank-Kamenetskii's theory[49,72,73], which greatly simplify the complexity of chemistry (assuming one-step global reaction) as well as the complexity of geometry (assuming same material for the whole bulk, homogeneous distribution) to achieve large-scale predictions. Direct experiments on such large-scale LIB ensemble usually monitor only a few key parameters (e. g. heat release rate), and then a global Arrhenius type of reaction is used to fit the data[74].

Due to all these difficulties, the current understanding of self-heating ignition of LIBs is very limited. In this thesis, I use numerical methods to explore this unknown field. Based on fundamental physics and known kinetics, I develop several computational models to step by step investigate theoretical fundamentals in the self-heating ignition of LIBs and explore and discuss several possible key influential factors. $LiCoO_2$ (LCO) type of battery is selected as an example to simplify kinetics and help to better understand the heat transfer related factors. Although the quantitative results are mainly based on an LCO type of battery, the numerical methodology and simplification methods developed in this thesis should be able to be applied to other types of LIBs. I hope my work can help the battery and fire safety community to better understand the self-heating ignition behaviour of LIBs and prompt an open thread for related research.

1.2 Outline of the thesis

Chapter 1 introduces the research background and motivations of the thesis.

Chapter 2 presents the fundamental physics and theoretical model for self-heating and introduces the chemical kinetics adopted for LCO type of LIBs in this thesis. The numerical simulations all over the thesis are based on commercial software COMSOL Multiphysics.

Chapter 3 introduces a computational model that incorporates multi-step kinetics to simulate the self-heating ignition of large ensembles of LIBs. In this chapter, I numerically investigate the differences in self-heating ignition behaviour of LIB ensembles across scales and put forward three parameters for effective evaluation.

Chapter 4 presents a box scale investigation to study the effects of complex isolation and spacing during LIB storage, which significantly affect the heat transfer ability of the LIB ensemble. In this chapter, I simulate the self-heating behaviour of a box with 100 cylindrical cells with different materials for isolation and different spacing to study the possible effects of heat transfer.

Chapter 5 introduces the development of an anisotropic model, which incorporates the effects of complex isolation and spacing, and could be used for large scale predictions. I put forward a method of simplification which transfer the complexity of geometry in real LIB storage into improved physics modelling. Such simplification incorporates the effects of complex heat transfer in LIB storage and greatly reduces the computations costs which enable large scale predictions.

Chapter 6 further investigates the possible effects of self-discharge during LIB storage on self-heating ignition of LIB ensembles. The possible heating by self-discharge during LIB storage is incorporated into my previous model to investigate whether the tiny heat generated by self-discharge could affect the self-heating behaviour of large ensembles of LIBs.

Chapter 7 compares numerical modelling performances of the commercial software COMSOL Multiphysics against the open-source tool Gpyro which has widely been used to model self-heating ignition of carbon-rich materials. I conduct several cases of comparison

which across scales and kinetics to benchmark the numerical performance of both tools on self-heating ignition of LIBs.

Chapter 8 summarizes the main conclusion of this thesis.

Chapter 2. Theoretical foundations of self-heating ignition and numerical modelling

2.1 Introduction to self-heating ignition theories

Self-heating, defined by ISO[75], is "a rise in temperature in a material resulting from an exothermic reaction within the material". In the chemistry community, this concept is often interpreted as chemistry focused, which defines the onset of exothermic reactions. However, it is also a concept significantly related to heat transfer. What is implicated in the definition is that the exothermic reaction should be adequate to cause a notable temperature rise, which lifts the temperature of the substance above the environment without an external energy supply[76]. In other words, self-heating is not only dependent on the internal chemistry of the substance, but also related to the environment the substance is surrounded by. Depending on the heat balance between the heat generation inside the reactive substance and heat dissipation to the surrounding, self-heating usually could result in two possible outcomes[72]. The first situation is self-heating in a mild manner, which could raise the temperature of the substance slightly above the environment, but the heat generation is not sufficient to cause thermal runaway and reaches a dynamic balance with the heat dissipation to the surroundings. Eventually, the temperature will drop down as the reactants deplete. The other situation is strong self-heating resulting in thermal runaway, which rapidly raises the temperature and triggers more violent reactions and causes an ignition, named self-heating ignition (also referred to as autoignition and spontaneous combustion [72]).

Self-heating ignition has been reported to be responsible for many large fires in nature when porous combustible materials were massively stacked[48,49]. Apart from the environment and chemistry involved, the geometric size and the shape of the body of the

reactive substance are also critical factors for self-heating ignition. For an ensemble of reactive substances with a typical length of L, the total heat generation is roughly proportional to the volume of the ensemble, which is proportional to L^3. While the heat dissipation is roughly proportional to the surface area of the ensemble, which is proportional to L^2. With a larger size, the heat generation grows much faster than the heat dissipation, which means the reactive ensemble on the large scale is easier to ignite and self-heating ignition could occur at a lower ambient temperature. Theoretically, there will be a critical size for a reactive ensemble to self-ignite at normal ambient temperature. To make effective strategies for prevention, it is crucial to understand the fundamental mechanisms and the critical influential factors of self-heating ignition.

The first mathematical solution of a self-heating ignition problem was developed by Semonov[49] in 1928. Based on a set of simplifications and assumptions, Semonov put forward a theoretical solution of the criticality of self-heating ignition of a lumped system. His student Frank-Kamenetskii[49] then further expanded Semonov's theory and developed a theoretical model to consider the effects of heat transfer and temperature gradient among a 1D system. Thomas[77] further modified the theory and proposed a more general model considering a wider range of boundary conditions. Bowes[49] wrote a monograph, *Self-heating: evaluating and controlling the hazards*, in 1984 to specifically discuss and explain this phenomenon and summarize related research. Babrauskas[76] also discussed this phenomenon and related theories in his book *Ignition handbook*, published in 2003. Gray[72] further updated the recent research in a chapter of the book, *SFPE Handbook of Fire Protection Engineering*, published in 2016.

This chapter briefly introduced Frank-Kamenetskii's theory (F-K theory), which is the theoretical foundation of self-heating ignition problems. Afterwards, the problems and

challenges introduced by LIBs in self-heating ignition were discussed and explained. A commercial numerical modelling tool, COMSOL Multiphysics, which is used for subsequent numerical modelling, was then introduced. The numerical models developed in this thesis (Chapters 3-6) were mainly based on COMSOL Multiphysics considering multi-step reaction kinetics. Chapter 7 introduced another self-heating ignition model for LIBs based on one-step global reaction kinetics using Gypro [78,79], which is an open-source simulation tool designed for pyrolysis modelling for combustible solids. The self-heating ignition models by Gypro were mainly developed by my colleague, Xuanze He [29,79,80]. A benchmarking analysis was conducted in Chapter 7 for the numerical models by COMSOL and Gpyro to analyse the potential effects of different simulation tools.

2.2 Classical self-heating theory--Frank-Kamenetskii's theory

Frank-Kamenetskii's theory is one of the most popularly used theoretical theories for analysing the criticality of self-heating ignition of reactive solids and has been used as guidance for many lab-scale experiments and evaluations of relevant parameters. The detailed theoretical deductions of Frank-Kamenetskii's theory has been carefully explained in many studies and monograph introduced before[49,72,76]. Here, this section summarizes the basic idea, adopted assumptions, and the major conclusion of this theory, which could help better understand the numerical model developed and related parameters discussed in this thesis.

The basic problem Frank-Kamenetskii's theory try to solve is the criticality of self-heating ignition of a reactive solid as an infinite plane slab. The governing equation for this problem is the energy conservation equation:

$$k\nabla^2 T + q''' = \rho c_p \frac{\partial T}{\partial t} \quad (2\text{-}1)$$

Where k is the thermal conductivity, q''' is the heat generation rate per unit volume, ρ is the density and c_p is the heat capacity. The classical F-K theory considers a Dirichlet boundary condition, which assumes the temperature of the walls equals the ambient temperature, T_{walls}=T_a.

To simplify calculations, the F-K theory adopted several basic assumptions[76]: (1) The reaction follows zero-order Arrhenius kinetics, (2) there is an infinite supply of reactants and oxygen, and (3) the only temperature gradients are in the thickness direction. To solve the Equation 2-1in a steady-state, F-K theory defined a dimensionless parameter δ[79]:

$$\delta = \frac{EL^2 f_0 \Delta H_c}{kRT_a^2} e^{-E/(RT_a)} \quad (2\text{-}2)$$

Where the L is the characteristic length of the reactive ensemble, f_0 is the mass fraction function at the initial state, ΔH_c is the effective heat of reaction, E is the effective activation energy, R is the universal gas constant. For a determined reaction, δ is related to the characteristic length, L and the ambient temperature, T_a.

Through mathematical analysis, if δ is below a critical value, δ_c, which is determined by the geometry of the reactive ensemble, a steady-state could exist, which means self-heating ignition would not occur. Therefore, self-heating ignition takes place when δ>δ_c, which could help to guide the choice of a suitable L of the reactive ensemble to ensure it would not self-ignite at a given ambient temperature T_a.

2.3 Numerical modelling by COMSOL Multiphysics

Equation 2-2 given by the F-K theory has been widely used to provide guidance and assessment of safe storage of reactive materials, especially for porous reactive solids[81,82] Many experimental studies[83,84] have proved that F-K theory could provide satisfying results for the engineering predictions. However, there are still certain scenarios with complex heat transfer, chemistries, or transient performance that could not fill the basic assumptions by the F-K theory. For those complex conditions, the governing equations could no longer be solved analytically. Numerical models were then proved to be effective methods for those complex scenarios.

LIB, as explained in Chapter 1, is a complex electrochemical system consisting of multiple components and various reactive materials. The fundamental chemical kinetics of possible reactions at elevated temperatures is very complicated and has been studied intensively for the last two decades but still not fully understood[11,85]. The complex real storage condition further hinders the understanding of the self-heating behaviour of large LIB ensembles. Therefore, numerical models are developed in this thesis to discuss and analyse the self-heating ignition behaviour of LIBs, especially large LIB ensembles.

The numerical models developed in this thesis are mainly based on commercial software, COMSOL Multiphysics[86]. COMSOL is a powerful numerical tool aiming to provide numerical solutions for all kinds of scientific and engineering problems, especially for problems involving multi-disciplines. It contains various basic modules and interfaces to solve governing Partial different Equations (PDE) based on the Finite Element Method (FEM) for a wide range of scientific and engineering phenomena. COMSOL has been widely used to analyse the electrochemical and thermal behaviour of LIBs[50,87,88], and it contains basic

modules for LIBs and heat transfer. Therefore, this tool is used in this thesis to model the self-heating ignition phenomenon for LIBs.

The basic idea for the numerical model is to simulate a typical self-heating test, oven test, as shown in Figure 2-1. A LIB ensemble with an initial temperature of T_0 is set in a warm environment with ambient temperature T_a. The ambient temperature is set to increase by steps until the system could self-ignite to determine the critical ambient temperature to initiate self-heating ignition, $T_{a,cr}$.

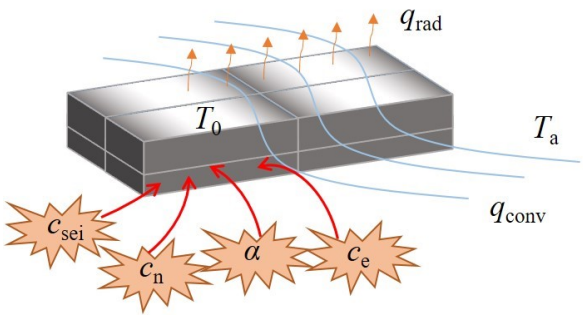

Figure 2-1. Diagram of self-heating of a LIB ensemble. A LIB ensemble with initial temperature T_0 is placed at environmental temperature T_a. Convective and radiative heat transfer q_{conv} and q_{rad} are considered for free surface boundaries. The possible reactions considered include: SEI decomposition (c_{sei}), negative-electrolyte reaction (c_n), positive-electrolyte reaction (α), and electrolyte decomposition (c_e).

The real physical and chemical changes inside a LIB at elevated temperature are very complicated, where chemical reactions generate gases changing the physical properties and dynamics. The internal structure of a LIB is also complex (usually jellyroll structure or layer structure). Many numerical models[39,89,90] have been developed to investigate the detailed kinetics and dynamics inside a single cell. However, self-heating ignition discussed in this thesis cares more about the general thermal behaviour of the whole battery ensembles with numerous cells, instead of tiny changes at locals inside a cell. Therefore, some simplifications are adopted in the numerical model.

First, instead of modelling the whole combustion behaviour of LIBs (usually cell temperature below 800℃), self-heating ignition focuses on the transition from a stable state (subcritical condition) to the onset of thermal runaway (supercritical condition) with cell temperature usually below 200℃. In this temperature range, the reactions are relatively mild, and the gases generated are still sealed inside the battery cell. The expansion of the cell usually would not be large, therefore, the thermophysical properties: ρ, c_p, k, could be taken as constant. The minimum unit analysed in this thesis is a 18650 cylindrical cell. Battery cells have a complex internal structure such as jellyroll structure or layer structure and are in principle heterogeneous. However, for the specific self-heating ignition behaviour, studies have proved that for a fully charged battery cell at a temperature below 200℃, a lump thermal model[11] already provides adequate accuracy for the temperature prediction for the single-cell when compared to a 3D heterogeneous model[66]. Therefore, a battery cell could be simplified as all reactants are homogeneously distributed inside the cell. The governing equation then could be simplified as [35]:

$$\rho c_p \frac{\partial T}{\partial t} = k\nabla^2 T + q'''_{\text{tot}} \tag{2-3}$$

Where q'''_{tot} is the heat generation rate per unit volume of all reactions. For the boundary conditions, both radiative and convective heat transfer are considered for free surface boundaries[35].

$$q''_{\text{conv}} = h(T_s - T_a) \tag{2-4}$$

$$q''_{\text{rad}} = \varepsilon\sigma(T_s^4 - T_a^4) \tag{2-5}$$

One of the major challenges for analysing the self-heating ignition behaviour of LIBs is the kinetics of the complex reaction at elevated temperatures. Even after the numerous studies [91–93] conducted in the past two decades, the complete kinetics for LIBs at elevated

temperature is still not fully understood. Furthermore, with the development of LIB technology, the materials used in LIBs have been updated massively, especially for the active materials of the PE, which have been used in different types of LIBs such as lithium cobalt oxide (LCO), lithium manganese oxide (LMO), lithium iron phosphate (LFP) etc. Even the same type of LIBs with different proportions of the metal oxide or different additives to electrolyte could significantly change the reaction mechanisms resulting in different thermal behaviour. There is no general mechanism for all LIBs, and it is impossible to investigate all of them.

Therefore, in this thesis, an LCO type of LIB which has been systematically studied in the literature[11,91,94,95] is taken as an example, and the multi-step reaction kinetics reported is used to represent chemistry for modelling and discussions of its self-heating ignition behaviour. Although the thermal tolerance of the LCO type of battery is lower than the commonly used batteries in the electric vehicle (EV) industry, the chemical composition of LCO is relatively simple, and ample data has been reported in the literature [5,32,33].

However, even for this simple LCO battery, its fire kinetics are still not fully understood. One widely accepted kinetics model is by Hatchard et al. [34] and Kim et al.[35]. By analysing and modelling the thermal behaviour of each component of the LIB and grouping them together, Hatchard et al.[34] and Kim et al.[35] made good estimations on thermal behaviours of a whole-cell in a totally different heat transfer condition, oven tests. Therefore, these kinetics should reveal some fundamental understanding of the thermal behaviour of LIBs and are reasonable to be used for upscaling analysis. The kinetics and parameters adopted in models I developed by COMSOL Multiphysics are by Hatchard et al.[34] for E-One/Moli Energy ICR18650 (18 mm diameter, 65 mm length) 1.65 Ah LCO/graphite cells at 100% state of charge (SOC). Batteries in storage and shipment are usually required to be stored at 30%-50% SOC. Unfortunately, there is no study reporting the relationship between these fundamental

kinetics and SOC. Therefore, kinetics based on 100% SOC is used in the multi-step models to represent the worst scenario in terms of reactivity.

The kinetics of the LCO battery adopted in the numerical models include four major reactions: the solid electrolyte interphase (SEI) decomposition, negative-electrolyte reaction, positive-electrolyte reaction, and electrolyte decomposition are the dominant heat generation terms at the early stage of thermal runaway of LIB in open circuit condition[34,35].

$$q'''_{\mathrm{tot}} = q'''_{\mathrm{sei}} + q'''_{\mathrm{n}} + q'''_{\mathrm{p}} + q'''_{\mathrm{e}} \tag{2-6}$$

Where q'''_{sei} is the volumetric heat generation by SEI decomposition, q'''_{n} is the volumetric heat generation by negative-electrolyte reaction, q'''_{p} is the volumetric heat generation by positive-electrolyte reaction, q'''_{e} is the volumetric heat generation by electrolyte decomposition, and q'''_{tot} is the volumetric heat generation by all four reactions.

It is commonly believed that reactions stemming from thermal abuse start at the SEI layer[1,5,22], which is a thin passivating layer formed around the negative electrode. At around 100 ℃, the meta-stable component inside the SEI layer starts to decompose[1]. While the SEI is decomposing, the intercalated lithium inside the negative electrode is exposed to the electrolyte and can react to form a new SEI layer. This reaction is called the negative-electrolyte reaction. For the positive electrode, MacNeil et al.[96,97] found an autocatalytic mode of reaction for LCO and electrolyte, named positive-electrolyte reaction in this study. Meanwhile, the organic solvent of the electrolyte can also decompose at relatively high temperatures and is named electrolyte decomposition. The detailed developments of these kinetics are explained in the work by Hatchard et al.[34] and Kim et al.[35]. The equations are summarized in Table 2-1. The descriptions of the related variables are listed in Table 2-2. The adopted values are based on the studies by Hatchard et al.[34] for E-One/Moli Energy ICR18650 (18 mm diameter,

65 mm length) 1.65 Ah LCO/graphite cells at 100% SOC. These equations are the theoretical basis for the numerical modelling in the following chapters (From Chapter 3 to Chapter 6), which adopt different adjustments and modifications to deal with the challenges introduced by the large geometric size, complex geometry, and complex chemistry.

Table 2-1

The kinetic model for $LiCoO_2$ Lithium-ion battery from the literature[34,35].

Chemical mechanisms		Eq.
SEI decomposition	$R_{\mathrm{sei}} = -\frac{\mathrm{d}c_{\mathrm{sei}}}{\mathrm{d}t} = A_{\mathrm{sei}}\exp\left(-\frac{E_{\mathrm{sei}}}{RT}\right)c_{\mathrm{sei}}^{n_{\mathrm{sei}}}$	(2-7)
	$q'''_{\mathrm{sei}} = \Delta H_{\mathrm{sei}} W_{\mathrm{n}} R_{\mathrm{sei}}$	(2-8)
Negative-electrolyte reaction	$R_{\mathrm{n}} = -\frac{\mathrm{d}c_{\mathrm{n}}}{\mathrm{d}t} = A_{\mathrm{n}}\exp\left(-\frac{z}{z_0}\right)\exp\left(-\frac{E_{\mathrm{n}}}{RT}\right)c_{\mathrm{n}}$	(2-9)
	$\frac{\mathrm{d}z}{\mathrm{d}t} = A_{\mathrm{n}}\exp\left(-\frac{z}{z_0}\right)\exp\left(-\frac{E_{\mathrm{n}}}{RT}\right)c_{\mathrm{n}}$	(2-10)
	$q'''_{\mathrm{n}} = \Delta H_{\mathrm{n}} W_{\mathrm{n}} R_{\mathrm{n}}$	(2-11)
Positive-electrolyte reaction	$R_{\mathrm{p}} = \frac{\mathrm{d}\alpha}{\mathrm{d}t} = A_{\mathrm{p}}\alpha(1-\alpha)\exp\left(-\frac{E_{\mathrm{p}}}{RT}\right)$	(2-12)
	$q'''_{\mathrm{p}} = \Delta H_{\mathrm{p}} W_{\mathrm{p}} R_{\mathrm{p}}$	(2-13)
Electrolyte decomposition	$R_{\mathrm{e}} = -\frac{\mathrm{d}c_{\mathrm{e}}}{\mathrm{d}t} = A_{\mathrm{e}}\exp\left(-\frac{E_{\mathrm{e}}}{RT}\right)c_{\mathrm{e}}^{n_{\mathrm{e}}}$	(2-14)
	$q'''_{\mathrm{e}} = \Delta H_{\mathrm{e}} W_{\mathrm{e}} R_{\mathrm{e}}$	(2-15)

Table 2-2

Physical and kinetic parameters used in the computational model.

Symbol	Description	Value	Unit
A_{sei}	SEI decomposition frequency factor	2.08E15 [98,99]	s^{-1}
A_{n}	Negative-electrolyte frequency factor	1.67E6 [98]	s^{-1}
A_{p}	Positive-electrolyte frequency factor	6.67E13 [34,35]	s^{-1}
A_{e}	Electrolyte decomposition frequency factor	5.14E25 [35]	s^{-1}
E_{sei}	SEI decomposition activation energy	1.35E5 [98,99]	J mol^{-1}
E_{n}	Negative- electrolyte activation energy	7.72E4 [98]	J mol^{-1}

E_p	Positive- electrolyte activation energy	1.40E5 [34,35]	J mol^{-1}
E_e	Electrolyte decomposition activation energy	2.74E5 [98]	J mol^{-1}
ΔH_{sei}	SEI decomposition heat release	2.57E5 [34,35]	J kg^{-1}
ΔH_n	Negative- electrolyte heat release	1.71E6 [34,35]	J kg^{-1}
ΔH_p	Positive- electrolyte heat release	3.14E5 [34,35]	J kg^{-1}
ΔH_e	Electrolyte decomposition heat release	1.55E5 [35]	J kg^{-1}
W_n	Specific negative active content	363 [34]	kg m^{-3}
W_p	Specific positive active content	726 [34]	kg m^{-3}
W_e	Specific electrolyte content	407 [35]	kg m^{-3}
n_{sei}	Reaction order for SEI decomposition	1 [34,35]	-
n_e	Reaction order for electrolyte decomposition	1 [35]	-
c_{sei0}	Initial value of c_{sei}	0.15 [34,35]	-
c_{n0}	Initial value of c_n	0.75 [34,35]	-
α_0	Initial value of α	0.04 [34,35]	-
z_0	Initial value of z	0.033 [34,35]	-
c_{e0}	Initial value of c_e	1 [35]	-
T_0	Initial temperature	301.15 [34]	K
k	Average thermal conductivity	3.4 [34]	W m^{-1} K^{-1}
ρ	Average density	2580 [34]	kg m^{-3}
c_p	Average heat capacity	830 [34]	J kg^{-1} K^{-1}
h	Convective heat transfer coefficient	7.17 [35]	W m^{-2} K^{-1}
ε	Surface emissivity	0.8 [35]	-

Chapter 3. Scale effects on self-heating ignition of Lithium-ion batteries stored in boxes, shelves and racks

Summary[1]

The fire safety of LIBs during their storage and transport is becoming of prime importance for the industry, with a number of such fires reported in recent years. It is crucial to understand the mechanisms and causes of these fires to provide insights for prevention. Previous studies mostly focused on small-scale LIBs testing and the chemistry involved. The possibility of ignition resulting from heat transfer within a large-size ensemble of LIBs has been poorly investigated. Focusing on the fire safety of large-scale stored LIBs, this chapter discusses the risk and likelihood of self-heating ignition, which is a known cause of fires in other industries (e.g. chemical storage). Taking LCO type of battery as a base case and using its chemical kinetics reported in the literature, this chapter develops a transient heat transfer model based on multi-step chemical kinetics to analyse the self-heating behaviour of ensembles of LIBs in four typical storage sizes, from a single cell to racks containing around 2 million cells, using COMSOL Multiphysics. The results show that the critical ambient temperature for self-heating ignition is significantly lower for a large-scale LIB ensemble (e.g. 60 ℃ for the rack), indicating spontaneous side reactions are not negligible heat sources in large LIB ensembles and self-heating could pose potential fire hazards in large-scale LIB storage. This work

[1] This chapter is based on "Hu, Z., He, X., Restuccia, F., Yuan, H., & Rein, G. (2021). Numerical study of scale effects on self-heating ignition of lithium-ion batteries stored in boxes, shelves and racks. Applied Thermal Engineering, 190, 116780."

provides insights into the effects of heat transfer of LIB ensembles across scales and helps better understand of self-heating ignition of LIBs.

3.1 Introduction

LIBs are an important type of power storage unit and are widely used in portable electronic devices[100]. The high energy density of LIBs boosts their commercial applications. On the other hand, this feature also imposes a safety risk, namely their susceptibility to ignition[61,101,102]. Many catastrophic fires related to large-scale LIB storage and transport have been reported in the past decade, while the possible causes of those large LIB fires are still not understood[56,103,104]. LIB manufacturers, recycling companies as well as storage and transportation industries have suffered great losses due to these fires, and are increasingly concerned about how to safely store and transport these highly reactive batteries.

The concept of self-heating ignition and the specific challenges introduced for LIBs are introduced in Chapters 1-2. The worst cases for self-heating ignition are whether it could occur at, or near to, normal ambient temperature, which usually requires a large stack of reactants. However, current studies on self-heating behaviour of LIBs were mainly focused on a single cell or small module[105]. The possibility of self-heating ignition of large-scale stacked LIBs has not been scientifically studied yet. It is crucial to develop a model to predict and analyse the possible self-heating ignition behaviour of large ensembles of LIBs.

This chapter develops a 3D numerical model to investigate the self-heating behaviour of LIBs across scales and discuss if self-heating ignition could be a possible cause of fires of large-scale stacked LIBs. Taking LCO type of LIBs as a base case, which has been systematically studied in the literature, this chapter models the self-heating behaviour of LIB

ensembles in four typical storage sizes. Four-step reaction kinetics reported in the literature are adopted the consider the complex reactions for LIBs. Sensitivity analyses are conducted to determine the most important input parameter for the model. Three parameters are put forward to assess the self-heating behaviour of LIB ensembles. Furthermore, the heat generations of each reaction for different LIB ensembles are compared to evaluate the dominant reactions that can trigger self-heating ignition.

3.2 Physical and mathematical model

3.2.1 Summary of the physical model and chemical kinetics

The fundamental physics and chemical kinetics of the numerical model developed for self-heating ignition of LIBs can be found in Section 2.3. The numerical model simulates a typical self-heating experiment, the oven experiment. LCO type of battery is selected as an example for quantitative analyse. The kinetics and parameters are from the studies by Hatchard et al.[34] for E-One/Moli Energy ICR18650 (18 mm diameter, 65 mm length) 1.65 Ah LCO/graphite cells at 100% SOC. Batteries in storage and shipment are usually required to be stored at 30% SOC. Unfortunately, the fundamental relationship between these kinetics and SOC has not been reported yet. Therefore, this thesis still uses kinetics based on 100% SOC, which represents the worst scenario in terms of reactivity. All of the numerical calculations are performed using commercial software COMSOL Multiphysics 5.3a.

3.2.2 Model validation

The accuracy of the simplified model is assessed by conducting a case analysis of a single cylindrical cell and comparing against the experimental data from the literature, as shown in Figure 3-1. The values of the required parameters are listed in Table 2-2. A mesh independence

analysis is conducted to simulate the single-cell case with three sets of meshes containing 384, 608, and 1128 elements, respectively. The calculated temperature with these three sets meshes all agrees well (within 1% relative errors). In this case, the mesh with 384 elements already provides adequate accuracy and is therefore used for the simulations.

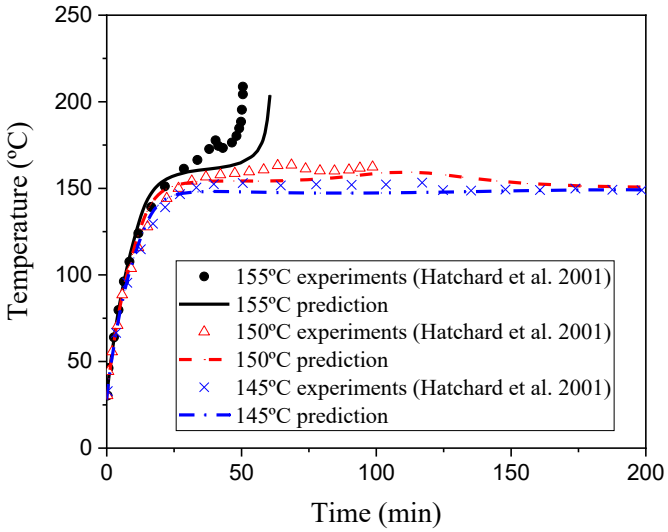

Figure 3-1. Comparison of temperature history between our COMSOL simulation (solid lines) and oven experiments (dot points) by Hatchard et al.2001[34].

As Figure 3-1 shows, at a subcritical condition (T_a= 145 ℃ and T_a=150 ℃), the temperature of the cell remained stable at ambient temperature. While at a supercritical condition, T_a=155 ℃, the temperature of the cell quickly rose above the ambient temperature and initiated thermal runaway. The temperature profiles given by the numerical model fit well with experiments for the subcritical conditions but are underestimated for the supercritical condition after thermal runaway. This underestimation is because this model focuses on predicting the onset of thermal runaway, not the whole fire behaviour of the LIB. Reactions considered are only for the early stage of thermal runaway at relatively low temperatures. Once the temperature of the battery cell reaches around 200 ℃, complex combustion reactions could occur. These combustion reactions are out of the scope of our model. However, the numerical

model gives a good prediction of the critical ambient temperature where thermal runaway starts to occur. This is the key parameter for self-heating ignition; therefore, it is reasonable to use this model to make predictions of the self-heating behaviour of LIBs.

3.2.3 Sensitivity analysis

As Table 2-2 shows, this model requires dozens of input parameters. Since most of these parameters require careful measurements to ensure accuracy, it is useful to perform a sensitivity analysis to determine parameters with significant effects and give priority to these parameters for further attention. One-at-a-time (OAT) method is therefore adopted for the scenario of one single cylindrical cell. The impact on the output Y is numerically assessed by applying a small variation ΔX_i on the nominal input parameter of interest $X_{i,0}$. s_i is the effective sensitivity coefficient defined by the following equation[82,106]:

$$s_i = \frac{Y(X_{i,0} + \Delta X_i) - Y(X_{i,0})}{\Delta X_i} \cdot \frac{X_{i,0}}{Y(X_{i,0})} \tag{5-1}$$

The output of interest is the critical ambient temperature to trigger thermal runaway $T_{a,\,cr}$. The small variation of the input parameter is chosen as 5% of the nominal value. 24 input parameters are analysed including chemical parameters, initial mass and concentration of reactants, and heat transfer parameters. The OAT analysis results are shown in Figure 3-2, which shows that the activation energy of positive-electrolyte reaction E_p is the dominant parameter predicting critical ambient temperature. The absolute effective sensitivity coefficient of E_p is about 20 times larger than any other parameters. This indicates that the positive-electrolyte reaction drives the thermal runaway of a single cell. These results agree with the simulation results by Kim et al.[66] that thermal runaway took place while the positive electrode was decomposing.

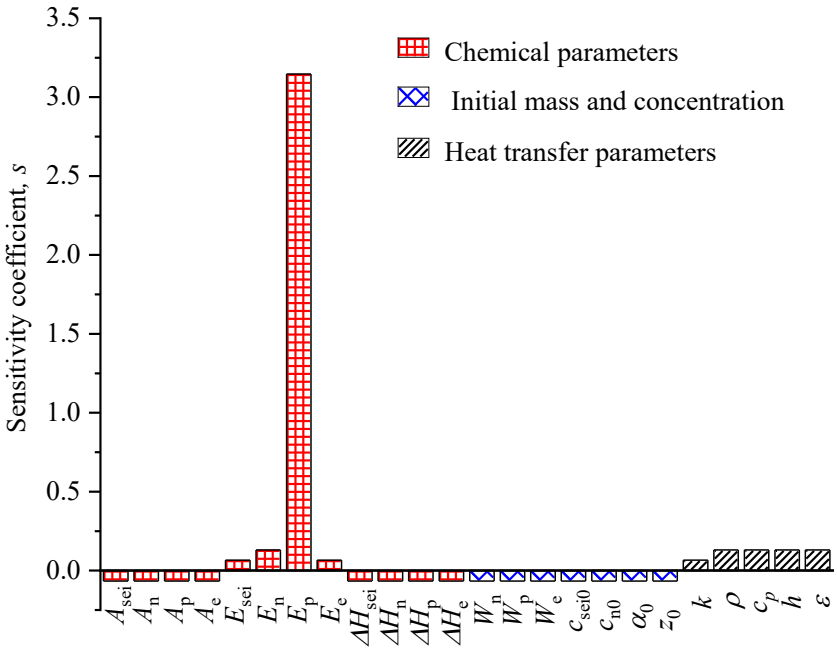

Figure 3-2. Sensitivity analysis of 24 input parameters on predicting the critical ambient temperature $T_{a,\,cr}$ based on the case of one single cylindrical cell.

3.3 Simulations of large battery ensembles

Arguably the most important case for self-heating of LIBs in terms of safety is whether LIBs in different storage sizes could self-ignite at normal ambient temperature or not. Therefore, this model considers four typical storage sizes: single cell, a box of cells, a shelf of boxes, and a rack of shelves, as shown in Figure 3-3. The detailed dimensions for the four sizes are listed in Table 3-1. For real LIBs storage, this involves a highly complex geometry due to the packaging material and the presence of various insulation materials. Modelling a large ensemble of LIBs with complex chemistries with the addition of a complicated packaging setup would become computationally prohibitive in terms of resources required. For these simulations, the model therefore initially considers a theoretical condition where all battery cells are tightly packed together, with no insulating materials between cells. The shape of the battery cells is simplified to a pouch shape with the same composition as the cylindrical cells

discussed in Section 2.3, where the kinetics and parameters are also the same. In this simplified case, the 3D homogenous model could be applied to the entire ensemble to finally achieve large-scale simulations. All four scenarios are simulated under different ambient temperatures until the systems could self-ignite to find the critical ambient temperature for self-ignition. The results are shown in Figure 3-4. In this chapter, three parameters are put forward to evaluate the self-heating behaviour of LIB ensembles: the critical ambient temperature $T_{a,\,cr}$, the onset time of thermal runaway t_{on}, and the onset cell temperature T_{on}.

Table 3-1

The dimensions of the four simulation scenarios modelled in this work

Scenarios	Dimensions	Number of cells inside	Number of mesh elements
Single cell	0.229×0.152×0.008 m	1	247
Box	0.431×0.343×0.165 m	80	1995
Shelf	3×1.5×1.5 m	24,000	1539
Rack	30×6×3 m	1.94×10^6	2432

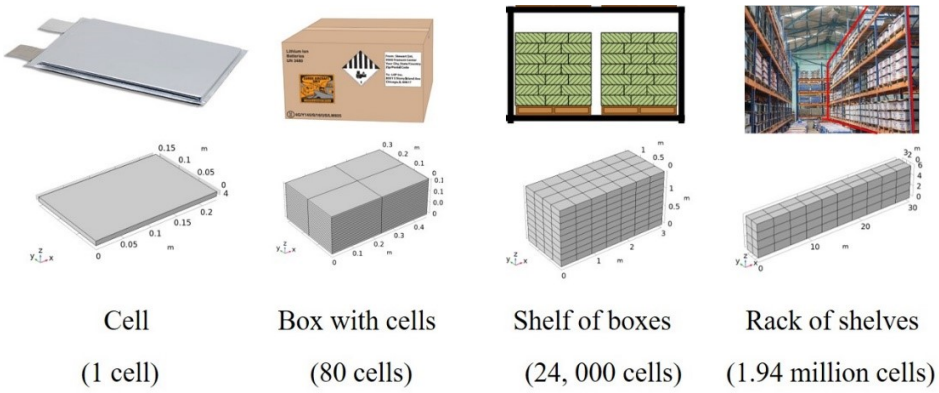

Figure 3-3. The schematics of simulation scenarios. The battery cells are assumed to have the same compositions as the cylindrical cells, and the shape is changed from cylindrical to pouch shape out of simplicity. The real packing configurations (top) and the computational domains (bottom) are presented in pairs for each size studied.

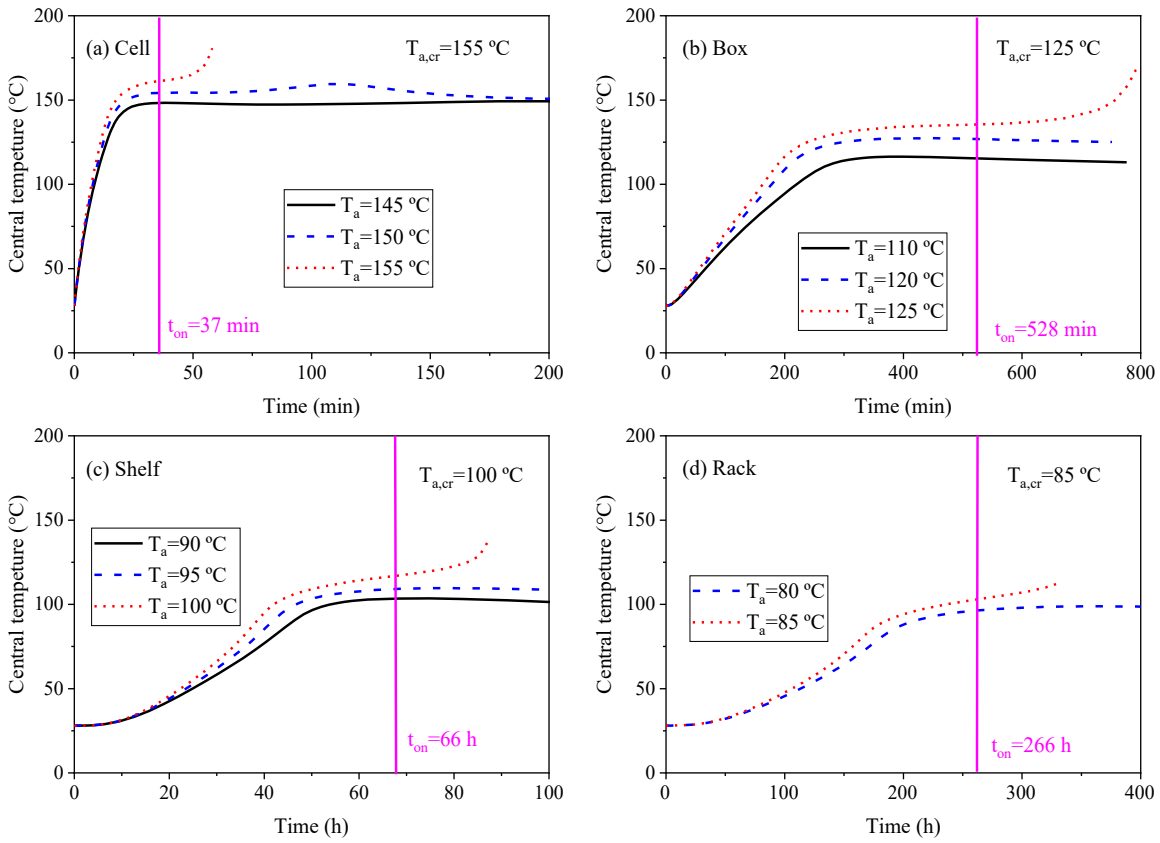

Figure 3-4. The calculated temperature history of the central point of four scenarios (from (a) single cell, (b) a box of cells, (c) a shelf of boxes, to (d) a rack of shelves) exposed to different ambient temperatures. The purple lines represent the time when thermal runaway starts to take place. $T_{a,cr}$ drops from 155 ℃ for the single cell to 85 ℃ for the rack of cells.

3.3.1 The critical ambient temperature $T_{a,\,cr}$

$T_{a,\,cr}$ is the minimum ambient temperature that LIB ensembles required to initiate self-heating ignition. The central points of the LIB ensembles are expected to be the local hot spot because of the adiabatic condition due to symmetry. Their temperature is therefore used to assess thermal runaway and self-heating ignition. Since LIBs have a large energy density, the model assumes that self-heating ignition would occur once the central cell goes into thermal runaway. According to the simulations, $T_{a,\,cr}$ decreases significantly with a larger LIB ensemble. A single cell could undergo thermal runaway at an ambient temperature of 155 ºC, while a rack of cells requires 85 ºC, which is even lower than the onset temperature of SEI decomposition

reported in the literature[1,5]. This is because the current adiabatic calorimetry techniques[38], such as the ARC technique, cannot provide a rigorously adiabatic environment. In these tests, reactions with a self-heating rate lower than 0.02 ℃ min^{-1} are omitted. These reactions with slow heat generation are difficult to observe for a small sample, which has a relatively strong ability to dissipate heat. However, when samples are stacked in large sizes, heat is harder to dissipate, and the heat generated by slow-rate spontaneous reactions could accumulate and lead to a temperature increase. After a long period of heat accumulation, the rack of cells is finally able to self-ignite at an ambient temperature of 85 ℃.

3.3.2 Onset time t_{on} and the onset cell temperature T_{on}

From Figure 3-4, it can be seen that in all thermal runaway cases, the temperature of the central point is quite different when the LIB ensembles start to undergo thermal runaway. To evaluate this phenomenon, this work puts forward two parameters, onset time t_{on} and the onset cell temperature T_{on}. t_{on} is defined as the time when thermal runaway starts to take place, while T_{on} is the onset temperature of the central point (hot spot) when thermal runaway starts. Although many comprehensive definitions of thermal runaway of LIBs has been proposed, the criteria of the onset of thermal runaway, which assess the transition of normal controllable temperature increase to an uncontrollable thermal runaway, is still controversial [29]. Most of the criteria proposed mainly focus on heat generation. For instance, some testing standards take the battery temperature exceeded the environment temperature to a certain degree (e. g. 50 ℃) as the criterion for thermal runaway, while some suggested using a certain heat generation rate as the criterion[29]. Without considering the effects of heat dissipation from the environment, these criteria, which are often developed based on single-cell tests, cannot be guaranteed to apply when used for large scale evaluation. Moreover, these criteria actually define what is

known as fully developed thermal runaway, in which the heat generation rate already greatly exceeds heat dissipation resulting in large temperature increase rates, rather than a precise criterion describing the transition of a normal controllable temperature increase to uncontrollable thermal runaway.

In this study, the onset state of thermal runaway is defined as the time where the second derivative of temperature over time, $\frac{d^2T}{dt^2}$, turns from negative to positive. For a subcritical condition, temperature increases in a controllable way, $\frac{dT}{dt} > 0$ and $\frac{d^2T}{dt^2} < 0$. In the end, the temperature would stabilize at a typical value. However, when the system transitions to a supercritical condition, $\frac{d^2T}{dt^2} > 0$, not only does the temperature increases with time, but the temperature increase rate, $\frac{dT}{dt}$, starts to increase, leading to uncontrollable temperature increase and runaway. The time it takes to reach this critical state is t_{on} and the temperature of the central point at this time is T_{on}. The values of t_{on} and T_{on} for all four scenarios undergoing thermal runaway are listed in Table 3-2.

Table 3-2

The calculated critical parameters for the four scenarios under thermal runaway

Scenarios	t_{on}	$T_{a,\,cr}$	T_{on}
Cell	37 min	155 ºC	165 ºC
Box	528 min	125 ºC	136 ºC
Shelf	66 h	100 ºC	117 ºC
Rack	266 h	85 ºC	103 ºC

As presented in Table 3-2, for a larger size of LIB ensemble, self-heating ignition could occur at a lower ambient temperature, however, it also requires much more induction time to accumulate heat inside to trigger ignition. t_{on} increases significantly with the increase of LIB ensemble size. The single-cell took about 40 min to reach thermal runaway at an ambient

temperature of 155 ºC, while the rack ensemble needs around 10 days to thermal runaway at an ambient temperature of 85 ºC. This means that although a large battery ensemble could self-ignite at relatively low ambient temperature, the time it needs can be significantly longer, which agrees with the classical self-heating theories[49,107]. This long induction period could explain why large-scale LIB storage fires are hard to predict. While the surface temperature of the LIB ensemble remains the same as the surrounding environment, the internal cells might keep accumulating heat for a long period, and may then undergo thermal runaway at a critical time.

Table 3-2 also shows that T_{on} declines with the increase of geometric size, from 165 ºC for the single-cell dropping to 104 ºC for the rack. Due to the decreasing of heat dissipation ability for the rack, the internal cells have lower thermal tolerance that heat generation at a lower temperature is adequate to overcome the heat dissipate and initiate thermal runaway. Therefore, the internal cells only need to be heated up to 104℃ to self-ignite. This again proves that a large LIB ensemble could self-ignite at a much lower temperature. The temperature of the central point only needs to reach 104 ℃, which is the temperature when SEI decomposition starts to be obvious[1,5], the low heat generation already overcomes heat dissipation and causes thermal runaway.

Figure 3-6 shows the relationships between $T_{a,\,cr}$, T_{on} with the number of cells. Both $T_{a,\,cr}$ and T_{on} drop significantly for a large LIB ensemble. According to the decreasing trend, it seems that self-heating ignition for a battery ensemble at environmental temperature is impossible to take place for it requires countless cells. However, these decrease trends clearly show that a large ensemble of LIBs is much more thermally vulnerable than a single cell, that they could self-ignite at much low ambient temperature. These predictions are based on the assumptions that all cells are tightly packed and there are no insulating materials nor contact resistance between cells. According to these assumptions, the effective thermal conductivity of the whole

battery ensemble is the same as that of LIB, 3.4 W $m^{-1}K^{-1}$. However, for real LIB storage, insulations are often required to separate battery cells to prevent short circuits and provide cushioning to avoid mechanical damage[27]. These insulations are usually thermally insulating and would introduce a large heat resistance and greatly deteriorate heat transfer within the ensemble. The effective thermal conductivity for the whole LIB ensemble with insulations could be quite low. To consider this effect, this study simply decreases the effective thermal conductivity of the system to 0.3 W $m^{-1}K^{-1}$, the results are shown in Figure 3-5 in the blue line.

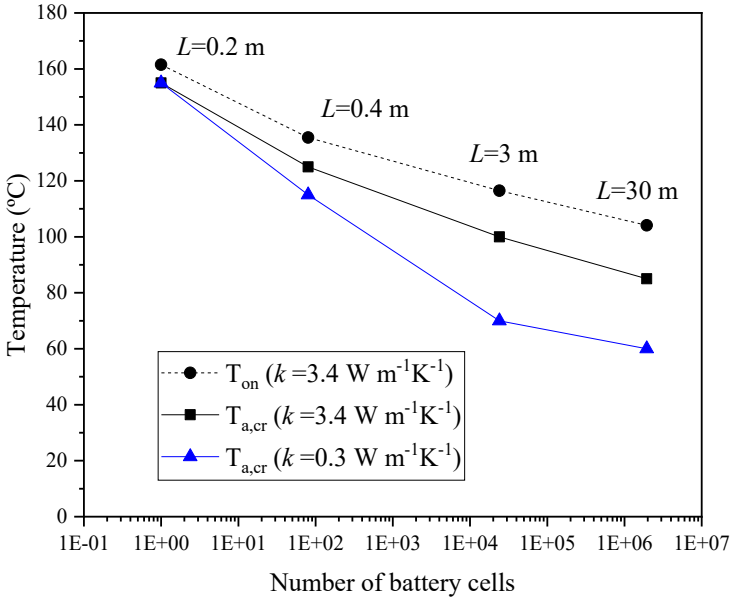

Figure 3-5. The calculated relationships between $T_{a,\,cr}$, T_{on} and number of cells in battery ensembles. Lines in black represent the results of initial calculations with average heat conductivity of 3.4 W $m^{-1}K^{-1}$, the dashed line represents the onset cell temperature T_{on}, the solid line represents the critical ambient temperature $T_{a,cr}$, the line in blue represents the results of $T_{a,cr}$ considering heat resistance between battery cells by assuming the effective heat conductivity of the system to be 0.3 W $m^{-1}K^{-1}$. L is the typical length, which is the longest dimension of LIB ensembles.

The calculations demonstrate that a large battery ensemble with good thermal insulation is much easier to self-ignite, the rack is predicted to self-ignite at T_a=60 ℃. Additionally, all these predictions are focusing on one type of LIB, and assume that all battery cells are in good condition. However, a large LIB ensemble with tens of thousands of cells might contain some

cells with tiny manufacturing defects. These defects might not be severe enough to cause a short circuit, but could lower the thermal stability of the cell, leading it to fail at a much lower temperature. These defective cells could be the local hot spots to start a fire, the critical ambient temperature could be much lower in this case. Self-heating ignition could pose potential fire hazards to LIBs.

Unfortunately, current safety guidelines and regulations [108,109] on LIB storage and transport do not consider this issue yet. Most of them focus on the prevention of short circuits[108,109] and fail to recognize that a warm storage environment might also pose a potential fire risk to LIBs.

3.3.3 The dominant reactions for thermal runaway

According to the computational results of Hatchard et al.[34] and Kim et al.[35], the dominant reaction triggering thermal runaway for a single cell is believed to be the decomposition of the positive electrode. However, as Table 3-2 shows, the $T_{a,\,cr}$ and the T_{on} for the rack-scale are predicted to be lower than the onset temperature of the positive-electrolyte reaction, which means the driving reactions for thermal runaway could change. In order to analyse this phenomenon, the residual concentration of reactants is recorded for these four scenarios undergoing thermal runaway. The results are shown in Figure 3-6.

The model predicts that the SEI layer is already consumed before thermal runaway takes place, while the electrolyte remains unreacted at the beginning of thermal runaway. The main changes in reactants are the intercalated lithium and the positive electrode. However, a large concentration change of a reactant does not guarantee this reaction producing the largest heat generation. In this case, the heat generation rate of each reaction q_i''' is integrated over the

whole volume of the system forming the heating power Q_i of each reaction. η_i is the heat generation fraction of i reaction, Q_i and η_i are defined as follows:

$$Q_i = \int_V q_i''' \tag{5-2}$$

$$\eta_i = \frac{Q_i}{Q_{tot}} \tag{5-3}$$

The heating power Q_i and heat generation fraction η_i of each reaction are shown in Figure 3-7 and Figure 3-8 respectively. The simulations predict that both heating power and heat generation fraction have a similar trend for different sizes of LIB ensembles. At the start of the simulation, the battery cells are all at a low temperature, where the negative electrolyte reaction generates most of the heat. As temperature increases, the SEI layer starts to decompose. η_{sei} forms a peak in the early stage with the consumption of meta-stable SEI. As the temperature increases further, positive electrolyte reaction begins to increase in speed. η_p rises sharply and quickly becomes the dominant reaction.

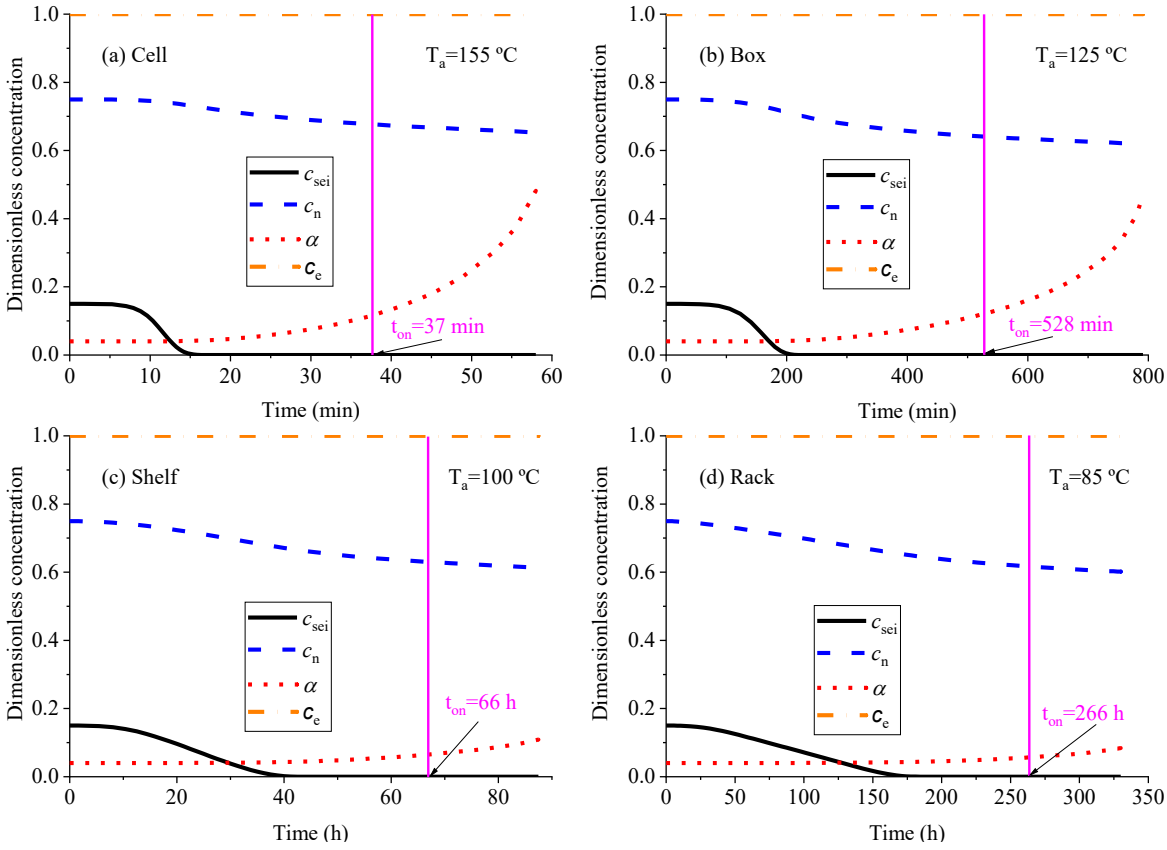

Figure 3-6. The calculated residual dimensionless concentration of four reactants in four scenarios (from (a) cell to (d) rack) undergoing thermal runaway. The vertical purple lines represent the time when thermal runaway starts to take place.

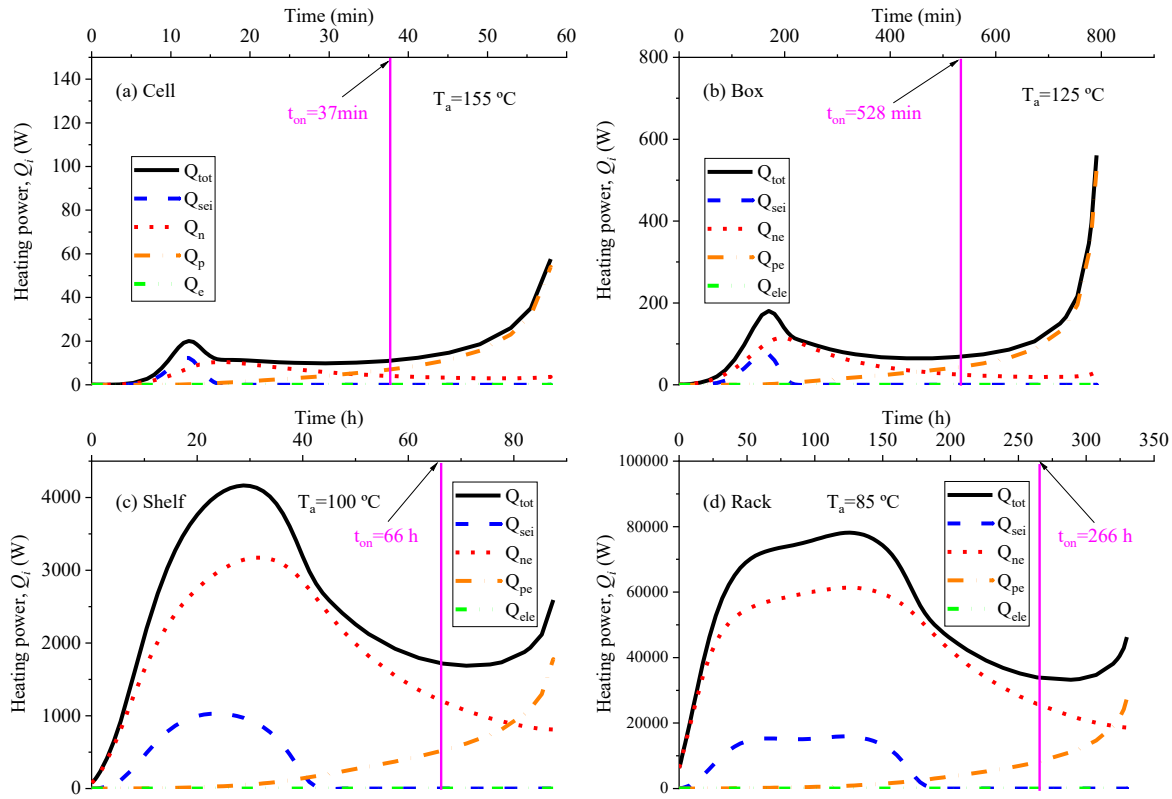

Figure 3-7. The calculated heating power of different reactions in four scenarios (from (a) cell to (d) rack) undergoing thermal runaway. Q_i is the heating power of *i* reaction, defined as the heat generation rate of *i* reaction integrated over the whole volume of the system. The vertical purple lines represent the time when thermal runaway starts to take place. The heating power of electrolyte decomposition, Q_e maintains around 0 for all scenarios.

However, when the size of the battery ensemble changes, there are some performance changes that need to be accounted for. As the size of the ensemble increases, the lasting time of the SEI reaction increases, making the peak flatten. Only for the single-cell scenario, the η_{sei} have a chance to rise above η_n. While for a large size, η_n is always higher than η_{sei}, which shows that the negative-electrolyte reaction has a stronger influence on self-heating behaviour for large LIB ensembles. Looking at the time when thermal runaway starts to take place, the positive-electrolyte reaction is dominating for small size (cell and box scenarios), while the negative-electrolyte reaction plays a more crucial role for large size (shelf and rack scenarios). This can be interpreted that as the size of the battery ensemble increase, the onset time of

thermal runway, the purple lines in Figure 3-8, move toward the left, which can be regarded as an earlier stage. This means for a large battery ensemble, it does not need that much heat generation to reach thermal runaway. The heat provided by the reactions taking place at lower temperatures might already be enough to trigger thermal runaway and self-ignition.

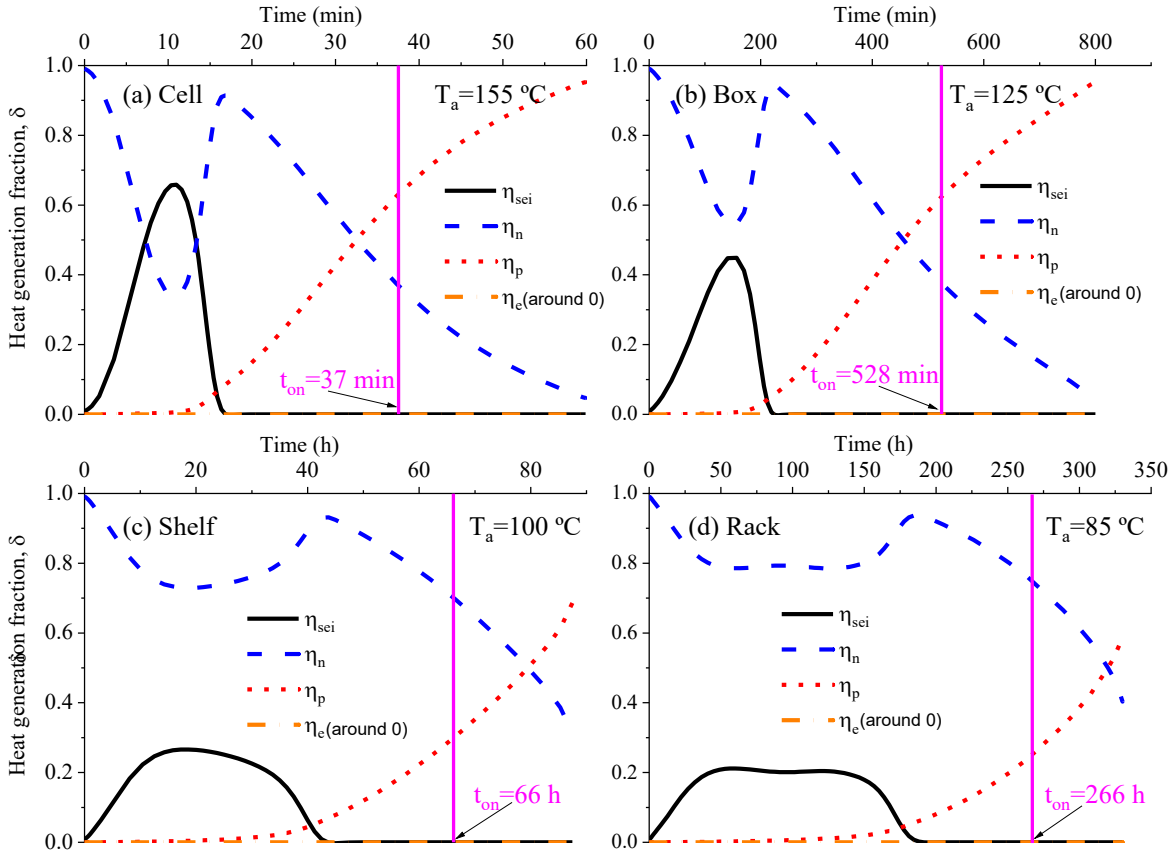

Figure 3-8. The calculated heat generation fractions of different reactions in four scenarios (from (a) cell to (d) rack) undergoing thermal runaway. η_i is the heat generation fraction of *i* reaction, defined as heat generation of *i* reaction divided by the total heat generation of all reactions. The vertical purple lines represent the time when thermal runaway starts to take place. The heat generation fraction of electrolyte decomposition, η_e maintains around 0 for all scenarios.

For a large ensemble of LIB, η_{sei} and η_n play a more important role in the early stage of self-heating. The changes of η_n vs. η_{sei} in the scenarios of single-cell and rack are plotted in Figure 3-9 to demonstrate the changing of dominating reactions for different scales. Both curves show the same trend. At the beginning (t=0), the temperature of LIBs remains low and

all other reactions have not started yet except negative electrolyte reaction, η_n=1. When cells are heated up, SEI starts to react and η_{sei} increases until reaching the maximum reaction rate (t= 0.18 h for the single-cell and t=59 h for the rack), where η_{sei} peaks. Afterwards, η_{sei} drops as the active component of SEI consumed. In this period, η_n goes back and starts to increase. However, η_n could not reach 1 again, where the positive electrolyte reaction starts to react and gradually becomes the dominating one, and thermal runaway starts (t_{on}=0.61 h for the single-cell and t_{on}=266 h for the rack). The peak value of η_{sei} of the rack is significantly lower than that of the single cell, which indicates that negative electrolyte reaction has a larger influence on self-heating for large LIB ensembles.

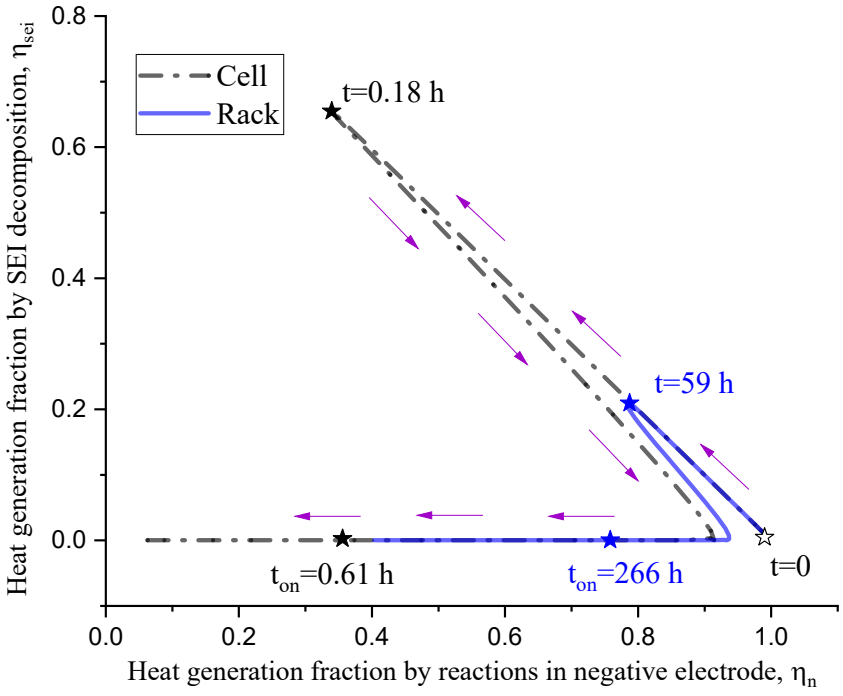

Figure 3-9. The relative value of the two most important heat generation terms η_n vs. η_{sei} in the scenarios of single-cell and rack to demonstrate the changing of dominating reactions when scale-up. The variation in time of η_n and η_{sei} is shown by directional purple arrows. At t=0, η_n=1 for both single-cell and rack scenarios. η_{sei} peaks at t=0.18 h and 59 h respectively for single-cell and rack. Thermal runaway starts at t=0.61 h and 266 h respectively for single-cell and rack. The peak of SEI heat generation decreases with the increase of size, indicating the negative reactions having growing importance on self-heating ignition of LIB ensembles.

3.4 Conclusions

In this study, a 3D transient heat transfer model is developed to investigate if a large ensemble of LIBs during storage could be ignited by self-heating ignition. LCO type of battery is chosen as an example for this case study and analysed based on multi-step chemical kinetics for four typical storage scales. The results show that heat transfer in different sizes of LIB storage systems could significantly change its self-heating behaviour. The upscaling modelling predicts that both the critical ambient temperature, $T_{a,cr}$, and onset cell temperature, T_{on}, decrease significantly with the increase of the size of battery ensembles. Simply considering a theoretical condition, $T_{a,cr}$ drops from 155 ℃ for a single cell to 85 ℃ for a rack of cells. The presence of insulations during LIB storage could further decrease the temperature threshold for self-heating ignition ($T_{a,cr}$=60 ℃). These indicate self-heating ignition can be a possible cause for fires of large-scale stocking of LIBs. Besides, the model predicts that the dominating mechanism of the self-heating ignition of LIBs changes with the size of LIB ensembles. While the positive reactions dominate self-heating ignition of small LIB ensembles, the negative electrolyte reactions are predicted to be more crucial for large LIB ensembles. Driven by heat transfer, the thermal behaviour of a large-scale application could in fact differ significantly from the lab-scale one. This work tries to provide insights into the effects of heat transfer in large scale LIB storage fires. For the sake of simplicity, the results presented in this paper focus on LCO batteries with no defects. However, other types of LIB as well as batteries with defects would have different kinetics and could increase the tendency to self-ignite.

Chapter 4. Heterogeneous model of self-heating ignition of a box of Lithium-ion batteries

Summary[2]

Many thermal events have been reported regarding the storage and transport of large numbers of LIBs, raising industry concerns and research interests in its mechanisms. Apart from electrochemical failure, self-heating ignition, driven by poor heat transfer could also be a possible cause for the fires of large-scale ensembled LIBs. The classical theories and models on self-heating ignition assume a simple lumped system, whereas LIBs storage involves complex geometry due to the packaging and insulation, which significantly changes the heat transfer within the system. These effects on the self-heating behaviour of LIBs have not been studied yet. In this chapter, the self-heating ignition behaviour of a box containing 100 LCO type of cylindrical cells with different insulation is numerically modelled using COMSOL Multiphysics. The model predicts that the critical ambient temperature triggering self-ignition of the box is 125°C, which is 30 °C lower than that for a single cell, and the time to thermal runaway is predicted to be 15 times longer. The effects of different insulating materials and packing configurations are also analysed. This work provides novel insights into the effects of heat transfer on self-heating of large-scale LIBs.

[2] This chapter is based on "Hu, Z., He, X., Restuccia, F., & Rein, G. (2020). Numerical study of self-heating ignition of a box of lithium-ion batteries during storage. Fire technology, 56(6), 2603-2621."

4.1 Introduction

LIBs are a popular type of rechargeable battery that have wide applications in portable devices such as cell phones, cameras, laptops, and even for vehicles and smart grids[110,111]. However, fire safety issues remain a severe challenge for their further development. Safe storage and transport of these batteries with high energy density is becoming a concern to LIB manufacturers, transport industries as well as recycling plants, because of many fire incidents having been reported in recent years. Figure 4-1 shows two large fires that took place at LIB manufacturer and warehouses, causing serious damage. It is crucial to understand the fundamental mechanisms of the cause of these large-scale LIB storage fires to help make strategies and better prevention.

Figure 4-1. Two large LIB storage fires. (Left) a battery recycle plant in the UK caught fire causing the burning of 4 tonnes of waste LIBs[112], and (right) a LIB factory warehouse in China caught fire, the area burnt was approximately 1000 m^2[113].

While the electrochemical community seek explanations mostly from the battery's chemistry, one important factor that has been omitted is that heat transfer also plays a significant role in ignition[49,107]. Self-heating ignition[49,107], which is a fundamental cause of fires for reactive materials[83,84,114], has barely been discussed in the battery community. The numerical model developed in Chapter 3 has shown the critical ambient temperature, $T_{a,cr}$, decreases significantly with the increase of the size of battery ensembles. A

rack of LIBs is predicted to self-ignite at an ambient temperature of 85°C, which is 70°C lower than that of a single cell. However, these results are based on a theoretical condition, which assumes all battery cells are tightly packed and there is no insulation or contact resistance between battery cells. Therefore, reactants are assumed to be continuously and homogeneously distributed inside the entire LIB ensemble. This is also the basic assumption for classical self-heating theories such as Semenov's theory and Frank-Kamenetskii's theory[76,107]. However, in real LIB storage, LIBs are required to be separated by insulations to prevent short circuits and provide cushioning to avoid mechanical damage[27,115,116]. These packaging materials are usually also thermally isolating, which might significantly change the self-heating behaviour of the system. It is crucial to build a model to quantitively analyse the effects of these complex insulations on the self-heating ignition behaviour of LIBs.

In this chapter, a heterogeneous numerical model is developed to analyse the self-heating behaviour of a box of cells (100 cylindrical cells) in storage and try to investigate the effects of insulations on its self-heating behaviour. LCO type of battery is chosen as a case study. Firstly, the self-heating behaviour of the LIB box is compared against one single 18650 cell as presented in Section 3.2.2. Afterwards, the impacts of different insulations and packing configurations are discussed.

4.2 Methods

In order to analyse the potential effects of complex insulations for real LIB storage, a typical storage box with 100 cylindrical cells is analysed. The schematic is shown in Figure 4-2. In the LIB box, the distance between adjacent cells is 20 mm, and there is a 5 mm gap between the front layer of cells and the cover of the box, as shown in Fig. 2 (a). The total

dimensions of the box are 0.208 m × 0.208 m × 0.075 m. To be noted, the size of the box analysed in this chapter is only one-eighth of that presented in Chapter 3. The batteries considered are the same batteries as explained in Section 2.3, which are batteries analysed in work by Hatchard et al[11]., E-One/Moli Energy ICR18650 (18 mm diameter, 65 mm length) 1.65 Ah cobalt cells in 100% SOC. Firstly, all gaps are assumed to be filled with air, which is the most common scenario for real LIB storage. In this packing configuration, the volume ratio of battery cells with respect to the whole box $\chi=V_b/V_{box}$ is 0.51. Due to the symmetry of the geometry, one-eighth of the box is chosen as a computational domain to save computational costs, just as shown in Figure 4-2 (b). The numerical calculations are performed using the finite element method (FEM) software COMSOL Multiphysics 5.4.

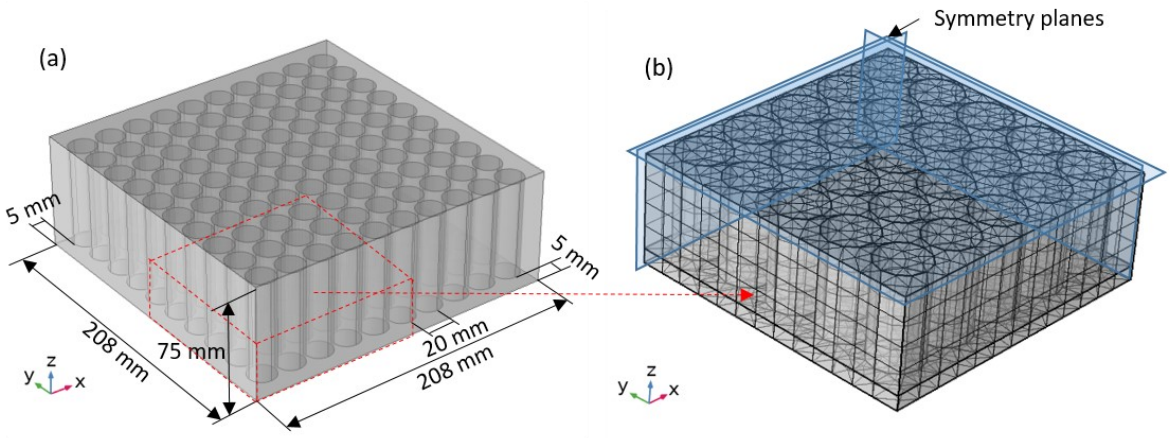

Figure 4-2. Domains of the battery boxes studied in this work. (a) The whole battery box containing 100 cylindrical cells, and (b) one-eighth of the box is chosen as a computational domain using geometrical symmetry.

4.2.1 Governing equations and kinetics for the heterogeneous model

The governing equations and battery chemical kinetics are mostly based on the model explained in Section 2.3. However, the presence of insulation changes the overall heat transfer within the box. Two computational regions are considered: the battery, where exothermic

reactions take place, and the air, which is inert. Therefore, the 3D governing equation is amended as:

$$\rho_i c_{p,i} \frac{\partial T}{\partial t} = k_i \nabla^2 T + q'''_{\text{tot},i} \tag{4-1}$$

where ρ_i is the density, $c_{p,i}$ is the heat capacity, k_i is the thermal conductivity of i material, and $q'''_{\text{tot},i}$ is the volumetric heat source in i. The thermophysical properties ρ, c_p, and k for i material are considered as constant effective values and do not change at the temperature range analysed. In this box scenario, the air gaps are very thin. The flow of air is constrained, therefore, only heat conduction is considered and natural convection within the constrained narrow gaps can be ignored. The heat transfer at interfaces between battery and air domain is calculated using the following equation:

$$\rho_b c_{p,b} \frac{\partial T}{\partial t}\bigg|_{\text{int,b}} = \rho_{air} c_{p,air} \frac{\partial T}{\partial t}\bigg|_{\text{int,air}} \tag{4-2}$$

At the free surface of the box, radiative and convective heat transfer are considered. Eq. 4-3 is used for the convective heat flux component.

$$q''_{\text{conv}} = h(T_s - T_a) \tag{4-3}$$

where h is the convection heat transfer coefficient, T_s is the temperature of the free surface boundary, and T_a is the ambient temperature. Eq. 4-4 is the radiative heat flux component at the boundary:

$$q''_{\text{rad}} = \varepsilon\sigma(T_s^4 - T_a^4) \tag{4-4}$$

where ε is the surface emissivity, and σ is the Stefan-Boltzmann constant. At symmetric boundaries, no heat passes through:

$$\rho_i c_{p,i} \frac{\partial T}{\partial t}\bigg|_{\text{sym}} = 0 \tag{4-5}$$

The chemical kinetics are the same as explained in Section 2.3, except, the reactions only occur in the battery region. In the air region, the heat source term is zero. The thermal physical properties for the LIB and air are listed in Table 4-1, while the chemical kinetic properties are the same as Table 2-2.

Table 4-1

Thermophysical properties of battery cells and insulating materials used in the model.

Materials	ρ (kg m^{-3})	c_p (J kg^{-1} K^{-1})	k (W m^{-1} K^{-1})
Battery cells [11]	2580	830	3.4
Air (Bubble wrap*) [117]	1.204	1007	0.025
Polystyrene [118]	19	1280	0.036
Polyurethane [118]	28	1537	0.024

* Since the thermophysical properties of bubble wrap change with the portion of polymer and air used, this study assumes the thermophysical properties of bubble wrap are the same as air at 20°C.

Table 4-2

Mesh independence analysis. The calculated results of the temperature of the central cell and total heating power of the whole battery box at the time of 2 h, 5 h, and 10 h based on three sets of meshes.

Number of elements	t=2 h		t=5 h		t=10 h	
	$T_{central}$ (°C)	Q_{tot} (J s^{-1})	$T_{central}$ (°C)	Q_{tot} (J s^{-1})	$T_{central}$ (°C)	Q_{tot} (J s^{-1})
3872	76.2	0.627	123.3	0.583	126.9	0.260
5150	75.9	0.589	122.8	0.582	126.8	0.259
7480	76.0	0.596	122.9	0.582	126.4	0.259

4.2.2 Mesh independence analysis

The mesh used for the single-cell presented in Section 3.2.2 contains 384 elements. It is relatively easy to grid such a small homogeneous domain. However, for a complex heterogeneous multi-cells system, mesh quality might play a crucial role in the accuracy of calculations. It is necessary to conduct a mesh independence analysis on such a system. Three

sets of meshes are used in this chapter with 3872, 5150, and 7480 elements respectively. The temperature of the central cell and the total heating power of the whole battery box are two crucial parameters for self-heating and are chosen as the criteria. The result of the mesh independence analysis is listed in Table 4-2. It shows that all three meshes give almost the same results. Using the results of 7480 elements as a baseline, the meshes with 3872 elements and 7480 elements provide enough accuracy. To ensure the accuracy for more complex simulation conditions, the mesh with 5150 elements is chosen.

4.3 Results and discussion

A series of numerical calculations under different ambient temperatures are conducted to determine the critical ambient temperature $T_{a,cr}$ that triggers self-heating ignition. All battery cells in the box are in open circuit condition with 100% SOC. The effects of chemical defects, insulating material, and packing configurations on the critical ambient temperature $T_{a,cr}$ are analysed in the following sections.

4.3.1 Critical ambient temperature

Figure 4-3 shows the temperature history of both the single-cell and the battery box exposed to different ambient temperatures. The central cell in the box is the local hot spot due to geometric symmetry, and its temperature is used to assess the onset of ignition. The $T_{a,cr}$ for the battery box is predicted to be 125℃, which is 30 ℃ lower than that of the single cell. This is because the heat dissipation condition for the central cell in the box is much worse than the single cell, which needs less heat generation and, therefore lower temperature to undergo thermal runaway.

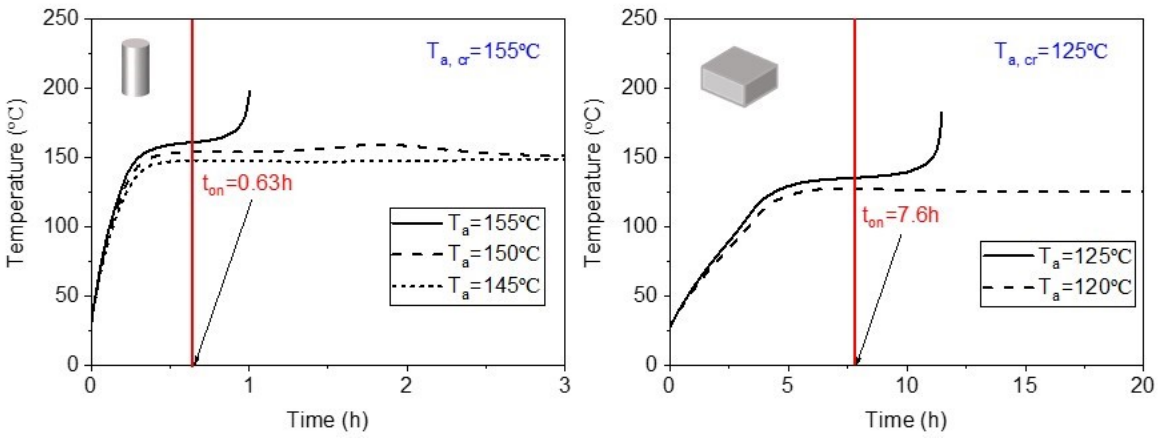

Figure 4-3. The calculated temperature history of the single-cell (left) and the box (right) under different oven temperatures. The vertical red line represents the time when thermal runaway starts to take place.

4.3.2 Time to thermal runaway

The numerical results show that the battery box can self-ignite at lower ambient temperature, the time it needs to run away is longer. As Figure 4-3 shows, under the critical ambient temperature (155 °C for the single cell, and 125 °C for the box), the time scale for the single cell is less than 100 min, while that for the battery box is over 10 h. In this study, the onset state of thermal runaway is defined as the time where the second derivative of temperature over time $\frac{d^2T}{dt^2}$ the first time turns from negative to positive. After this critical time, not only does the temperature increase with time, but also the temperature increase rate $\frac{dT}{dt}$ starts to increase, which leads to an uncontrollable temperature increase and runaway. This time is t_{on}, and the cell temperature at this time is defined as the onset cell temperature T_{on}. To be noted, T_{on} is the temperature of the central point of the system, while $T_{a, cr}$ is the critical temperature of the ambient. In this case, the single-cell starts to thermally run away at t_{on}=38min, while the t_{on} of the battery box is 7.6h. The t_{on} for both the single-cell and the box is marked using a red vertical line shown in Figure 4-3. The t_{on} is the criterion to assess the onset of thermal runaway. After this point, without any external measures being applied to cool

down the system, the system can heat itself up, which means it already goes into a hazardous state. The t_{on} is ahead of the time when there is a sharp temperature increase, which can be called a fully developed thermal runaway state.

4.3.3 The temperature distribution inside the battery box

Figure 4-4 shows the calculated temperature distribution inside the box at 11h (Ta=125 °C). At this point, the box already is undergoing thermal runaway. The hot spot is located at the central point of the box because of its lowest heat dissipation due to geometric symmetry. There is an obvious temperature difference between different cells, while the temperature gradient inside one cell can be omitted. This is because of the difference in thermophysical properties between the batteries and air. The batteries have a much larger volumetric heat capacity ρc_p than that of the air, which means that battery cells have a stronger ability to store energy and maintain their temperature.

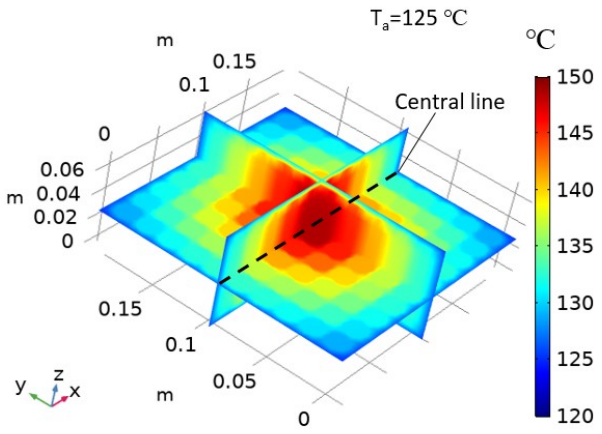

Figure 4-4. The calculated temperature distribution along middle cross-section planes inside the whole box (t=11 h, T_a=125 °C). The dark dashed line is the line used to analyse the temperature distribution history afterwards.

The temperature distribution of the central line (the black dashed line in Figure 4-4) as a function of time is monitored to analyse the development of thermal runaway, as shown in

Figure 4-5. Due to the geometry symmetry, the temperature distribution in the y-direction is the same as that in the x-direction. The x-axis of Figure 4-4 is normalised to the length of the box. In the early stage, the temperature of the outer layer of cells increases sharply. After 5h, the battery cells in the central part of the box reach the environmental temperature. The heat generated by side reactions heats the battery cells, leading the temperature of cells to be higher than the environment. After a further 2 h where heat is accumulating in the box, the temperature of the central cell reaches thermal runaway conditions.

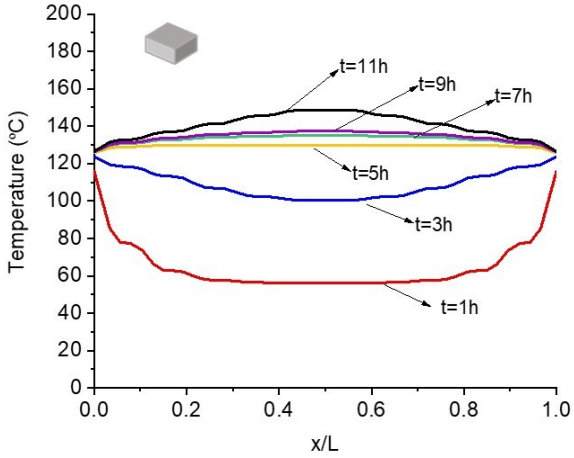

Figure 4-5. Predicted temperature distribution at the centre line in the x-direction at different times. The x-axis is normalised by the total length (L) of the box (at T_a=125 °C).

4.3.4 Dominating chemical reactions

To analyse the mechanisms that initiate thermal runaway, the dimensionless concentration of the reactants is studied, as shown in Figure 4-6. All reactants show very similar trends for both cell and box. The meta-stable SEI component for both scenarios is already consumed by the time thermal runaway is initiated, while the electrolyte remains unreacted because the temperature range interested is lower than the temperature to initiate electrolyte decomposition. The intercalated Lithium in the negative electrode decreases slowly, while the positive electrode decomposes rapidly just after thermal runaway. To analyse the most important

reactions triggering thermal runaway, the heat generation of each reaction is calculated. Heating power Q_i is defined as the volume integration of the heat generation rate q_i''' of i reaction.

$$Q_i = \int_V q_i''' \tag{4-6}$$

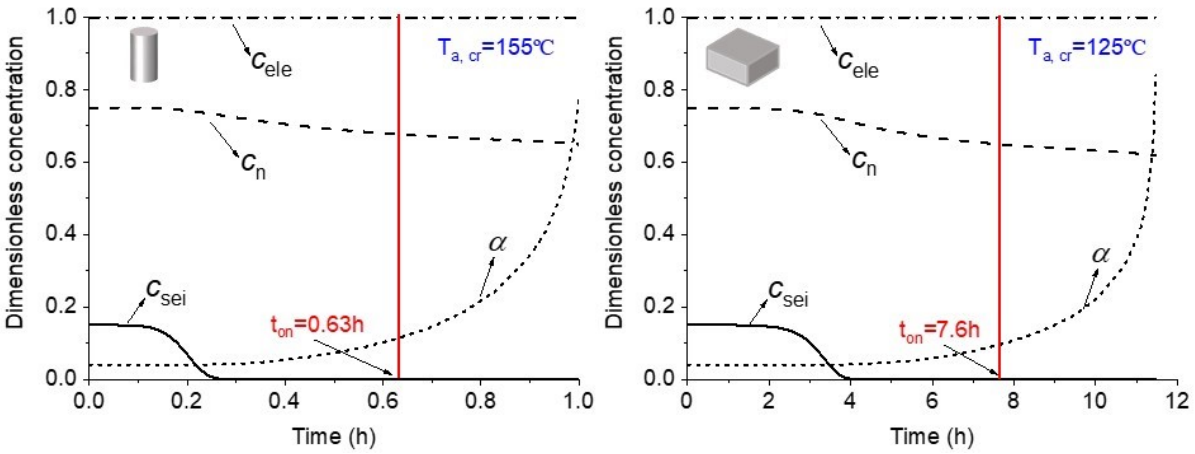

Figure 4-6. Predicted dimensionless concentration of reactants for the single-cell (left) and the box (right) at their critical ambient temperature. The vertical red line represents the time when thermal runaway is initiated.

The predictions are shown in Figure 4-7. The left plot shows the heating power of one single cell, while the right graph shows the heating power of the whole box with 100 cells. Q_{tot} has a peak at an early stage, around 0.2 h for the single-cell and 3 h for the battery box due to the SEI decomposition. Thermal runaway is initiated at 38 min for the cell and 7.6 h for the box. After this critical time, the positive-electrolyte reaction is the dominant reaction to trigger thermal runaway for the single cell, while for the battery box, the positive-electrolyte reaction and the negative-electrolyte reaction share the same contribution on triggering thermal runaway. It is because the battery box requires a lower temperature to initiate thermal runaway, which the reactions at low temperature contribute more heat to trigger thermal runaway. While the

single-cell thermal runaway at a relatively high temperature that only the reactions at high temperature could initiate thermal runaway.

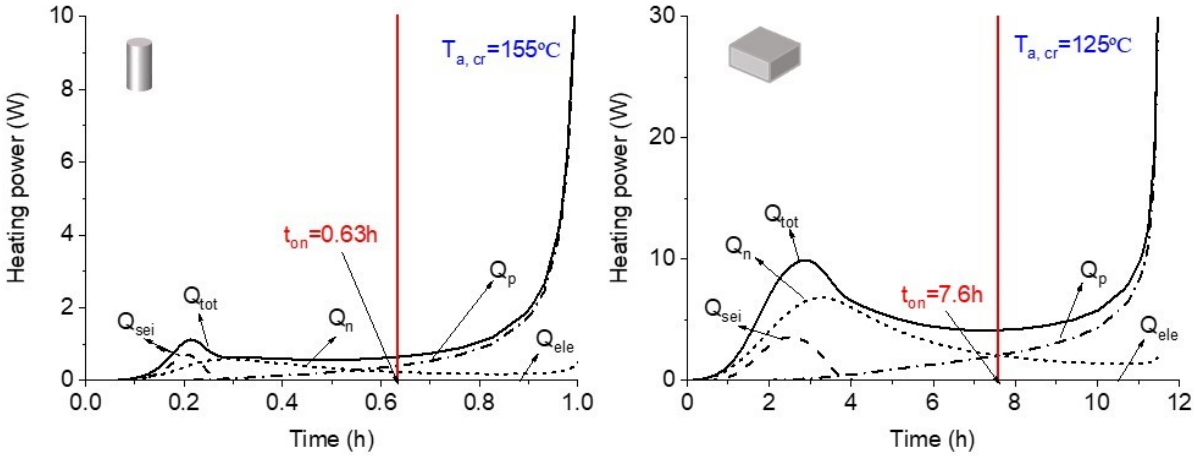

Figure 4-7. Predicted heating power of reactions for the single-cell (left) and the box (right) at their critical ambient temperature. The vertical red line represents the time when thermal runaway starts to take place.

4.3.5 Effects of activation energy

The sensitivity analysis presented in Section 3.2.3 has shown that the activation energy of the positive reaction E_p is the most sensitive parameter for the single cell. In this chapter, the influence of E_p on $T_{a,cr}$ for the whole LIB box is also evaluated. The E_p varies from 90%-110% of the baseline from Table 2-2. The calculated results are shown in Figure 4-8. It shows that E_p also has a large influence on the $T_{a,cr}$ of the box of cells. With ±10% variation of E_p, the $T_{a,cr}$ could decrease to 65 °C or increase to 165 °C for the box.

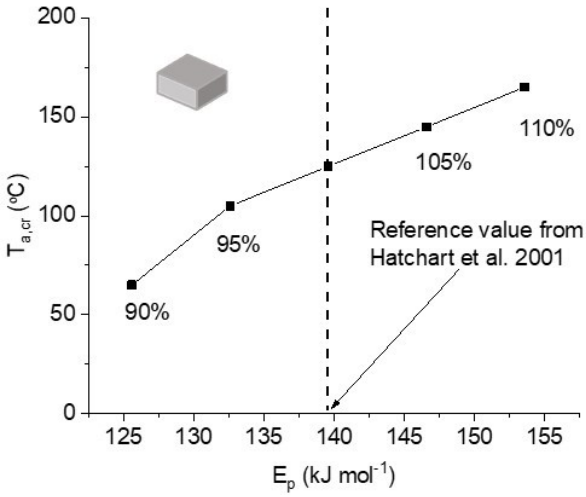

Figure 4-8. Predicted $T_{a,cr}$ of the battery box using different E_p (Basic value is taken from Hatchard et al.[11]).

4.3.6 Effects of packaging materials

For the storage and transport of LIBs, electrical and mechanical insulation between cells is required to avoid short-circuits and mechanical collisions. Several kinds of materials are available with different thermophysical properties, which may change the self-heating behaviour of the box. In this chapter, three commonly used packaging materials: bubble wrap, polystyrene, and polyurethane are analysed. The thermophysical properties of these three materials are listed in Table 4-1. The predictions are shown in Figure 4-9. $T_{a,cr}$ of the box case with different packaging materials are estimated to be the same, 125 °C, the type of insulating materials has a negligible influence on $T_{a,cr}$. This is mainly because the thermal conductivity k for all three packaging materials are similar compared to the thermal conductivity of the batteries, which is 2 orders of magnitude higher. This means the packaging materials introduced the same order of magnitude of heat resistance inside the box system, while the heat resistance by battery cells is much smaller and can be neglected. This makes the self-heating ignition of the box with these packaging materials almost identical. Although boxes with these three different insulation materials are predicted to self-ignite at the same critical ambient

temperature, the temperature profiles still have slight differences. The box with polyurethane is predicted to have the lowest temperature increase rate in the early stage (first 7 h), but the fastest temperature rise when thermal runaway is initiated. While the box with polystyrene is just the opposite that which has the fastest temperature increase rate in the early stage, but is lowest after the onset of thermal runaway. The box with bubble wrap is predicted in the middle.

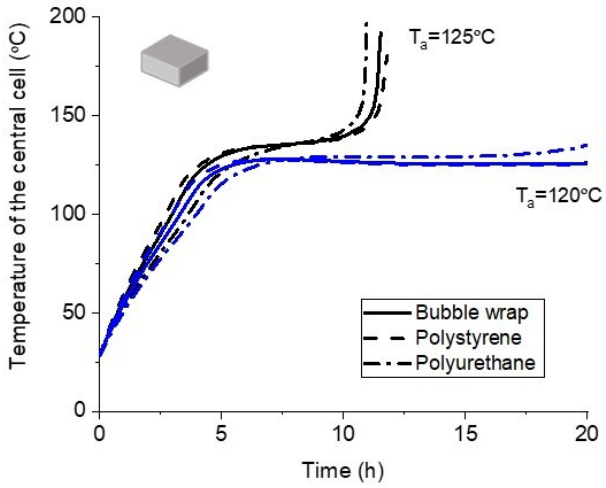

Figure 4-9. Predicted temperature history of the central cell with different insulating materials. The boxes with different packaging materials are all thermal runaway at 125 °C.

4.3.7 Effects of packing configurations

There is no standard or guideline for the distance of gaps between adjacent cells for the package of LIBs. However, the industry tends to use smaller gaps to allow more cells to be stacked as long as the gaps provide reasonable protections for electrical insulation and mechanical cushion. The gap between cells could influence the critical condition for self-ignition. The effects of packing configuration with different spacing of cells are analysed in this chapter. The same box with dimensions of 0.208 m × 0.208 m × 0.075 m is chosen for all packing configurations, with different numbers of cells inside (100, 49, 25 and 9 respectively), and the volume ratio of batteries over the total box $\chi=V_b/V_{tot}$ are 0.510, 0.250, 0.127, and 0.046 respectively, as shown in Figure 4-10. While the former analysis has shown that the box with

all three types of packaging materials has almost the same self-heating behaviour. This work assumes gaps between cells are filled with bubble wrap. The theoretic case, χ=1, is considered as the extreme case for comparison. The predictions are shown in Figure 4-11.

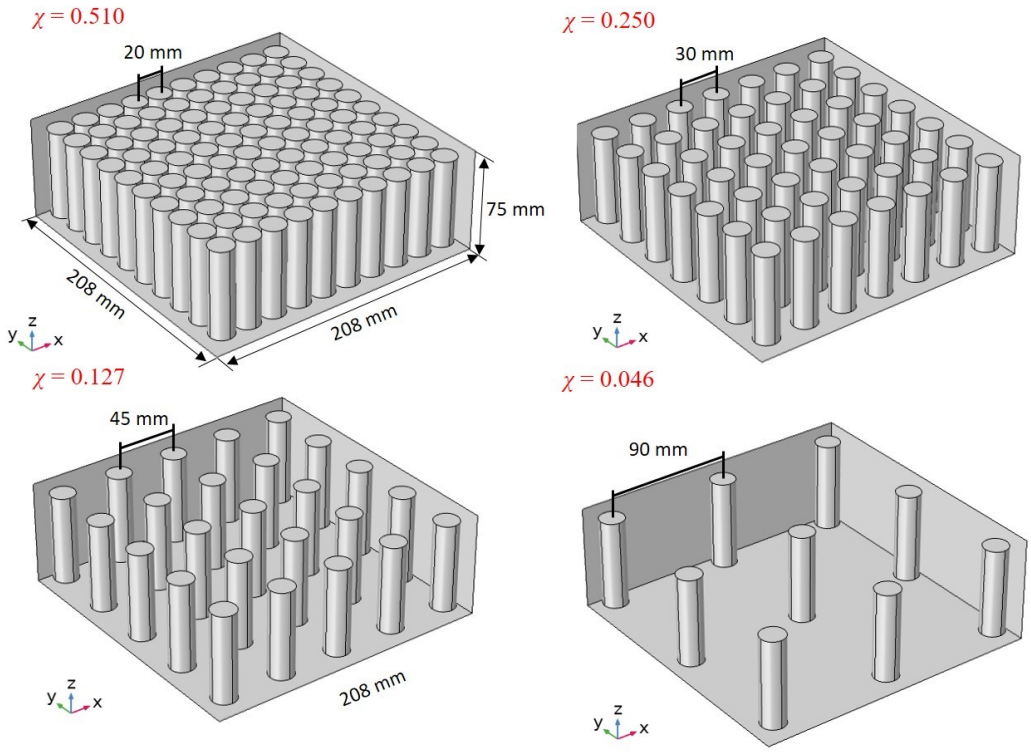

Figure 4-10. The Sketch of domains for different packing configurations using the same box (0.208 m × 0.208 m × 0.075 m) with 100, 49, 25, and 9 cells. The volume ratio of battery cells $\chi=V_b/V_{box}$ is 0.510, 0.250, 0.127, and 0.046 respectively.

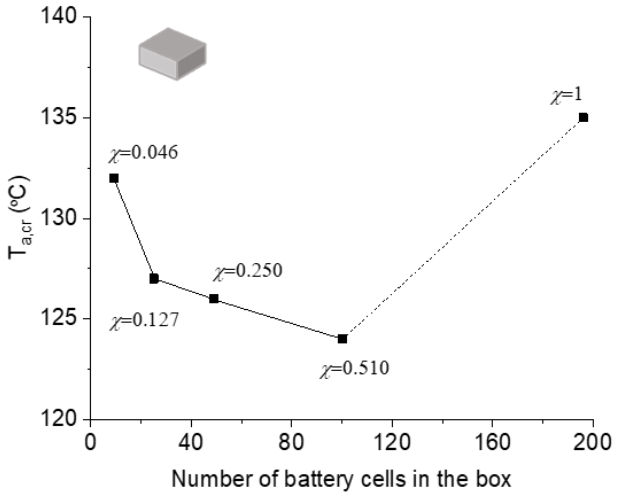

Figure 4-11. Predicted $T_{a,cr}$ for different packing configurations. The same box containing 9, 25, 49, 100, and 196 (theoretical) battery cells, with χ=0.046, 0.127, 0.250, 0.510, and 1 respectively.

Interestingly, Figure 4-11 shows that the box with χ=0.510 has the lowest $T_{a,cr}$, which means it has the worst thermal stability and can self-ignite at the lowest ambient temperature. Compared with the theoretical condition, χ=1, the $T_{a,cr}$ for the scenario with χ=0.510 is around 10 ℃ lower, which means the presence of packaging material actually could significantly promote self-heating ignition. This is because the presence of thermal insulation significantly changes the effective thermophysical properties of the system.

For the theoretical case, χ=1, it has the maximum number of battery cells as well as the highest heat generation. However, its ability to dissipate heat is also strongest because the heat conductivity of batteries is over 100 times higher than the packaging material. In this ideal scenario, the heat resistance of the whole box is much lower than other scenarios, leading to the system to tolerate a higher ambient temperature. Once the insulating materials are incorporated, the heat resistance by the insulating materials are dominating compared to the heat resistance by the battery cells. Therefore, the total heat resistance of the system does not change much for different spacing with different χ. However, the system with lower χ has significantly lower heat generation density, which allows the system to tolerate a higher temperature environment and self-ignite at a higher temperature. Therefore, the box with χ=0.046 has the minimum number of battery cells, which means lower heat generation, and has a higher $T_{a,cr}$. This phenomenon should be similar to other LIB storage systems.

4.4 Conclusions

In this chapter, a heterogeneous model is developed to analyse the self-heating ignition behaviour of a box with 100 LCO type of cylindrical cells under storage. The impacts of

packaging materials and packing configurations during LIB package on self-heating behaviour are analysed to provide insights for predicting the self-heating behaviour of large-scale LIB storage systems. It is found that the critical ambient temperature triggering self-ignition of the battery box is 30 ^{o}C lower than that of a single cell, indicating that the safety guidance based on tests on single cells does not guarantee the safety of a large pack of battery cells. The model predicts that the presence of packaging materials could accelerate self-heating ignition, while the type of materials used has a negligible influence on the self-heating ignition of the box as long as thermal conductivities of the insulation are the same order of magnitude as that of air. It is predicted that the box with the volume ratio of battery cells in the box of around 0.51 has the highest tendency to self-ignite. This study shows that the insulations during the LIB package have crucial impacts on the self-heating behaviour of the LIB storage system. This study shows that the insulations used during LIB packaging have a crucial impact on the self-heating behaviour of the LIB storage system

Chapter 5. Anisotropic and homogeneous model of large ensembles of Lithium-ion batteries

Summary[3]

Self-heating ignition is a fire hazard in warehouses when stacking large quantities of reactive materials and is also a cause of fires for large ensembles of the lithium-ion battery (LIB) during storage. Current self-heating models on LIBs are either too computationally expensive to be applied to the predictions of large LIB ensembles, or capable of large ensemble predictions but missing important heat transfer characteristics like insulation in packaging. This chapter develops a 3D anisotropic homogeneous (Ani-Hom) transient model that can incorporate both complex packaging and be useable for large ensemble predictions using COMSOL Multiphysics. Lithium Cobalt batteries (LCO) are used as a case study. This Ani-Hom model was verified by comparing a box-scale simulation against an isotropic heterogeneous (Iso-Het) model developed in Chapter 4. Both the predictions of temperature evolution and the heat generation agreed to within 5%, while the computational time of the Ani-Hom model is one order of magnitude lower than the Iso-Het model. The Ani-Hom model is then applied to LIB ensembles in four possible storage sizes, ranging from a single cell to a rack with around 10 million cells, with different packing configurations and spacing between cells. The model predicts that the presence of packaging insulation promotes self-heating ignition. A rack of these LCO LIBs is predicted to self-ignite at an ambient temperature of

[3] This chapter is based on "Hu, Z., He, X., Restuccia, F., & Rein, G. (2021). Anisotropic and homogeneous model of heat transfer for self-heating ignition of large ensembles of Lithium-ion batteries during storage (accepted). Applied Thermal Engineering."

45℃, which indicates that LIBs in a warehouse are vulnerable to fire hazards in warm environments. The presence of defects or abuse will even lower this critical ambient temperature. This work provides insights into the effects of complex insulation and spacing on self-heating ignition of LIBs during storage and contributes a better understanding which can help mitigate such fires.

5.1 Introduction

Self-heating ignition, as introduced in Chapter 1 and Chapter 2, is a fundamental cause of fires when reactive materials are heavily stacked. Unfortunately, this phenomenon has seldom been discussed in the battery community. The worst cases for self-heating ignition are whether it could occur at, or near to, normal ambient temperature, which usually requires large stacking of reactants. For LIBs, it is difficult to conduct such large-scale experiments due to the high costs and severe hazards involved, which significantly block the understanding in this field. Current feasible approaches are through investigating the critical kinetics by lab-scale experiments[52,119,120] and then applying it to a self-heating theory or fundamental heat transfer model to make large-scale predictions[62]. However, simulating such a large-scale LIB ensemble is still a challenge for the current state-of-the-art models in the literature. As introduced in Chapter 1 and demonstrated in Figure 1-2, self-heating ignition of LIBs at the warehouse-scale (may contain thousands of or millions of cells[54]) involves three major challenges: the complexity of chemistry, the complexity of geometry, and the geometric scale. While the thermal models in the literature usually focus on one aspect with little attention to the other two.

In Chapter 3, a homogeneous model is developed to achieve large scale predictions of self-heating ignition of LIBs with consideration of four-step reaction kinetics. The results show that the geometrical size of the LIB ensemble has a vital influence on the critical ambient temperature for self-heating ignition. However, the model does not consider the complex heat transfer introduced by the packaging and insulation. Chapter 4 develops a heterogeneous model to consider the complex geometry and heat transfer for a box with 100 cylindrical cells. The results predict that the insulation significantly deteriorates the internal heat transfer within the battery box and facilitates self-heating ignition. Therefore, the effects of these insulations should not be ignored for large scale predictions. The problem is that directly simulating these narrow structures with the heterogeneous model would introduce more refined meshes (millimetre scale) and is numerically affordable for large-scale (warehouse-scale) predictions. It is important to develop a model, which could incorporate the complex heat transfer introduced by insulations during LIB storage and also is capable of large-scale prediction to better understand the self-heating ignition behaviour for large-scale LIB storage.

The objective of this chapter is to build such a model. Based on the models developed in Chapter 3 and Chapter 4, a simplification methodology is put forward. The model developed in this chapter firstly decouples heat transfer from complex chemical reactions to calculate the key effective heat transfer properties, and then recouples the multi-step chemical reactions to achieve fast simulations for large-scale LIB ensembles. The improved model simulates the box case presented in Chapter 4 and validates against the heterogeneous model. Afterwards, the improved model is applied for large-scale predictions and compared against the large-scale predictions by the homogeneous model developed in Chapter 3 to understand the effects of insulation on self-heating ignition of large LIB ensembles.

5.2 Modified anisotropic and homogeneous model

The fundamental modelling of self-heating ignition of LIBs is based on the homogeneous model presented in Chapter 3. The chemical kinetics are the same as explained in Section 2.3. Still, the LCO type of LIBs from the work by Hatchard et al.[11] and Kim et al.[66] is selected as a case study. The detailed input parameters are mostly from Table 2-2 based on E-One/Moli Energy ICR18650[11] (18 mm diameter, 65 mm length) 1.65 Ah cobalt cells in 100% SOC. All of the numerical calculations are performed using a finite element method (FEM) commercial software, COMSOL Multiphysics® V5.4.

5.2.1 Simplification methods

A major obstacle for predicting self-heating of the real large-scale LIB storage system is that battery cells are usually separated by small gaps or insulations to avoid mechanical abuse or short-circuits. These composite structures created by the insulations significantly change the heat transfer performance of the whole LIB storage system, and therefore are not negligible for self-heating modelling. However, direct simulations by considering these narrow structures would introduce refined meshes, which is numerically unaffordable for large-scale predictions. Proper simplification needs to be taken for the current model. When discussing simplification of calculations, this work introduces another concept, anisotropy (isotropic/anisotropic), which needs to be distinguished from heterogeneity (homogeneous/heterogeneous).

Homogeneous defines all material properties to be identical in all locations (otherwise heterogeneous), while isotropic defines that material properties are the same in all directions (otherwise anisotropic). Based on a simple LIB structure, Figure 5-1 uses thermal conductivity, k, as an example to illustrate the differences of these characteristics. Heterogeneity is

introduced by analysing heat transfer between different materials, often adding difficulties on numerical discretization and meshing, quantitatively increasing computational costs but with the controlling equations remaining unchanged. Anisotropy is an intrinsic property of some materials, which have a strong directional heat transfer tendency. It does not geometrically change the discretization, but physically changes the controlling equations (for each property, it introduces three directional variables), increasing computational costs by adding complex calculations. While most models[121–123] considered the heterogeneity of the system, the concept of anisotropy has seldom been discussed, and therefore by default, isotropic distribution is assumed, especially for large-scale predictions requiring massive simplifications.

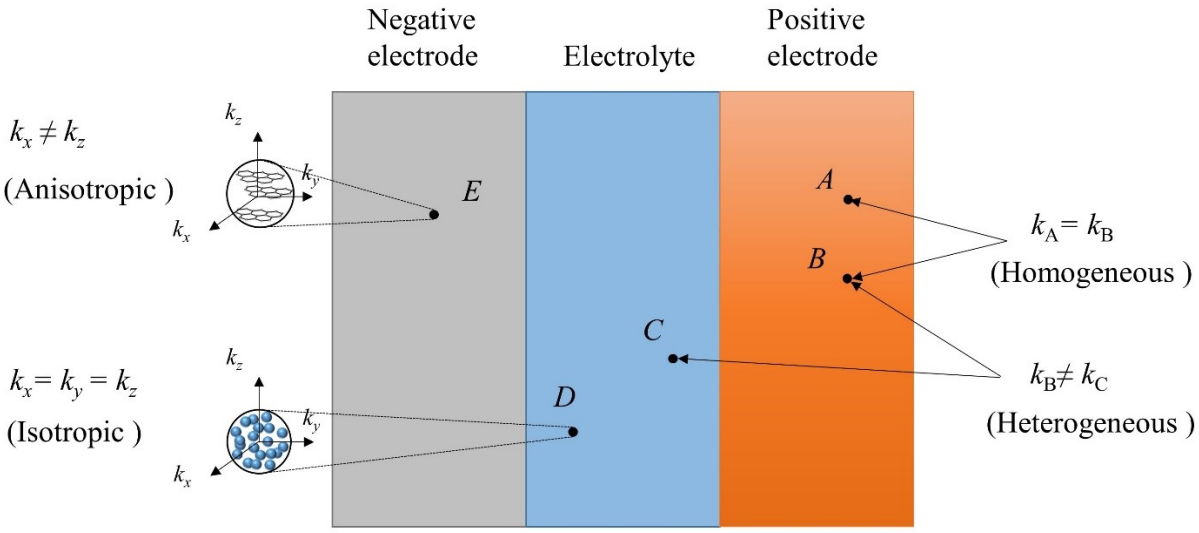

Figure 5-1. Diagram to identify homogeneous (heterogeneous) vs. isotropic (anisotropic). Using thermal conductivity, k, as an example, homogeneous describe material properties to be identical in all locations (the positive electrode consists of the same material, $k_A = k_B$, and therefore is homogeneous), otherwise, it is heterogeneous (the entire battery consists of different materials with different properties, $k_B \neq k_C$, and therefore the entire battery is heterogeneous). Isotropic describe material properties to be the same in all directions (Point D in the electrolyte, in which different molecules are randomly distributed, resulting in macroscopically the same thermal conductivity in all directions), otherwise it is anisotropic (Point E in the negative electrode, which graphite has a layer molecular structure, resulting in different thermal conductivity along the axial direction and radial direction).

Although a LIB cell consists of multiple components and has a complex internal structure, the lumped model[11] (isotropic homogeneous, named Iso-Hom afterwards) using effective properties could provide adequate accuracy for self-heating prediction of the single-cell compared with the 3D isotropic heterogeneous (Iso-Het) model by Kim et al. [66]. Furthermore, a large-scale LIB storage system has a highly periodical structure (as shown in Figure 5-2 (a)) and consists of multiple cells. While each cell is a closed system where complex reactions couple with heat transfer, the interaction between cells is merely by heat transfer, which allows a method to simplify calculations.

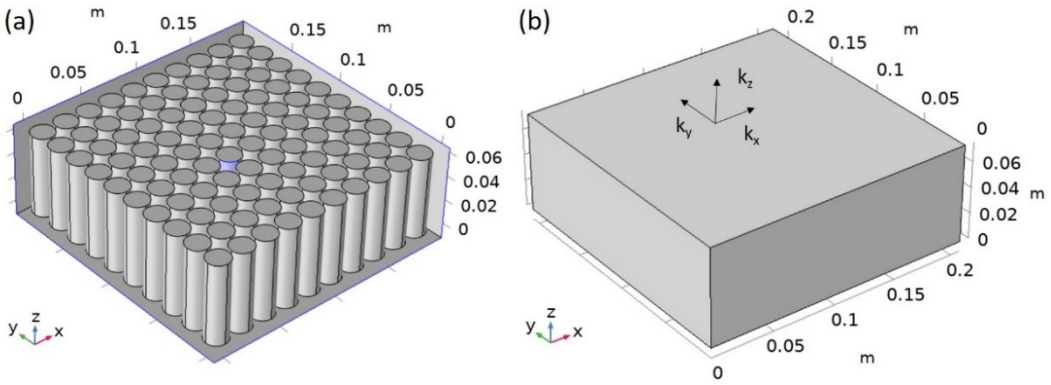

Figure 5-2. Geometric diagrams of the Iso-Het model by Hu et al.[124] (a), which consider the detailed heterogeneous structure of a box containing 100 cylindrical cells, and the Ani-Hom model (b) developed in this study, which simplify the same LIB box as a homogeneous media with anisotropic heat transfer characteristics.

This chapter puts forward a method to decouple the complex chemical reactions and heat transfer, using anisotropic homogeneous (Ani-Hom) heat transfer properties to simplify the Iso-Het transfer with the LIB storage system. The box with 100 cylindrical cells presented in Chapter 4 (as shown in Figure 5-2 (a)) is used as a case study to explain the methodology. The basic box has dimensions of 0.208m ×0.208m ×0.075m. The gaps between cells are filled with insulation (air) as inert. This study assumes the same amount of reactants (100 cells) and inert (air) are equally distributed to the same size of the box (Figure 5-2 (b)), which is homogeneous.

The lumped thermophysical properties such as ρ_l, $c_{p,l}$ of the homogenous box could be calculated as:

$$\rho_l = \chi\rho_b + (1-\chi)\rho_{air} \tag{6-1}$$

$$\chi = V_b/(V_b + V_{air}) \tag{6-2}$$

$$c_{p,l} = \frac{\chi\rho_b c_{p,b} + (1-\chi)\rho_{air}c_{p,air}}{\chi\rho_b + (1-\chi)\rho_{air}} \tag{6-3}$$

where χ is the volumetric ratio of batteries in the storage system. The different placements and orientation of the battery cell within the box could lead to different heat transfer ability in different directions. Therefore, heat transfer differences in different directions are considered by anisotropic thermal conductivity in this study. Three effective directional thermal conductivities k_x, k_y and k_z are used to consider the effects of insulations and orientations of cells on the heat transfer through the whole battery box. As discussed before, the interactions between battery cells are merely by heat transfer, and therefore could be decoupled from the complex chemical reactions. Also, the effective directional thermal conductivities k_x, k_y and k_z are inherent properties of the box and could be calculated by conducting steady-state simulations, just like a steady-state experiment to measure thermal conductivity.

Figure 5-3 shows an example of a numerical setup used to calculate k_x. Firstly, heat transfer is decoupled from chemical reactions by turning off all reactions to consider a pure heat transfer condition. The two boundaries in the x-direction are set as fixed temperatures T_L and T_R. Boundaries in the other directions are set as adiabatic. In this condition, heat only transfers along the x-direction, following Fourier's law:

$$\int_{S_x} q_x'' ds_x = l_y l_z k_x (T_L - T_R)/l_x \tag{6-4}$$

where l_x, l_y and l_z are the lengths of the box in different directions, and S_x is the surface area along the x-direction. Given an arbitrary temperature difference, T_L-T_R, the total heat flux in the x-direction can be calculated using a steady-state simulation. Then, the effective thermal conductivity in the x-direction k_x can be deducted by Eq. 5-4. Due to the geometric symmetry, k_y equals k_x. k_z can be calculated using the same method, by conducting steady-state simulation to calculate the heat flux with a given arbitrary temperature difference between the bottom and top boundaries, T_B-T_T.

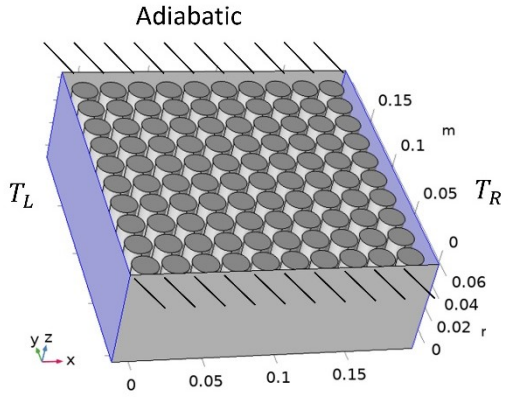

Figure 5-3. Example of the steady-state model used to calculate effective directional thermal conductivity in the x-direction. A pure heat transfer condition is considered. The 2 boundaries in the x-direction are set as fixed temperature T_L and T_R, while the other 4 free boundaries are set to be adiabatic.

The calculated effective directional thermal conductivities of the box are listed in Table 5-1. In this packing condition, k_x is equal to 0.052 W $m^{-1}K^{-1}$, approximately half of the value for k_z. Compared to the thermal conductivity of LIBs, these effective directional thermal conductivities of the whole box are 1 to 2 orders of magnitude lower, agreeing with the result presented in Chapter 4 that the presence of insulating materials could significantly change the heat transfer properties of the LIB storage system. This is because the insulating materials between cells introduce a large heat resistance to the box, while the heat resistance from the battery cells is small and negligible.

Table 5-1

Packing configurations and the effective thermal conductivities of LIB ensembles with different sizes.

No.	Cells arrangement	k_x W m^{-1}K^{-1}	k_y W m^{-1}K^{-1}	k_z W m^{-1}K^{-1}
1	10×10×1	0.052	0.052	0.131
2	20×20×1	0.052	0.052	0.130
3	10×10×2	0.052	0.052	0.130
4	10×10×4	0.052	0.052	0.130
5	20×20×4	0.051	0.051	0.129

5.2.2 Box case validation

Replacing the thermal properties in Eq. 2-3 with these calculated effective thermal properties and coupled with chemical reactions (turning on all reactions), a 3D Ani-Hom model is developed, where the effects of insulations during storage are included. With identical input kinetic parameters, the self-heating ignition behaviour of the equivalent Ani-Hom battery box is simulated and compared with the results by the Iso-Het model for the box with 100 cylindrical cells presented in Chapter 4. The results are shown in Figure 5-4.

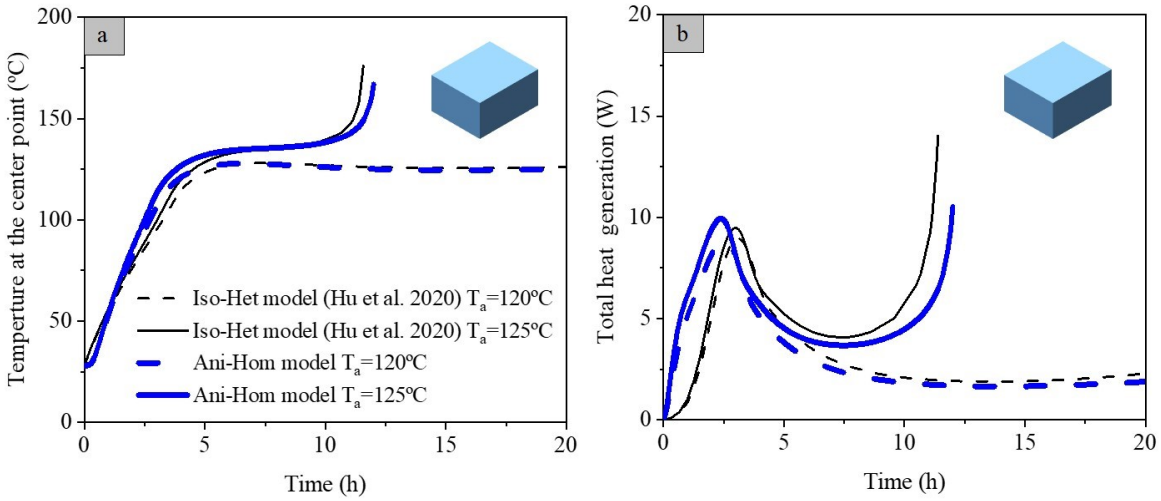

Figure 5-4. The calculated temperature history at the centre point of the box (a) and total heat generation of all reactions (b) though Iso-Het model (black) presented in Chapter 4 and Ani-Hom model (blue) in this study.

The centre point of the box is most vulnerable to self-heating ignition due to geometrical symmetry. As a result, its temperature can be used to quantify the propensity of self-heating ignition. As Figure 5-4 (a) shows, the simplified Ani-Hom model successfully captured the same transition from a subcritical condition (T_a= 120℃) to a supercritical condition (T_a= 125℃) as the Iso-Het model. Also, the Ani-Hom model gives quite good predictions (within 5%) on the temperature history of the centre point against the Iso-Het model. Another important comparison criterion is the total heat generation by the four reactions for the whole box with 100 cells (shown in Figure 5-4 (b)).

Both models predicted the early peaks resulting from SEI decomposition, and the decay for subcritical condition and the exponential growth for the supercritical condition resulting from the positive-electrolyte reaction. Compared to the Iso-Het model, the total heat generation in the Ani-Hom model has almost the same peak value (within 5%) in the early stage (at around 3h). However, the total heat generation given by the anisotropic homogenous model occurs slightly earlier (around 30min) in the early stage and slightly later (around 30min) after thermal runaway. This is because of the difference in geometry between the two models. Compared to the Ani-Hom model, the Iso-Het model shown in Figure 5-2 (a) has a thin layer (5 mm) of insulation attached to the outer covers. Heat is much more difficult to transfer in this insulating layer. In the initial stage, this thin layer delays the heat flux from the environment to the cells, causing a delay of the temperature increase and therefore less heat generation due to chemical reactions. As the temperature of the box increases, the temperature of the cells rises above the external environment and starts to have a net heat release towards the ambient. The box insulation again delays the heat flux toward the external ambient with respect to the no insulation case, causing the total heat generation curve to be ahead of that given by the

anisotropic homogeneous model. This could also explain the slight differences in the temperature given by these two models.

However, the magnitude of total heat generation by these two models is almost the same, which confirms the same self-heating criterion, i.e., the same critical ambient temperature $T_{a,cr}$. While the modified Ani-Hom model predicts almost the same self-heating behaviour, its computational time is less than 10% of that taken by the Iso-Het model. Time efficiency can be even higher for a larger LIB ensemble. This great advantage of Ani-Hom is achieved by these decoupling and recoupling processes when calculating heat transfer and chemical reactions. While the traditional Iso-Het model with refined meshes (5150 elements) needs to solve the energy conservation and the species conservation within every single element, the Ani-Hom separate these two processes and simplifies the heat transfer model and solves the energy conservation on a large scale by considering the special geometric structure of the LIB box. Although these decoupling and coupling processes complicate calculations, they enable the adoption of coarser meshes (845 elements), which greatly reduce the number of elements that need to be calculated, and therefore achieve higher computational efficiency. The comparison of the box case simulations with the two models is to demonstrate that with proposed simplifications, the modified model developed in this study could achieve almost the same numerical prediction of the isotropic heterogeneous model considering complex geometry, but crucially with much lower computational costs and therefore support large-scale predictions.

5.3 Results and discussion

After the box-scale validation, the Ani-Hom model is then applied for upscaling prediction. The key issue is whether these effective parameters from the box-scale simulation could be applied for a much larger LIB ensemble. The chemical kinetics are developed based on fundamental tests on individual components of LIB[91,95,125] and are regarded to be independent of the geometrical size. According to Eq. 5-1 and 5-3 ρ_l and $c_{p,l}$ are constant with a fixed χ and are independent of the size of the LIB ensemble. The effective directional thermal conductivities are calculated by the numerical method and may change with the size of ensembles. To determine the relationship of effective directional thermal conductivities on the size of the system, LIB ensembles in 5 sizes, ranging from 1 box (100 cells) to 16 boxes (1600 cells) are calculated. The detailed diagram of these LIB ensembles packages is shown in Figure 5-5. The effective directional thermal conductivities of all ensembles are also listed in Table 5-1. It is found that k_x, k_y and k_z for all ensembles with different sizes are almost the same, indicating that this basic box is representative of large-scale LIB ensemble scenarios. k_x, k_y and k_z are generally independent of the size of LIB ensembles and could be used for upscaling analysis.

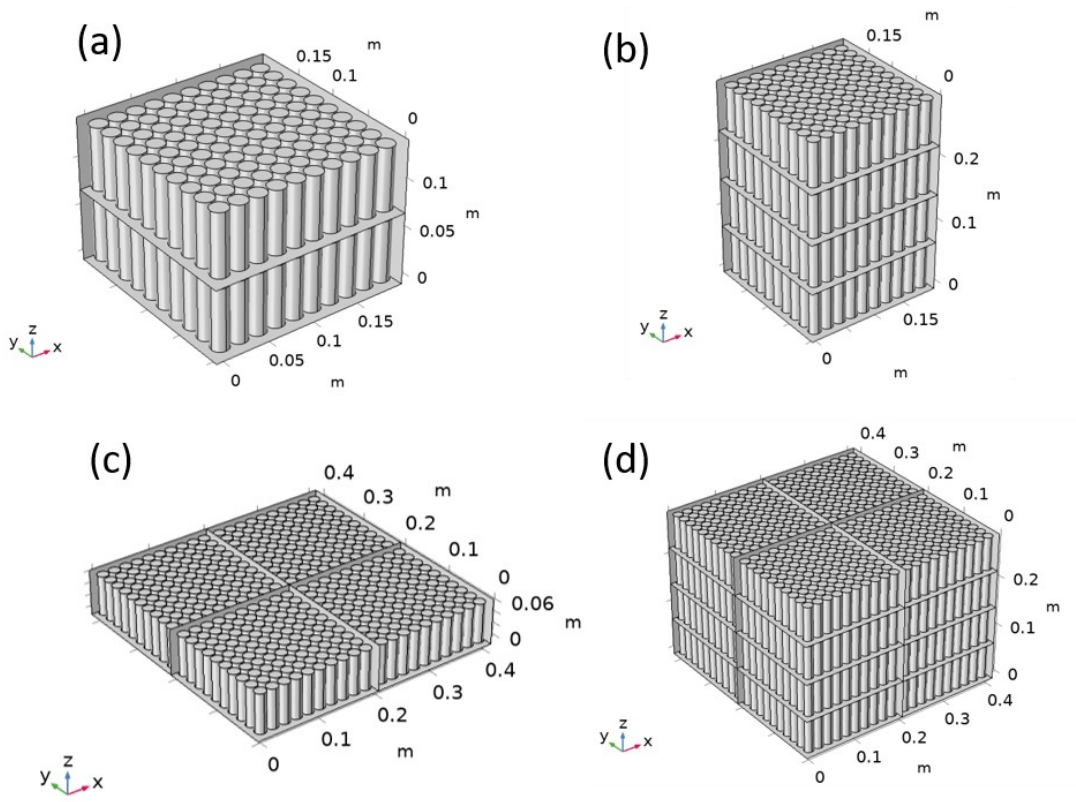

Figure 5-5. The diagram of LIB ensembles used to calculate the relationship between geometric size and directional thermal conductivities. Range from 2 boxes to 16 boxes.

For the predictions of self-heating ignition of LIB ensembles, this study considers four typical storage sizes used in Chapter 3: (1) a single cell, (2) a cardboard box of cells (0.431m × 0.343m × 0.165m), (3) a shelf of boxes (3m × 1.5m × 1.5m), and (4) a rack of shelves (30m × 6m × 3m). Chapter 4 shows that the boxes with different spacing between cells (different χ) have quite different self-heating behaviour. In this chapter, the effects of χ are also investigated. The same χ range are adopted as: 0.046, 0.127, 0.250, 0.510, and 1. The detailed diagrams of different packaging configurations are presented in Figure 4-10. The effective thermophysical properties of these LIB ensembles with different χ are calculated and listed in Table 5-2. With all these parameters, the self-heating ignition behaviour of different LIB storage scenarios with different χ was then simulated and presented in Figure 5-6.

Table 5-2

The effective thermophysical properties of LIB ensembles with different battery volume ratio χ.

χ	ρ_l kg m^{-3}	$c_{p,l}$ J kg^{-1}K^{-1}	k_x W m^{-1}K^{-1}	k_y W m^{-1}K^{-1}	k_z W m^{-1}K^{-1}
1	2580	830	3.4	3.4	3.4
0.510	1316	830	0.052	0.052	0.130
0.250	646	830	0.033	0.033	0.083
0.127	329	831	0.033	0.033	0.080
0.046	120	832	0.026	0.026	0.038

Figure 5-6 also compares the result from the isotropic homogeneous (Iso-Hom) model developed in Chapter 3, the square points. These square points represent the theoretical condition χ=1, where all ensembles are assumed to be fully filled with battery cells. As Figure 5-6 shows, all ensembles with insulations have lower $T_{a,cr}$ compared with the theoretical condition without insulations. This is because, for χ=1, the effective thermal conductivity of the storage system is the same as that of LIB, which is almost two orders of magnitude higher than that for other χ values. Although the mass of reactive materials in this theoretical scenario is much higher, the high thermal conductivity supports a much stronger heat transfer to the environment and thus leads to a higher critical self-ignition temperature.

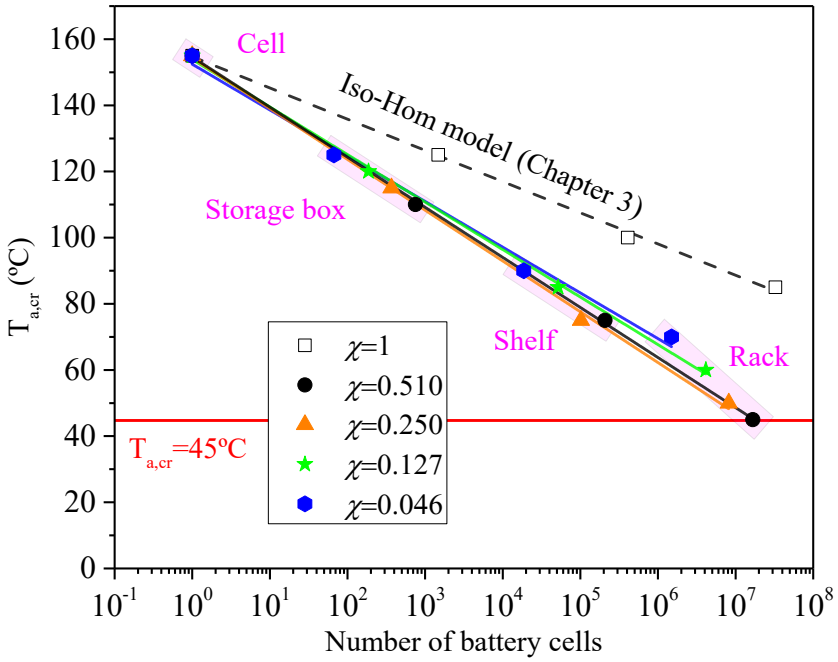

Figure 5-6. The calculated relationship between $T_{a,cr}$ and number of battery cells in LIB ensembles of four typical storage sizes in different packing configurations. The square points are results from the homogeneous model developed in Chapter 3 for the case of pure LIB storage (χ=1). The corresponding straight lines are linear fits of $T_{a,cr}$ verse logarithmic of the number of cells. The purple shaded areas represent different scenarios ranging from a single cell to a rack of cells. The worst calculated condition could self-ignition at $T_{a,cr}$=45 °C.

According to Figure 5-6, in a limited storage space such as the storage box, shelf, and rack scenarios (highlighted in purple), ensembles with higher χ (except χ=1) have lower thermal tolerance and are more prone to self-ignite. This is because, in limited storage space, a system with higher χ has more reactive materials, which means more heat can be generated. In contrast, the heat transfer ability of systems with different χ are quite similar. These coupled factors make the system with higher χ more prone to self-ignite at a given ambient temperature.

The rack-scale LIB ensemble with χ=0.510 (the red circle point in Figure 5-6) is predicted to self-ignite at an ambient temperature of 45°C, which is 40°C lower than the result given by the homogeneous model developed in Chapter 3. This lower critical ambient temperature is even lower than the LIB's normal working temperature range (below 60°C), and seems to be

defying observed phenomena for single cells. However, the normal working temperature for lithium-ion is usually specified for a single cell or a small module. For those small-scale cases, the surface-volume ratio is significantly larger than the large-scale cases, which means much more effective heat transfer and much easier to balance with the environment. These LIBs in small scales have much higher thermal tolerance that needs to be heated up to a much higher temperature to generate adequate heat to overcome the heat dissipation to initiate thermal runaway. However, for a large LIB ensemble, the internal cells are surrounded by other cells, which also generate heat. The heat generated is much more difficult to dissipate that the low-temperature reactions may already be enough to overcome its heat dissipation and initiate thermal runaway. Although the environmental temperature is merely 45℃, the unbalanced heat generation may heat the internal cells up to a much higher temperature after a long time of storage and initiate a fire.

This again confirms that the presence of insulations significantly accelerates self-heating of large LIB ensembles. These results consider the worst condition, which assumes LCO types of LIB (which is relatively easy to ignite) intensively stacked (χ=0.51) in an extremely large size (30×6×3 m) at 100% SOC. Such a condition is not likely for real LIB storage that LIBs are usually stored at 30-50% SOC with large spacing. However, compared to the $T_{a,\,cr}$ for a single cell ($T_{a,cr}$ =155 ℃[11,66]), the rapid drop of $T_{a,cr}$ for the rack scenario indicates that the thermal stability of large LIB ensemble is lower than thought. The potential risks of self-heating ignition for large LIB ensembles are much higher. Furthermore, if there were some battery cells with defects in the ensemble, thermal stability could be lower, thus leading to a lower ambient temperature for self-ignition. Unfortunately, the current safety regulations on LIB storage[27,109] do not consider this phenomenon, the industry for LIB storage sometimes do not provide proper ventilation to save on costs. This might pose a hazard of self-heating ignition.

This study suggests that for large-scale LIB storage, additional cooling or thermally conductive insulations could be used to lower the hazard of fires.

Figure 5-6 also shows that for each χ, $T_{a,cr}$ seems to have a linear relation with the logarithm of N, the number of cells. Therefore, a linear relation is assumed as follows:

$$T_{a,cr} = a + b \log N \tag{6-5}$$

A linear fit is made for each χ, with corresponding parameters listed in Table 5-3. The corresponding fitting curves are also plotted in Figure 5-6. For each χ, R^2 is above 0.99, which proves the linear relation between $T_{a,cr}$ and log$N$. According to these fits, the safety thresholds of LIB storage system with different spacing under three typical storage temperatures, T_a=60°C, 40°C, 25°C, are plotted in Figure 5-7.

Table 5-3

The parameters of linear fits of LIB storage system in different χ

χ	a	b	R^2
1	154.68	-9.435	0.9983
0.510	154.61	-15.142	0.9997
0.250	154.35	-15.353	0.9985
0.127	153.87	-14.370	0.9989
0.046	152.4	-13.827	0.9926

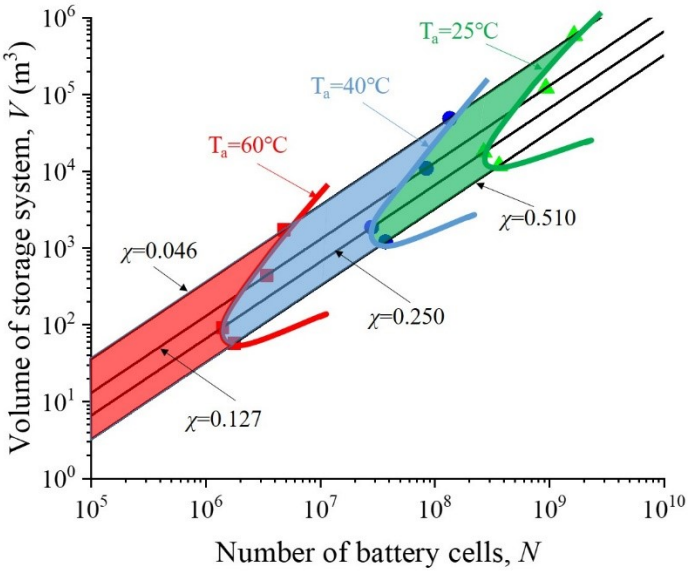

Figure 5-7. Thresholds for safely storing different numbers of LIBs with different spacing under three typical storage temperatures: ambient temperature Ta= 60°C (red), 40°C (blue), and 40°C (green). The black solid lines are LIB ensembles with different spacing, χ ranges from 0.046 to 0.510. The coloured curves are safety thresholds for different storage temperatures. Beneath the curves are corresponding safety zones (shaded in colours), which mean that LIBs stored in that volume and number of cells would not self-ignite when stored at that ambient temperature.

It is crucial for the industry to find a suitable spacing and battery volume ratio, χ, which satisfies the requirement of safety and minimizes storage space to lower the costs. According to Figure 5-7, the battery ensembles which is most prone to self-ignite is predicted to lie in $0.250<\chi<0.510$. For a given number of battery cells, Figure 5-7 helps evaluate whether the storage space is sufficient or not for the safety requirement, or it can be used to optimize safe spacing. For the analysed range of χ ($0.046<\chi<0.510$), storing less than 1 million of 18650 LCO type cells at an environmental temperature lower than 60°C is predicted to be safe from self-heating ignition (20 million cells for T_a<40°C, and 200 million cells for T_a<25°C).

5.4 Conclusions

This chapter put forward an anisotropic homogeneous (Ani-Hom) model to study self-heating ignition of LIBs. The modified Ani-Hom model considers the effects of complex packaging and could achieve predictions for large ensembles. This model is validated by simulating the box scenario against the isotropic heterogeneous (Iso-Het) model developed in Chapter 4, while the computational efficiency of the Ani-Hom model is 10 times higher. Afterwards, this Ani-Hom model is used to analyse the self-heating ignition of LIBs stored in four typical sizes. The model predicts the presence of insulations during LIB packaging could significantly facilitate self-heating ignition because the presence of insulations dramatically reduces heat transfer within the whole storage system. However, the model shows that the smaller spacing between cells, the lower the critical temperature needed to reach self-ignition. For the worst scenario, the rack with the volume ratio of batteries over the whole storage system, χ=0.510, is predicted to self-ignite at an ambient temperature of 45℃, while for a single cell the critical ambient temperature is 155℃. This critical ambient temperature predicted by the proposed Ani-Hom model is 40℃ lower than the prediction by an isotropic homogenous (Iso-Hom), which shows the insulation in battery packaging have significant impacts on self-heating of the battery ensembles. The low critical ambient temperature also indicates that warehouse storage of LIBs could suffer from the potential hazards posed by self-heating ignition, and self-heating ignition could be a possible cause of large-scale LIB storage fires.

Due to the complexity of battery kinetics, the quantitative results are based on a specific type of battery in a specific condition, which is closer but still does not represent the real LIB storage condition. However, the large drop of critical ambient temperature by considering the insulations and spacing indicates that the complex heat transfer due to insulation and spacing

could significantly facilitate self-heating ignition of LIBs. The potential hazard by self-heating ignition of LIBs should be considered during storage and transport and be included in the safety regulations. This work proposes that additional cooling means or thermally conductive packaging should be adopted for large ensembles of LIB during storage to control the hazards.

Chapter 6. Effects of self-discharge on self-heating ignition of Lithium-ion batteries

Summary[4]

Previous self-heating ignition models for LIBs are developed based on four-step reaction kinetics at a temperature above 100°C, while the potential heating from parasitic reactions at lower temperatures has not been discussed. This chapter tries to investigate the potential effects of low-temperature self-discharge processes. Based on experimental data from a calendaring study from the literature, an empirical correlation is developed for the generally self-discharge behaviour of LCO type of LIB. The heat generation by self-discharge is then incorporated with the model developed in Chapter 5 to discuss its potential influence on self-heating ignition of LIB ensembles across scales. The results show that for the single-cell and box scenarios, the predicted critical ambient temperature $T_{a,cr}$ is the same as the previous model, indicating the effects of self-discharge could be neglected for these scenarios. However, a significant drop of $T_{a,cr}$ is predicted for the shelf scenario, where the predicted $T_{a,cr}$ is 20°C, which is 55°C lower than the results by the previous model, showing that self-discharge processes may significantly facilitate self-heating ignition for large LIB ensembles. Afterwards, the effects of different battery volume ratios χ are also analysed, which shows that $T_{a,cr}$ drops with the increase of χ, indicating increasing the gaps between cells could be an effective method to lower the risk of self-heating ignition. This work helps better understand self-heating hazards for LIBs storage and contribute to making related safety strategies for prevention.

---

[4] This chapter is based on "Hu, Z., He, X., Restuccia, F., & Rein, G.. Effects of self-discharge on self-heating ignition of Lithium-ion batteries during storage (to be submitted)."

6.1 Introduction

Fire safety is a major concern for the industries of storage, transport, and recycling of large quantities of LIBs, which have undergone exponential growth in global markets since their first commercialization in the 1990s[126]. Many fire incidents [29,124] have been reported related to large-scale storage of LIBs, however, the understanding of the fundamental mechanisms of the causes of these fires and preventive solutions are limited. As a fundamental cause of fire driven by heat transfer, self-heating ignition is theoretically possible for LIBs, but has barely been studied in the battery community.

As explained in Figure 1-2, simulating the self-heating ignition behaviour of large ensembles of LIBs involves three major challenges: the complexity of chemistry, the complexity of geometry, and the geometric scale. In the previous chapters, three numerical models are developed to investigate and better understand the challenges introduced by large-scale geometry and complex heat transfer. Chapter 3 focuses on large-scale predictions with consideration of four-step reaction kinetics for LIBs, while Chapter 4 aims at analysing the potential effects of complex heat transfer during LIB storage. Chapter 5 then further incorporates both large-scale geometry and complex heat transfer and develops a modified model to better understand self-heating ignition of large LIB ensembles.

However, all three models developed are based on the four-step kinetics developed by experiments through adiabatic calorimetry techniques[38], such as the ARC technique. Unfortunately, none of these techniques could provide a rigorously adiabatic environment and usually have a sensitivity around 0.01-0.1 °C min^{-1}[91,94], which means the exothermic parasitic reactions with a self-heating rate lower than this value could not be observed and therefore are omitted. The heat generated by these parasitic reactions with an extreme low self-

heating rate is very tiny and easy to balance with environmental cool for single-cell or small modules. However, the heat may accumulate when thousands of millions of cells are stacked with a poor heat transfer condition, which is the core concept for self-heating ignition. Therefore, it is crucial to investigate and understand if these parasitic reactions with extreme low self-heating rates could affect self-heating ignition of LIB ensembles.

With the given sensitivity by current adiabatic calorimetry techniques[38], the first observed parasitic reaction reported in the literature was the decomposition of solid electrolyte interphase (SEI) at around 80-100℃[91]. However, there are many other exothermic parasitic reactions under 80℃, which although could not be observed by current thermal techniques, still exist. One such parasitic reaction is the self-discharge processes[127–129] during LIB storage. When a LIB is charged to a certain SOC, which represents a relatively high energy state, it has the potential to naturally discharge at a slow rate under storage conditions, lowering its energy state[130]. Many related studies[131–133] have been conducted to analyse this phenomenon with a general interest to understand and predict the lifespan of LIBs. The spontaneous losses of charge capacity could be divided into a reversible part, which could be restored after recharge, and an irreversible part, which permanently loses the capacity and cannot be restored by recharging[134]. The reversible part has often been attributed to the formation of sub-stable or intermediary substances, which would dissociate during recharge processes[130,134]. The irreversible part has been reported to mainly be caused by SEI formation/growth, which consumes recyclable lithium and causes impedance growth[130,135]. The electrochemical community has more interest in the irreversible part, which is related to the decay of LIB lifespan and is often named the ageing or degradation of the battery. The reversible part receives little attention. The definition of the term self-discharge has not reached a consensus in the literature and has been used to define the overall capacity losses[130],

reversible capacity losses[134], or even the irreversible losses[136]. In this thesis, self-discharge is referred to the overall capacity losses.

While the current thermal technologies are incapable of measuring the energy released by the parasitic reactions with super-low rate, the corresponding electrochemical changes could be measured and provide additional information to deduct the energy release for modelling. In this chapter, an empirical correlation about the energy release of self-discharge processes is developed based on an experiment study from the literature. This relation is then applied to the model developed in Chapter 5 to analyse its potential effects on self-heating ignition of LIB ensembles.

6.2 Modelling of self-discharge

Current studies on self-discharge mainly focus on its effects on LIB electrochemical behaviours, especially the degradation processes, which are vital to understand and predict the lifespan of LIBs. Research on the fundamental mechanisms of reversible capacity losses received less attention. The related energy changes and thermal behaviour with self-discharge have barely been discussed. It is because the current studies on self-discharge usually focus on a single cell, in which case, the low energy released can easily be balanced with the environment and is not even measurable for the current thermal techniques. While the information about the energy released by self-discharge cannot be detected by direct thermal techniques, it can be deduced by observing the related electrochemical changes with much higher sensitivity. For example, the open-circuit voltage (OCV) and capacity generally represent the energy state of a LIB, the energy losses by self-discharge could be deducted by long term observation of its related changes.

According to this methodology, the energy release could be modelled if the mechanisms of the capacity changes during self-discharge are understood. Unfortunately, self-discharge itself is an important and challenging research topic with tremendous studies published to investigate this phenomenon[137–139]. Different types of batteries or even the same type of battery in different sizes with different amounts of content could have different self-discharge behaviour. Even for a given LIB, both reversible and irreversible capacity losses involve multiple reactions and complex mechanisms such as internal electron leakage due to the electrolyte partial electronic conductivity, poor battery sealing, impurities, partial dissolution of electrodes etc[130]. A lot of experimental studies[138,140,141] have found that for a given LIB, its self-discharge performance is highly related to the initial stare of charge (SOC), storage temperature, and storage time. Therefore, most experimental studies on calendar ageing conducted experiments with sets of different SOC and storage temperature under months or years storage to observe the capacity losses, which involved heavy work and were also time-consuming. Furthermore, both reversible capacity loss and irreversible capacity loss are indirect parameters, which need to interrupt the experiments to discharge and recharge to measure these losses for a typical time[134]. Although many empirical, semi-empirical, and theoretical models have been developed, the fundamental mechanisms of self-discharge are still not fully understood.

Focusing on self-heating behaviour, this chapter does not attempt to pursue modelling self-discharge with high accuracy as most related complex electrochemical models developed in the literature. A general model which could predict self-discharge rate with around the same order of magnitude is already acceptable for the self-heating analyses, considering the uncertainty of the heat by the four-step reactions introduced in Section 2.3 might be orders of magnitude higher. Studies[130,142] have shown that the parasitic reactions at the negative

electrode (graphite) are the most important mechanism for self-discharge. Therefore, an empiric correlation between the energy released by self-discharge, storage time, and storage temperature is developed based on the experimental study by Utsunomiya et al. [143], which measured the OCV changes of three types of graphite half-cell at sets of different storage temperature during 52 days of storage. The correlation is applied and validated against 30-day self-discharge experiments from the literature. The energy released by self-discharge is then incorporated into the previous model developed in Chapter 5 to investigate the potential influence on self-heating ignition.

6.2.1 Development of an empiric correlation for self-discharge

In principle, the heat release of self-discharge processes is path-dependent, which is related to processes how charges lose and need to integrate through the whole period. However, considering the special condition for LIB storage that most of the chemical energy finally releases in the form of heat (no external or internal work for storage condition), the heat released by self-discharges could be simplified as a state function, which related to the initial and final states of the LIB. Empirical estimation of the chemical energy stored in a LIB could be given by:

$$\Phi(t) = C(t) \cdot \overline{U} \tag{6-1}$$

$$\Delta Q \approx \Delta\Phi(t) = \Delta C(t) \cdot \overline{U} \tag{6-2}$$

$$\Delta Q = C_0 \cdot \overline{U} \cdot \varphi(t) \tag{6-3}$$

Where Φ is the stored chemical energy that could transfer to output work, $C(t)$ is the capacity of the battery with a unit of Ah, and $\overline{U}$ is the nominal voltage of the battery, which is a constant for a given battery, ΔQ is the heat release and $\varphi(t)$ is the self-discharge ratio, which is the ratio of overall capacity losses to the initial capacity. For the storage condition, the energy

release $\Delta\Phi$ mostly transfers into heat release. In this study, we consider the worst scenario that assumes all the energy release transfers into heat release ($\Delta\Phi$=ΔQ). Therefore, the key issue for calculating the heat release turns into determining the self-discharge ratio, $\varphi(t)$.

Utsunomiya et al. [143] measured the open-circuit voltage (OCV) changes with time at sets of different storage temperatures during 52 days of storage and deducted the overall capacity losses. Figure 6-1 shows their experimental results of hard carbon graphite. They found that the overall capacity losses during the storage increased linearly with the square root of time and had an Arrhenius type of relation with temperature (Figure 6-2). The experiments by Utsunomiya et al. [143] focused on fully charged cells representing 100% SOC. Other studies[140] have found that the initial SOC have higher nonlinear relations with self-discharge. This chapter considers 100% SOC condition coordinating with four-step reaction kinetics developed for 100% SOC in Chapter 2, which represents the worst scenario. Therefore, the empirical correlation of capacity could be given as follows:

$$\varphi(t,T) = (At^{0.5} + B) \cdot \exp(-\frac{E_{SD}}{RT}) \tag{6-4}$$

Where E_{SD} is the activation energy of self-discharge processes. After numerical fitting and optimization, the final form of φ is determined as:

$$\varphi(t,T) = (0.0714t^{0.5} + 16.23) \cdot \exp\left(-\frac{E_{SD}}{RT}\right) \tag{6-5}$$

E_{SD} is determined by the slope of the plot of $1/T$ vs $\ln\varphi$, as Figure 6-2 shows. The value is determined as 16800 J mol^{-1}.

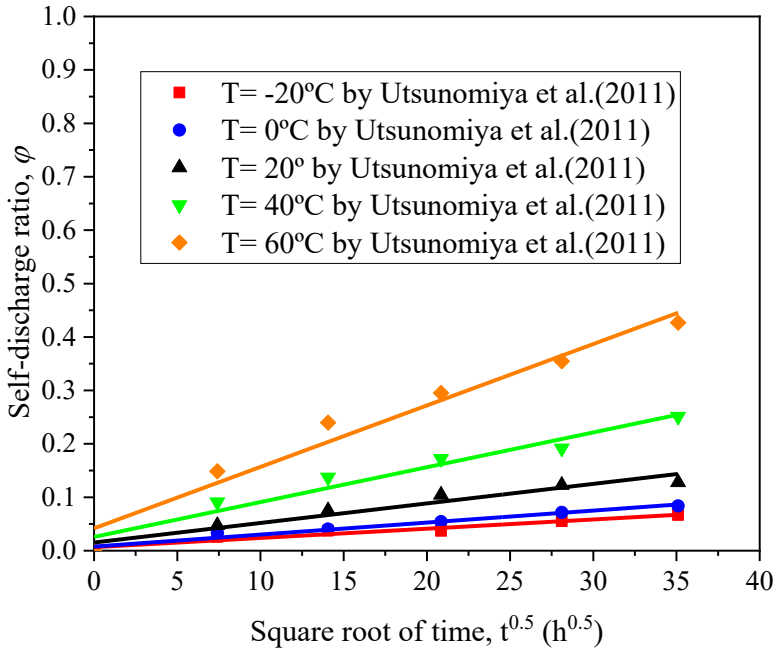

Fig. 1 The self-discharge of fully charged graphite half-cell at different storage temperatures by Utsunomiya et al. [143] plotted with the square root of time and corresponding linear fits.

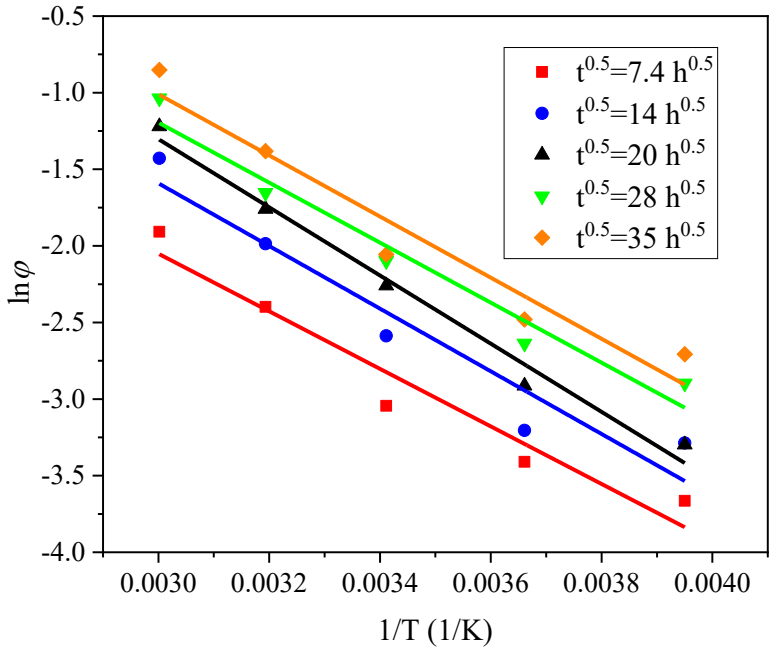

Fig. 2 Arrhenius plots of self-discharge of fully charged graphite half-cell at the different testing time by Utsunomiya et al. [143]

6.2.2 Validation

With all parameters determined, the predictions given by the developed empirical correlation are plotted to compare against the experimental data by Utsunomiya et al. [143], as shown in Figure 6-3. It shows that the function developed has quite good predictions (the absolute errors for all data points are less than 0.06, and the relative errors are less than 10%) for all experimental data points across 52 days and a temperature range from -20℃ to 60℃. Although this correlation is developed merely based on graphite half-cell experiments, it also has a quite good prediction for the self-discharge of a whole cell. Byun et al.[144] tested the self-discharge of LCO pouch cell in 100% SOC at 25℃ after 30 days of storage, and reported reversible (8.84%), irreversible (5.59%) and overall loss (14.43%, the star point in Figure 6-3). The correlation is then used to predict the self-discharge at 25℃ (the purple curve in Figure 6-3) and give the prediction of self-discharge of 14.94% for 30 days storage, with a relative error of 3.5%. This shows that the function developed could be used to predict self-discharge of LCO type of cells, at least in the same order of magnitude. The heat generation by self-discharge could be given by:

$$Q_{SD}(t)/V_{cell} = \int q'''_{SD}(t)\, dt \tag{6-6}$$

$$q'''_{SD}(t) = \frac{C_0 \cdot \overline{U}}{V_{cell}} \cdot \frac{d\varphi(t)}{dt} \tag{6-7}$$

Where V_{cell} is the volume of the single cell, and q'''_{SD} is the corresponding heat source term by self-discharge. The heat generation by self-discharge transfers into a heat source, which depends on the derivative of self-discharge ratio dφ/dt. This chapter assumes the self-discharge ratio of the LCO type of battery introduced in Section 2.3 follows the correlation given by Eq. 6-5. The self-discharge ratio φ is a function for both time and temperature. Considering self-

discharge is a slow process with slow heat generation. For a small period, δt, the temperature could be treated as unchanged. Therefore, q'''_{SD} could be simplified as:

$$q'''_{SD}(t) = \frac{C_0 \cdot \bar{U}}{V_{cell}} \cdot (0.0714 \times 0.5) \cdot t^{-0.5} \cdot \exp\left(-\frac{E_{SD}}{RT}\right) \quad (6\text{-}8)$$

In this function form, *t* should not start at 0s, which could lead to infinite $q'''_{SD}(t)$. Therefore, a small initial t=100s is selected as the initial state, and the final form of $q'''_{SD}(t)$ is:

$$q'''_{SD}(t) = \frac{C_0 \cdot \bar{U}}{V_{cell}} \cdot (0.0714 \times 0.5) \cdot (t + 100)^{-0.5} \cdot \exp\left(-\frac{E_{SD}}{RT}\right) \quad (6\text{-}9)$$

The corresponding parameters for the LCO analysed are listed in Table 2-2. The heat source by self-discharge is for all kinds of side reactions at low temperature (below 80℃), which already contains the heat generation by the four-step reactions explained in Section 2.3 at low temperature. However, when the temperature goes higher (around 100℃), the heat generation transfers into a four-step reactions scheme. To distinguish the heat by four-step reactions with the heat by self-discharge, we use subscript D to identify the overall decomposition heat by the four-step reactions:

$$q'''_D = q'''_{\mathrm{sei}} + q'''_{\mathrm{n}} + q'''_{\mathrm{p}} + q'''_{\mathrm{e}} \quad (6\text{-}10)$$

The final overall heat source is the larger one of q'''_D and q'''_{SD}:

$$q'''_{tot}(t) = \max\left(q'''_D(t), q'''_{SD}(t)\right) \quad (6\text{-}11)$$

To be noted, the four-step kinetics, as well as empirical correction for self-discharge, are all based on experiments on 100%SOC, which represents the worst scenarios. In principle, the chemical kinetics of LIBs are very complicated, depending on the state of batteries, such as SOC, state of health (SOH), the internal materials etc. The detailed kinetics are still not fully understood even with thousands of studies published every year. It is impossible to incorporate all possible complex chemical kinetics for a large LIB storage system, where the computational

costs are unaffordable. This thesis focuses more on the effects of heat transfer. Here, the batteries with 100%SOC are considered as a worst-case scenario to demonstrate a threshold. Researchers could adapt updated kinetics into the models this thesis provides to analyse the specific different battery types of interest and obtain more accurate predictions.

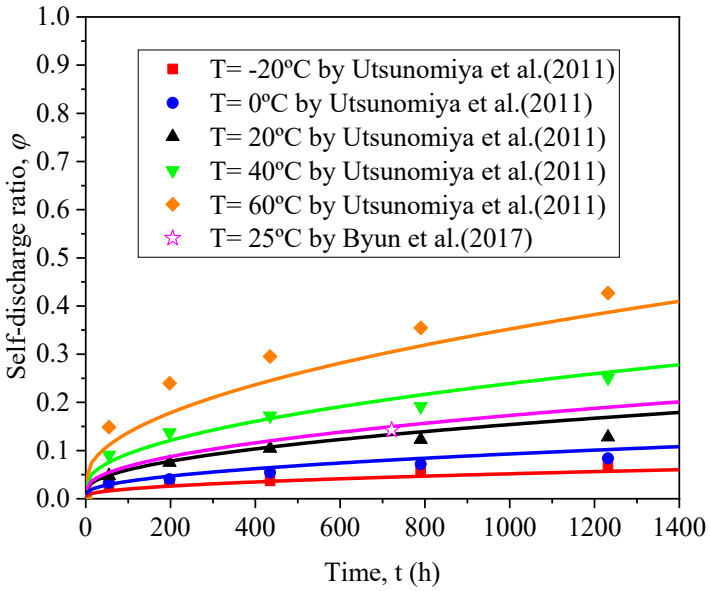

Figure 6-3 The comparison of predictions by the developed self-discharge function against experiments by Utsunomiya et al. [143] for 52 days of storage at the temperature range from -20°C to 60°C. The purple start point is the self-discharge of the LCO pouch cell at 25°C for 30 days storage, and the purple line is the corresponding prediction by the developed self-discharge function.

6.3 Results and discussion

The modified total heat source term in Eq. 6-11 is then applied to the previous self-heating model developed in Chapter 5 to investigate if self-discharge processes could affect self-heating ignition of LIB ensembles. The packaging style and spacing pattern are considered the same as introduced in Chapter 4 and Chapter 5, with battery volume ratio χ=0.51 representing the worst scenarios. Results are shown in Figure 6-4 to Figure 6-6.

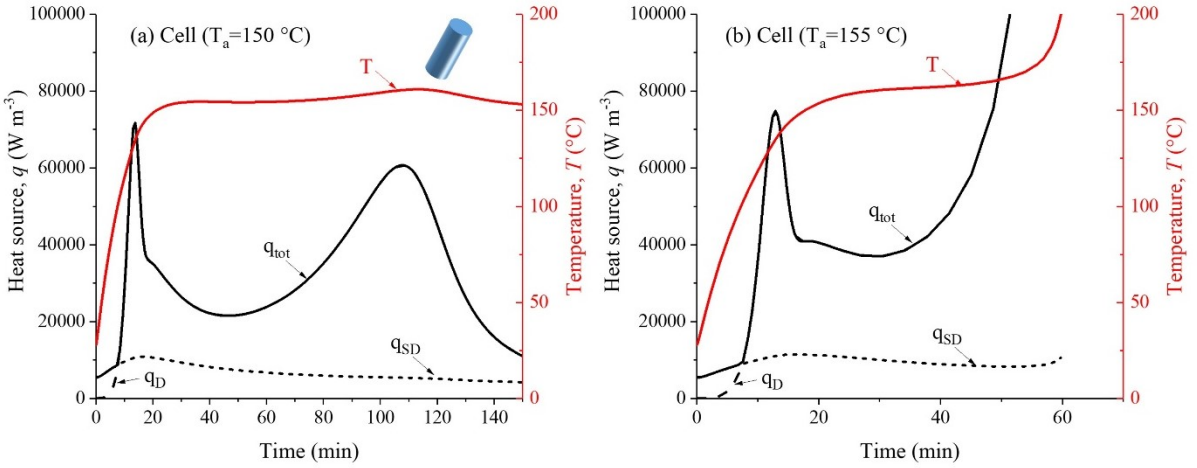

Figure 6-4. The predicted profiles of heat source terms and temperature of the single-cell scenario introduced in Chapter 5 at (a) subcritical condition (T_a=150°C) and (b) supercritical condition (T_a=155°C). Heat sources resulting from four-step decomposition reactions q_D, self-discharge processes q_{SD}, and overall total heat generation q_{tot} are presented by curves in black. The red curve is the temperature of the central point of the cell.

Figure 6-4 is the results for the single-cell case. The modified model considering self-discharge processes predict thermal runaway occurs at $T_{a,cr}$=155°C, which is the same as the results presented in Chapter 5. According to the profiles of the different heat source terms, the total heat generation is dominated by four-step decomposition reactions ($q'''_{tot} = q'''_D$) for the most of period for both subcritical and supercritical conditions, except the initial stage (t<10 min), where heating from self-discharge processes is higher ($q'''_{tot} = q'''_{SD}$). The heating from self-discharge processes has negligible effects on the self-heating ignition behaviour of the single-cell scenario. This is because the heat dissipation condition for the single-cell scenario is much higher, which requires higher ambient temperature ($T_{a,cr}$=155°C) with higher heat generation to trigger thermal runaway. At this critical ambient temperature, the dominating reactions are the reactions at high temperature, where the heat generation by self-discharge q'''_{SD} is orders of magnitude lower than the decomposition heat by four-step reactions. Therefore, the effects of self-discharge for the single-cell scenario are negligible.

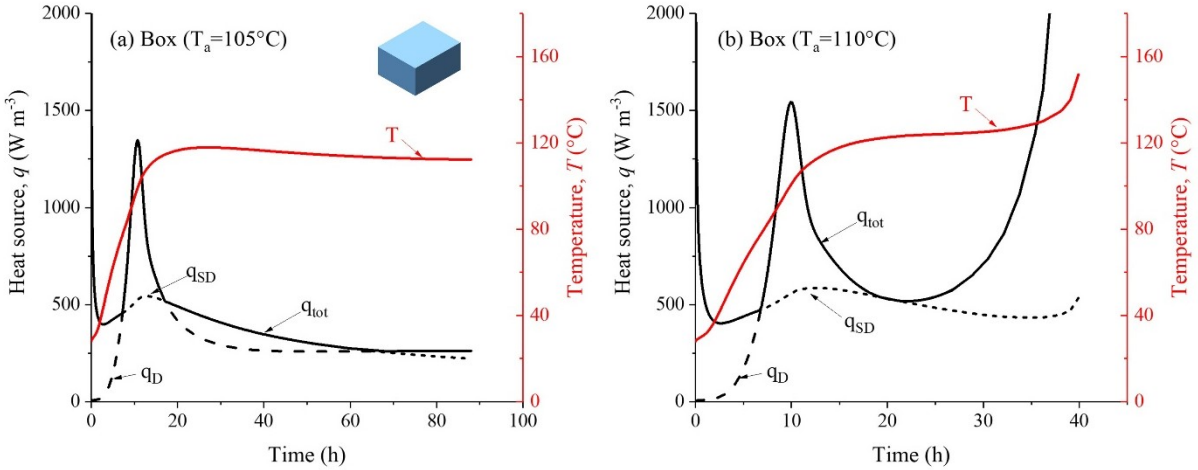

Figure 6-5. The predicted profiles of heat source terms and temperature of the box scenario introduced in Chapter 5 at (a) subcritical condition (T_a=105°C) and (b) supercritical condition (T_a=110°C). Heat sources resulting from four-step decomposition reactions q_D, self-discharge processes q_{SD}, and overall total heat generation q_{tot} are presented by curves in black. The red curve is the temperature of the central point of the box.

The results for the box scenario (Figure 6-5) are similar, that the modified model considering self-discharge processes still predicts the same critical ambient temperature ($T_{a,cr}$=110°C) as the results by the model developed in Chapter 5. However, notable changes take place for the heat source terms. q'''_{SD} dominates q'''_{tot} in the initial stage (t<10 h) where the initial cell temperature is low (T_0=28°C), but is quickly exceeded by q'''_D when the temperature rises. An early peak is formed at 10<t<20 h resulting from the SEI decomposition. With the depletion of meta-stable SEI components, q'''_{SD} once again takes over q'''_{tot} for the subcritical condition with plateaued temperature, while q'''_D is still in charge of q'''_{tot} for the supercritical condition, where the temperature keeps increasing and triggers positive electrolyte reaction resulting in thermal runaway. From the heat source curves at subcritical conditions, q'''_{SD} is around the same order of magnitude of q'''_D, which means the heating by self-discharge processes start to affect the self-heating ignition behaviour of the box scenario.

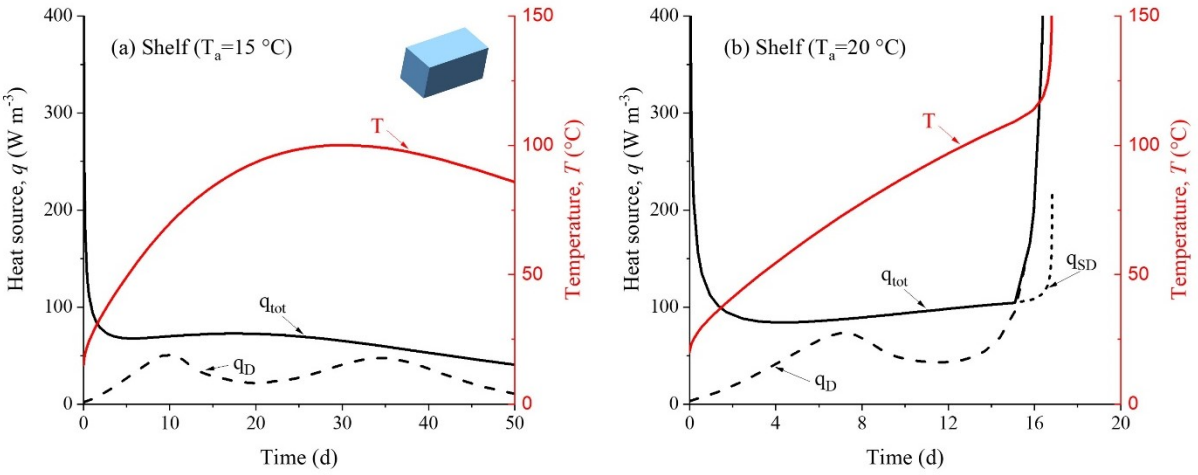

Figure 6-6. The predicted profiles of heat source terms and temperature of the shelf scenario introduced in Chapter 5 at (a) subcritical condition (T_a=15°C) and (b) supercritical condition (T_a=20°C). Heat sources resulting from four-step decomposition reactions q_D, self-discharge processes q_{SD}, and overall total heat generation q_{tot} are presented by curves in black. The red curve is the temperature of the central point of the shelf.

Significant changes are predicted for the shelf scenario, as shown in Figure 6-6. $T_{a,cr}$ of the shelf scenario is predicted to be 20°C, which is 55°C lower than the results by the model in Chapter 5. According to the profiles of heat source terms, q'''_{SD} dominates q'''_{tot} for the entire period for the subcritical condition, while q'''_D takes over only at the supercritical condition when thermal runaway is initiated. These results indicate that self-discharge processes could have crucial impacts on self-heating ignition of large LIB ensembles and self-discharge processes are the dominating reactions for self-heating ignition of LIBs at a low-temperature range. Again, these quantitative results consider the worst scenario, where the battery is LCO type, which is relatively easy to ignite, and assume all battery cells are stored in 100% SOC with high battery volume ratio (χ=0.51) and small spacing gaps and assume no extra ventilation methods during storage that heat dissipates only through natural convection and radiation. The initial SOC representing the energy state of LIBs and has been reported[145–147] significantly affect the self-discharge processes that the self-discharge ratio of LIBs with lower SOC could

be orders of magnitude lower than the fully charged cells[134]. In the industry, LIBs are usually required to discharge to 30-50% SOC for storage or transport with a much lower fuel load and could be separated with a much larger spacing[108]. Additionally, the correlation developed for the heat generation by self-discharge is a general empirical correlation, which may cause large uncertainty at low temperatures. Therefore, the $T_{a,cr}$ for the real LIB storage, should be much higher than the predications. However, the quantitative comparisons conducted in this chapter by considering heat from discharge reveal a possibility that there might be other dominating reactions for self-heating ignition of LIBs at the low-temperature range, and potential hazards from self-heating ignition might be worse than thought.

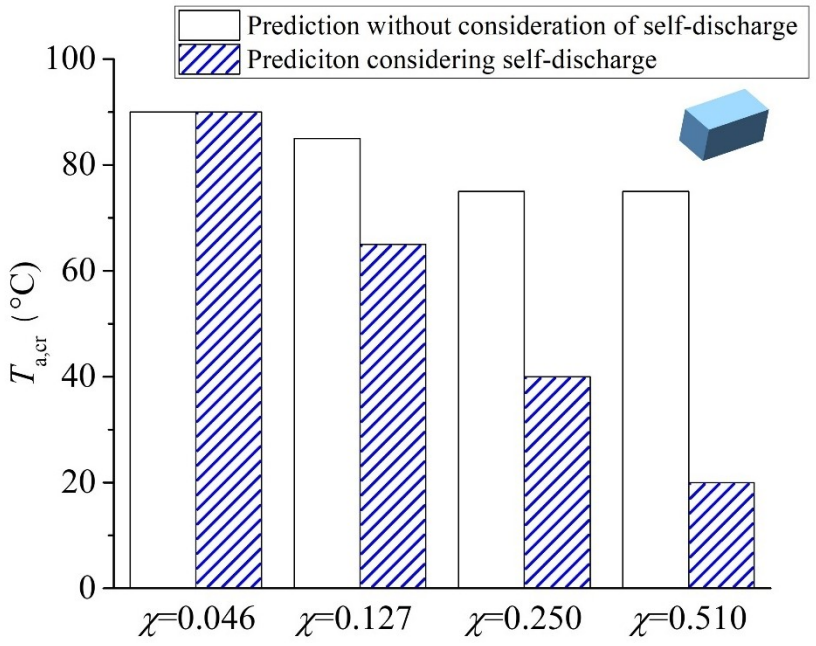

Figure 6-7. The predicted $T_{a,cr}$ for the shelf scenarios with different battery volume ratios χ. The blank bars are results based on the anisotropic model developed in Chapter 5, while the shaded bars are results based on the anisotropic model with further consideration of heating from self-discharge processes.

While significant changes are predicted for the shelf scenario, another important factor, the battery volume ratio, χ, which indicate the distance of gaps between adjacent cells is also analysed in this scenario. Results are shown in Figure 6-7. The previous model developed in

Chapter 5 is used as a baseline, which considers the effects of complex insulations during LIB storage and is capable of large-scale predictions. However, the chemical kinetics considered are four-step kinetics, which focuses on temperature ranges between 80-200℃. The modified model developed in this chapter further considers the possible reactions at lower temperature range, the self-discharge processes at a temperature below 80℃.

The modified model predicts that $T_{a,cr}$ drops with the increase of χ due to the increased energy density and fuel loads. For the worst case, χ=0.510, the difference of the predicted $T_{a,cr}$ due to self-discharge reaches 55℃, while for the case with large spacing (χ=0.046), the predicted $T_{a,cr}$ is the same, which means negligible effects by self-discharge. These results show that the modified model with consideration of self-discharge is more sensitive to the insulations. for a large LIB ensemble (above the shelf scale), increasing the gaps between cells could be an effective method to lower the risk of self-heating ignition.

6.4 Conclusions

Based on the self-heating model developed in Chapter 5, this chapter considers the heating by self-discharge processes at low temperatures to investigate if it could affect the self-heating ignition behaviour of LIB ensembles. An empirical correlation is developed to describe generally self-discharge development with different storage times and storage temperature based on experiments in the literature. The corresponding heat generation by self-discharge is then deducted and applied to the model developed in Chapter 5 to incorporate its effects. The results show that self-discharge processes have negligible effects on self-heating ignition of LIB ensembles in small sizes (single cell and box scenarios), while they are predicted to be dominating reactions for the shelf scenario with a larger size. The self-discharge processes are

predicted to significantly facilitate self-heating ignition for the shelf scenario, where the critical ambient temperature, $T_{a,cr}$, triggering self-heating ignition is predicted to be 20℃, which is 55℃ lower than the results by the model in Chapter 5. Afterwards, the effects of different battery volume ratios χ are also analysed, which shows that $T_{a,cr}$ drops with the increase of χ, indicating increasing the gaps between cells could be an effective method to lower the risk of self-heating ignition.

The quantitative results conducted in this chapter consider the worst condition, with a specific type of LIB in a specific condition, which overestimates the real LIB storage condition. However, the comparisons reveal a possibility that there might be other dominating reactions for self-heating ignition of LIBs at the low-temperature range, and potential hazards from self-heating ignition might be worse than thought.

Chapter 7. Benchmarking between COMSOL and Gpyro models in predicting self-heating ignition of Lithium-ion batteries

Summary[5]

Self-heating ignition of LIBs usually involves a large number of battery cells and is mainly studied using numerical methods. Different numerical simulation tools with different capabilities may have significant differences in predicting the self-heating ignition behaviour of LIBs. This chapter presents a benchmarking analysis between COMSOL Multiphysics, which is one of the prevailing tools used in modelling LIBs, and Gpyro, which is widely used for modelling self-heating ignition of carbon-rich solids. Four cases studies are conducted to analyse their respective numerical performance in predicting: (1) kinetics at the microscale (pure chemical reactions), (2) heat transfer at the mesoscale (pure heat transfer), (3) overall self-heating behaviour at the mesoscale (coupled chemical reactions and heat transfer) for a single cell and (4) a four-cell ensemble. The results of case studies 3 and 4 are compared with the oven experiments for a single prismatic LCO cell and a four-cell ensemble. The results show that although COMSOL and Gpyro have large differences in their numerical discretization methods, modelling of chemical dynamic and heat transfer, both tools can accurately predict the transition from the subcritical to supercritical conditions, which validates their capability in predicting the self-heating ignition of LIBs.

[5] This chapter is based on "Hu, Z., He, X., Restuccia, F., & Rein, G.. Benchmarking between COMSOL and Gpyro models in predicting self-heating ignition of Lithium-ion batteries (to be submitted)."

7.1 Introduction

In the previous chapters, several numerical models have been developed to analyse challenges for self-heating ignition of LIBs introduced by geometry size, the complex heat transfer, and the complex chemistry, respectively. These numerical models are all developed based on the commercial simulation software COMSOL Multiphysics, which is a popular simulation tool used in modelling LIBs. The introduction of COMSOL and related self-heating models is presented in Chapter 2. While COMSOL has been prevailing in simulating multi-disciplinary problems, there are also other numerical tools with a special focus on ignition and heat transfer and could be used for self-heating modelling. An example of such a tool is Gpyro, a powerful open-source tool designed for pyrolysis modelling of combustible solids based on the Finite Difference Method (FDM). The embedded coding covers mechanisms of mass transfer, heat transfer, and chemistry in both gas and condensed phases, and has been validated against many self-heating ignition studies[79,82,148]. Focusing on self-heating ignition of LIBs, the two numerical tools may have different computational performances since they are prevailing in a different area and may have different capabilities in simulating chemical dynamics, heat and mass transfer, and multi-discipline coupling. It could be interesting to benchmark COMSOL and Gpyro for the predictions of self-heating ignition of LIBs, and analyse their pros and cons.

This Chapter conducts a benchmark study to analyse the numerical modelling by both COMSOL and Gpyro in self-heating ignition of LIBs. The self-heating ignition model for LIBs by Gpyro was developed by my colleague Xuanze He [29,79,80], and I adapted his existing model for the simulations in this chapter. Several case studies are conducted with different levels of complexity, including (1) kinetics at the microscale (pure chemical reactions), (2) heat

transfer at the mesoscale (pure heat transfer), (3) overall self-heating behaviour at the mesoscale (coupled chemical reactions and heat transfer) against our oven experiments for a single cell and (4) a four-cell ensemble.

7.2 Theoretical framework

While COMSOL has been prevailing in modelling LIBs, Gpyro has widely been used to model the self-heating ignition problems of carbon-rich materials. Some adaptions and adjustments need to be made for both tools to successfully simulate self-heating ignition of LIBs. This section introduces the basic setup for both COMSOL and Gpyro with specific consideration of self-heating ignition of LIBs.

7.2.1 Numerical set up for COMOSL

The detailed development of self-heating ignition model using COMSOL is presented in Section 2.3 of this thesis and will not be discussed in detail here. This section summarizes the governing equations, boundary conditions, chemical kinetics, and basic simplification adopted by considering the special characteristics during self-heating ignition of LIBs for comparison with Gpyro.

Self-heating ignition focuses on the transition from a stable state to the onset of thermal runaway, with a special focus on early-stage reactions at a temperature below 200°C. The thermophysical properties: ρ, c_p, k, are assumed to be constant in this temperature range. While studies have shown that a lump thermal model[11] already provides adequate accuracy for the temperature prediction for the single-cell compared to a 3D model[66], a battery cell could be simplified as all reactants are homogeneously distributed inside the cell. The governing equation could be simplified as:

$$\rho c_p \frac{\partial T}{\partial t} = k\nabla^2 T + q'''_{\text{tot}} \tag{2-3}$$

COMSOL supports simulations on complex geometries with 0D, 1D, 1D axisymmetric, 2D, 2D axisymmetric, and 3D modelling. It also contains various types of interfaces for boundary conditions. For self-heating ignition analysis, the most used thermal boundaries include: temperature, heat flux, and thermal insulation. In regards to the chemical models used, COMSOL has a powerful module with sets of well-developed interfaces to simulate multi-step reactions, the interaction between reactions, and species transport. The chemical reactions considered in this chapter include four major reactions: Solid electrolyte interphase decomposition (SEI decomposition), negative-electrolyte reaction, positive-electrolyte reaction, and electrolyte decomposition. These four reactions are the sources considered for internal heat generation. There might be other dominating reactions at low temperatures as shown earlier in this thesis, in Chapter 6. However, the benchmark in this chapter compares against experiments for a single cell and a four-cell ensemble at a temperature around 150 ℃, for which the low-temperature reactions have negligible effects and could therefore be neglected. The heat generated by the four reactions is given by:

$$q'''_{\text{tot}} = q'''_{\text{sei}} + q'''_{\text{n}} + q'''_{\text{p}} + q'''_{\text{e}} \tag{2-6}$$

One of the most appealing features of COMSOL Multiphysics is its flexibility. While the software provides basic interfaces for most of the physical problems, it also has easy ways for users to make their own definitions and self-coding, even changing the governing equations. This allows users to adjust and develop specific models for the specific problems being studied. However, this requires the user to have a good understanding of the problem interested. Lots of definitions and self-coding might be involved during the set-up stage of simulations.

7.2.2 Numerical set up for Gpyro

Gpyro is a powerful open-source tool designed for pyrolysis modelling for combustible solids. The governing equations of the original model of Gpyro include the conservation equations[78,79] for: Eq. (2-3) mass, Eq. (2-4) species, Eq. (2-5) energy in condensed phase and, Eq. (2-6) mass, Eq. (2-7) species, and Eq. (2-8) momentum (Darcy's law) in the gas phase as follows:

$$\frac{\partial \bar{\rho}}{\partial t} = -\dot{\omega}_{fg}''' \tag{7-1}$$

$$\frac{\partial (\bar{\rho} Y_i)}{\partial t} = \dot{\omega}_{fi}''' - \dot{\omega}_{di}''' \tag{7-2}$$

$$\frac{\partial (\bar{\rho}\bar{h})}{\partial t} = k\frac{\partial}{\partial z}\left(\frac{\partial T}{\partial z}\right) + \dot{\omega}_{di}'''(-\Delta H_i) - h_{vl}(T - T_\infty) \tag{7-3}$$

$$\frac{\partial}{\partial t}\left(\rho_g \bar{\phi}\right) + \frac{\partial \dot{m}''}{\partial z} = \dot{\omega}_{fg}''' \tag{7-4}$$

$$\frac{\partial}{\partial t}\left(\rho_g \bar{\phi} Y_j\right) + \frac{\partial}{\partial z}\left(\dot{m}'' Y_j\right) = -\frac{\partial}{\partial z}\left(\rho_g \bar{\phi} D \frac{\partial Y_j}{\partial z}\right) + \dot{\omega}_{fj}''' - \dot{\omega}_{dj}''' \tag{7-5}$$

$$\dot{m}'' = -\frac{\kappa}{v}\frac{\partial p}{\partial z} \tag{7-6}$$

Where $\dot{\omega}'''$ is the volumetric reaction rate, Y is the mass fraction, $\bar{h}$ is the specific enthalpy, h_{vl} is the lumped volumetric heat transfer coefficient, D is the mass diffusivity, ϕ is the porosity, κ is the permeability, v is the viscosity. The subscript f represents formation reactions, d represents destruction reactions, g represents gases.

The original equations in Gpyro consider a 1-D problem, and therefore are not capable of simulating heat transfer with a complex 3D geometry. However, for some simple shapes, the 3D heat transfer could be considered by incorporating the heat transfer from the other

dimensions into a source term in the governing equation. For example, Eq. (7-3). h_{vl} [80,149] is the volumetric heat transfer coefficient considering the heat transfer from x and y directions.

With special consideration of self-heating ignition of LIBs and the assumptions explained in Section 7.2.1, the governing equations could also be simplified to Eq. (7-3), the energy conservation for the condensed phase. Gpyro also has various interfaces to set typical thermal boundaries such as temperature, heat flux, and thermal insulation.

The reactions scheme considered in Gpyro is similar to the classical self-heating theories which assume an effective overall Arrhenius type of reaction. Despite chemical reactions being naturally complex and usually containing multi reactions, the problem usually can be simplified with a focus on the dominating one for a specific temperature window. Such simplification can greatly facilitate fast assessments and is robust and easy to validate and analyse for engineering applications. For LIBs, the one-step effective reaction considered is:

$$1\ LIB \longrightarrow v\ Residue + (1 - v)\ Off\text{-}Gases \tag{7-7}$$

$$\dot{\omega}_d''' = \bar{\rho} A e^{-E/RT} Y_i^{n_c} \tag{7-8}$$

The most attractive feature of Gypro is that it is developed specifically for pyrolysis modelling for combustible solids, therefore already embedding many interfaces with consideration of most of the possible complex situations that are encountered in pyrolysis modelling. Users can easily set up the parameters and simplify the problem based on the module provided. The limitation is that if the problem analysed exceeds the range of the module provided, it is not easy for users to make their own definitions, as it requires extensive coding to change these parameters in the source code.

7.2.3 Set up for benchmarking

Considering the differences between COMSOL and Gpyro, this chapter conducts four case studies to compare and analyse the numerical performances for (1) kinetics at the microscale (pure chemical reactions), (2) heat transfer at the mesoscale (pure heat transfer), (3) self-heating ignition of a single cell, and (4) a four-cell ensemble. Case (1) and case (2) consider a theoretical condition while case (3) and case (4) are compared against the oven experiments for Sanyo LCO prismatic cells [36,79,80]. The dimensions of these cells are 34 mm×10 mm×50 mm, with a nominal capacity and voltage of 1.88 Ah and 3.7 V, respectively. The thermophysical properties of this type of battery are listed in Table 7-1.

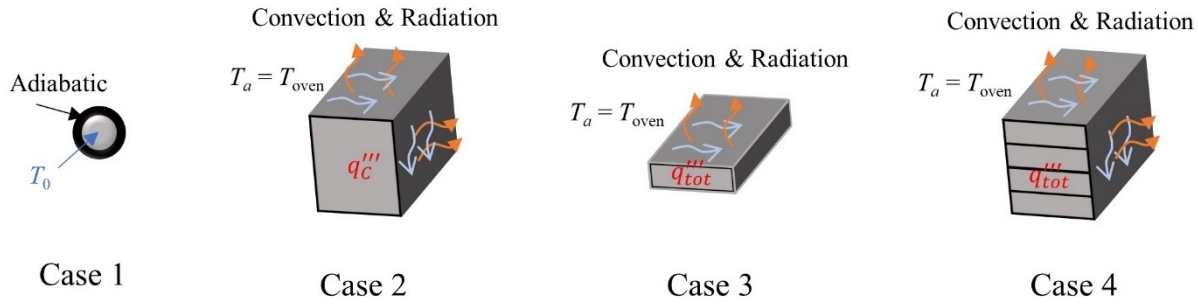

Figure 7-1. Diagram of 4 cases of benchmarking between COMSOL and Gpyro. Case 1 benchmarks the chemical kinetics by considering self-heating of 1 g of the LIB with an initial temperature of T_0 placed in an adiabatic condition, Case 2 considers the heat transfer between the bulk of solid sample with a constant internal heat source q_c''' and ambient at T_a. Case 3 and case 4 benchmark the oven experiments of one single cell and a four-cell ensemble, respectively.

Table 7-1

Heat transfer and kinetic parameters used in Gpyro simulations and simulations by COMSOL with the one-step reaction model for Sanyo LCO prismatic cells at 100% SOC. [80]

Parameters	Description	value	unit
A	Frequency factor	1.42E23	s^{-1}
E	Activation energy	3.25E5	J mol^{-1}
ΔH	Heat of reaction	8.87E5	J kg^{-1}

k	Thermal conductivity	1.08	W $m^{-1}K^{-1}$
ρ	Density	2164.7	Kg m^{-3}
c_p	Heat capacity	990.0	J $kg^{-1}K^{-1}$
ε	Emissivity	0.8	-
h_c	Surface convective heat transfer coefficient	11	W $m^{-2}K^{-1}$
h_v	Volumetric heat transfer coefficient	902.3	W $m^{-3}K^{-1}$

In case 1, an adiabatic condition is considered for a small battery (such as a coin cell) with a mass of 1 g at an initial temperature of T_0. In this condition, the heat generated by internal chemical reactions can be fully used to heat the battery sample up. Therefore, the temperature information is directly related to the chemical kinetics, and can be used to benchmark chemical kinetics, as shown in Eq. (7-9):

$$\rho c_p \frac{dT}{dt} = \dot{\omega}_d'''(-\Delta H) \tag{7-9}$$

With such a small size of the battery sample, the internal temperature gradient can be ignored, and the battery sample can be assumed to be a lumped system, which eliminates the effects of heat transfer and purely focuses on chemistry. While Gpyro considers a one-step global reaction, COMSOL also supports multi-step reactions as presented in Section 2.3. Therefore, both the one-step global reaction scheme (same as Gpyro) and four-step reaction scheme (presented in Section 2.3) are simulated to benchmark with Gpyro. One issue for the four-step reaction scheme is that the kinetic parameters are based on an old generation of E-One/Moli Energy ICR18650 (18 mm diameter, 65 mm length) 1.65 Ah LCO/graphite cells at 100% SOC by the work conducted by Hatchard et al. [34] in 2001. The battery techniques in terms of energy density and material safety have improved dramatically since then, and the parameters may no longer suit the current LCO batteries. Also, it is difficult for the industry to

obtain all the detailed kinetic parameters for a specific battery of interest, as it will require fundamental experimental analysis of every separate component making up the battery.

In this chapter, an energy proportional ratio, β, is used to consider the effects resulting from the different energy densities between batteries. The heat generated by the four-step reactions is assumed to proportionally change with the stored chemical energy (which is roughly proportional to the capacity). Eq. (2-6) is then modified as:

$$q'''_{\mathrm{tot}} = (q'''_{\mathrm{sei}} + q'''_{\mathrm{n}} + q'''_{\mathrm{p}} + q'''_{\mathrm{e}}) \cdot \beta \tag{7-10}$$

$$\beta = \frac{C}{C_{\mathrm{ref}}} \tag{7-11}$$

Where, C is the capacity of the targeted battery and, C_{ref} is the capacity of the reference battery, which is 1.65 Ah. This work tries to investigate if the assumed function could give a reasonable prediction of the self-heating ignition behaviour of the battery.

Case 2 considers a heat transfer scenario. A constant heat source is used in this case to eliminate the complex chemical reactions. The geometry considered in this case is the dimensions of the four-cell ensemble in the oven experiment, which is 34 mm×40 mm× 50 mm. Gpyro solves equations in one dimension, and adopts a volumetric heat transfer coefficient, h_{vl} [80,149] to consider the heat transfer from the other two dimensions. COMSOL supports simulations on a complex 3D geometry. Therefore, both 1D and 3D simulations are conducted for COMSOL to benchmark with Gpyro. The boundary conditions consider both convective and radiative heat transfer with the ambient.

Case 3 and case 4 simulate the oven experiments on a single cell and a four-cell ensemble, respectively. The two cases consider the coupling effects of both chemistry and heat transfer when predicting self-heating ignition of the batteries. Both a one-step reaction scheme and a four-step reaction scheme are simulated by COMSOL and compared with the results of Gpyro

and the oven experiments. Convective and radiative heat transfer with the surroundings are considered for the boundaries.

7.3 Results and discussion

7.3.1 Microscale chemistry

Figure 7-2 shows the benchmarking results for case 1 considering microscale chemistry. The heat transfer and chemical kinetic parameters for Gpyro are listed in Table 7-1. The one-step reaction model considered in COMSOL uses the same parameters as Gpyro for comparison. The parameters for the four-step reaction model considered in COMSOL is the same as the parameters listed in Table 2-2, except for the thermophysical properties, ρ, c_p, k, which uses the values listed in Table 7-1. The energy proportional ratio, β, considers two values: β =1, which represents the same chemical kinetics for the battery with 1.65 Ah [11] presented in Chapter 3, and β =1.14, which is adapted to the battery with 1.88 Ah [79,80]. Two initial temperatures are considered: T_0=130℃, and T_0= 140℃.

As Figure 7-2 shows, the predictions by the one-step model of COMSOL and Gpyro agree well for both initial temperatures. At T_0=130℃, a small increase of temperature (within 2.5℃) after 200 min in the adiabatic condition is predicted for both the one-step model of COMSOL and Gpyro. The internal reactions are limited, with low heat generation at this initial temperature. However, for a rigorous adiabatic condition, the heat will accumulate inside, and the temperature will always run away giving enough storage time. For T_0=140℃, both models predict the exponential increase of temperature after 75 min, while the temperature predicted by COMSOL one-step model is a little bit (within 3 min) ahead of that by Gpyro. Those small differences may result from the different numerical methods (FEM for COMSOL and FDM

for Gpyro) and different criteria for numerical convergence by the two tools. Overall, COMSOL and Gpyro agree well with the one-step modelling of chemical dynamics.

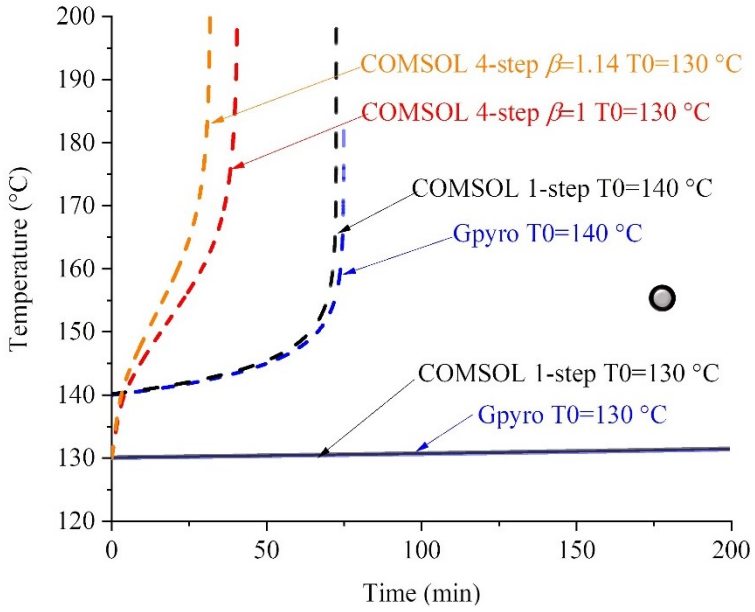

Figure 7-2. The predictions of temperature development for case 1 by Gpyro, COMSOL one-step model, and COMSOL four-step model, considering two initial temperatures T_0=130°C and 140°C. The results for Gpyro and COMSOL one-step model are presented with curves in black and blue, respectively. The COMSOL four-step model considers two energy densities, with β=1(the curve in red) and β=1. 14 (the curve in yellow).

However, the four-step model by COMSOL considering two β values predicts a fast temperature increase at T_0=130°C. For β=1, which represents the same kinetic parameters as Table 2-2, the temperature is predicted to grow exponentially at t= 37 min, which is even earlier than the result from the one-step models at T_0=140°C. The temperature for β=1.14, which is modified by considering the variation of energy density, are predicted to grow faster, around 10 min ahead of that for β=1. These fast temperature increases by the four-step model are because of the SEI decomposition reaction, which is predicted to take place at around 100°C and generate a certain amount of heat. The heat generated by the SEI decomposition reaction

will raise the temperature fast in the adiabatic condition and initiate other reactions, resulting in a rapid temperature increase in a short period.

7.3.2 Mesoscale heat transfer

Figure 7-3 is the benchmarking results for case 2, which considers the heat transfer in a mesoscale. The COMSOL 1-D model uses the same governing equations and boundary conditions as Gpyro. A 3-D heat transfer is also considered for COMSOL. A constant heat source ($q_c''' = 10000$ W m^{-3}) is assumed for the solid bulk to eliminate chemical dynamics. Convective and radiative heat transfer is considered for the solid bulk and the ambient at T_a=140℃. The thermophysical properties and heat transfer coefficients are the same as Table 7-1.

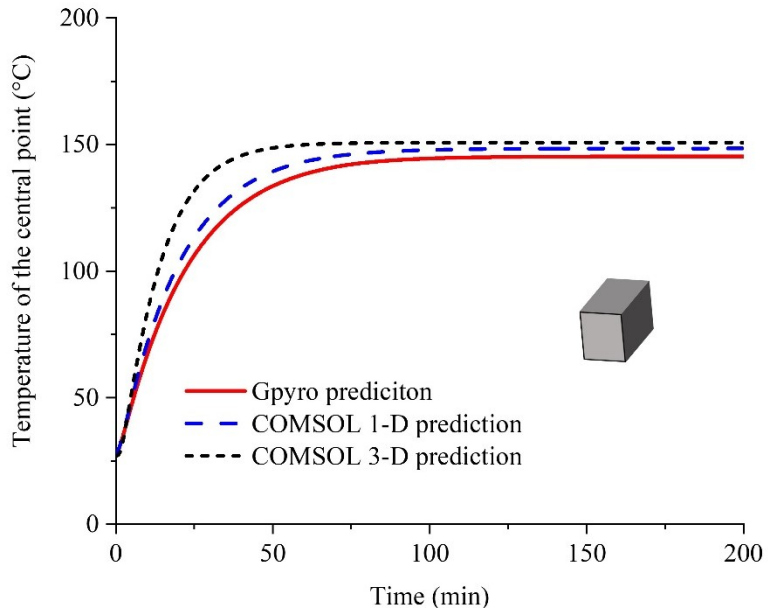

Figure 7-3. The predictions of temperature development for case 2 by Gpyro, COMSOL 1-D model, and COMSOL 3-D model. The results of the three models are presented by curves in red, blue, and black, respectively.

As Figure 7-3 shows, all three curves stabilize at around 150℃. The temperature prediction by the COMSOL 1-D model has the same trend as the results by Gpyro, but is a

little bit (around 3℃) higher. The 3-D model by COMSOL gives a higher prediction of temperature in the first 50 min. This difference may result from the consideration of 3D heat transfer. Gpyro and the COMSOL 1-D model use a volumetric heat transfer coefficient h_{vl} as a source term to consider the heat transfer from other dimensions. This treatment assumes the same temperature distribution for each cross-section perpendicular to the dimension analysed. While the COMSOL 3-D model directly solves equations in 3 dimensions, which can consider the temperature gradience in the cross-sections. Overall, the final equilibrium temperatures by all three models are in agreement, which shows the same capability of modelling mesoscale heat transfer for COMSOL and Gpyro.

7.3.3 Single-cell comparison

Figure 7-4 and Figure 7-5 are the benchmarking results for case 3, which are compared against the oven experiments on a single prismatic LCO cell. The COMSOL one-step model uses the same governing equations, boundary condition, kinetic and heat transfer parameters as the model developed by Gpyro. The COMSOL four-step model uses the parameters based on the model developed in Chapter 3 and considers two energy proportional ratios β =1 and 1.14 for 3D heat transfer. The corresponding kinetic parameters for the four reactions are the same as Table 2-2, while the heat transfer parameters are the same as Table 7-1.

Figure 7-4 presents the numerical results by the COMSOL one-step model and Gpyro against the oven experiment for one single cell. Different ambient temperatures are simulated until the transition to thermal runaway is predicted. The oven experiment showed that the temperature of the single-cell stabilized at T_{sub} =147 ℃ (subcritical condition) and undertook thermal runaway at T_{sup}=149 ℃ (supercritical condition). Gpyro predicts the same subcritical and supercritical conditions as the experiment, while the COMSOL one-step predicts T_{sub}=146 ℃

for the subcritical condition and T_{sup}=147°C for the supercritical condition. The temperature profiles for the subcritical condition by the two models agree well with the experiment, with an error below 3°C. While for the supercritical condition, both models underestimate the time needed for the cell to develop into thermal runaway. Using temperature equals 200°C as a criterion, it took around 150 min for the experiment to reach that temperature, while Gpyro predicts around 50 min and the COMSOL one-step model predicts around 40 mins at T_a= 149°C and 100 min at T_a= 147°C. These results show that the reactivity of the one-step global reaction might be a little higher than the reactivity a battery experiences under these conditions. However, both models have a good prediction of the transition from the subcritical condition to the supercritical condition, which is the key parameter to assess self-heating ignition. Therefore, both COMSOL and Gpyro are capable of predicting self-heating ignition of LIBs with the one-step global reaction assumption.

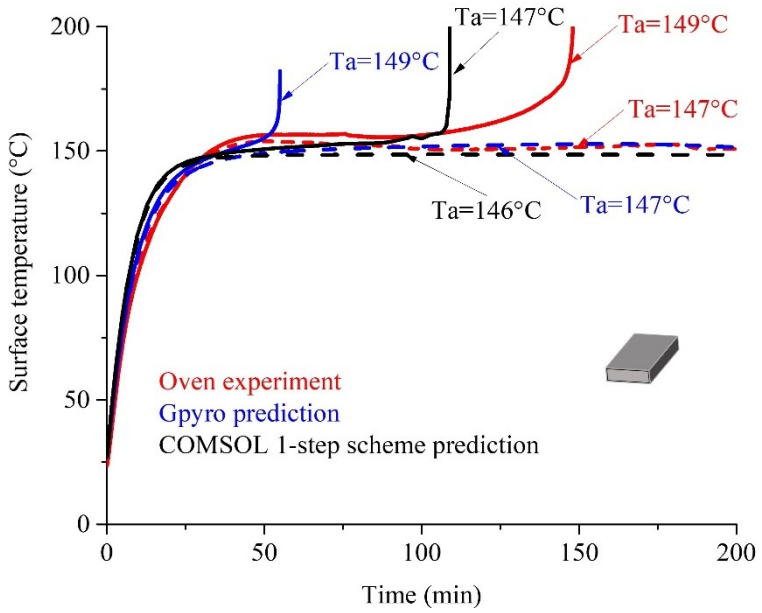

Figure 7-4. The benchmarking results for the COMSOL one-step model and Gpyro against the oven experiments for a single prismatic LCO cell for both subcritical condition (dashed curves) and supercritical condition (solid curves). The results for the experiments, Gpyro, and the COMSOL one-step reaction are presented by curves in red, blue, and black, respectively.

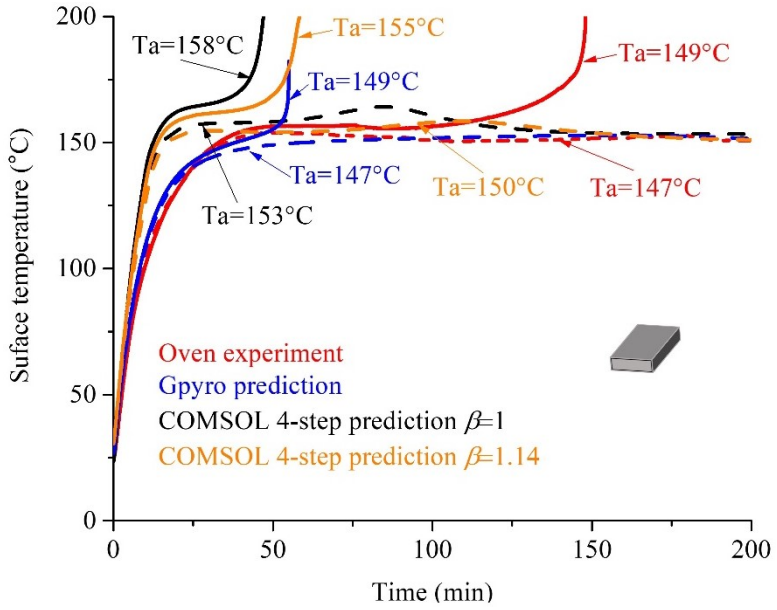

Figure 7-5. The benchmarking results for the COMSOL four-step model against results by the oven experiments and Gpyro for a single prismatic LCO cell for both subcritical condition (dashed curves) and supercritical condition (solid curves). The results for the experiments, Gpyro, and the COMSOL four-step reaction with β= 1 and 1.14 are presented by curves in red, blue, black, and yellow, respectively.

Figure 7-5 shows the numerical results by the COMSOL four-step model to compare with the results by the experiments and Gpyro. Since the kinetic parameters used in the COMSOL four-step model are mainly from the work by Hatchard et al [11] for a different battery cell, the predictions are different. For β= 1, which represents exactly the same kinetic parameters as Table 2-2, the battery cell is predicted to stabilize at T_{sub}= 153 ℃ and thermal runaway at T_{sup}= 158 ℃. While for β= 1.14, which adjusts the heat generation by considering the energy difference between the cylindrical cell in Chapter 3 and prismatic cell in this work, the predicted subcritical and supercritical conditions are T_{sub}= 150 ℃ and T_{sup}=155℃, respectively. As explained in Section 7.3.2, the 3D heat transfer predicts a faster temperature increase for the first 30 min, and the early-stage reactions such as SEI decomposition explained in Section 7.3.1 further accelerate this temperature increase rate. These results indicate that the prismatic

cell analysed in this chapter may have a large difference in early-stage reactions compared with the cylindrical cell analysed in Chapter 3. This may also result from the improvement of the safety of LIB techniques.

7.3.4 Four-cell comparison

Figure 7-6 and Figure 7-7 are the benchmarking results for case 4, which compare against the oven experiments on a four-cell ensemble. The numerical set-up and parameters for the COMSOL one-step model, four-step model, and Gpyro are the same as introduced in Section 7.3.3, except the geometry considered is a four-cell ensemble. This case with a larger size is supposed to demonstrate the effects of heat transfer.

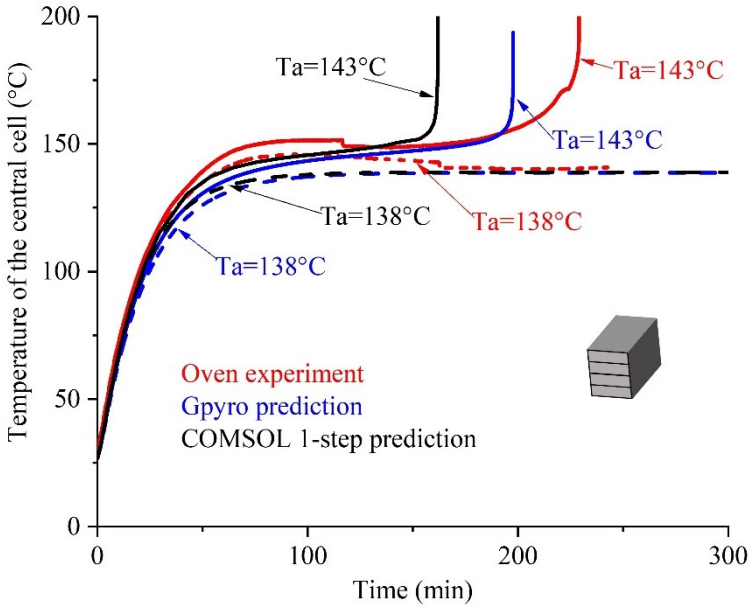

Figure 7-4. The benchmarking results for the COMSOL one-step model and Gpyro against the oven experiments for a four-cell LCO ensemble for both subcritical condition (dashed curves) and supercritical condition (solid curves). The results for the experiments, Gpyro, and the COMSOL one-step reaction are presented by curves in red, blue, and black, respectively.

As Figure 7-6 shows, both COMSOL one-step model and Gpyro predict the same subcritical (T_{sub}=143°C) and supercritical (T_{sup}=138°C) conditions as the results obtained by

the oven experiment. Again, the temperature profiles predicted by both COMSOL one-step model and Gpyro agree well for both subcritical and supercritical conditions, except the temperature predicted by COMSOL grows a little bit faster than Gpyro for the supercritical condition. The temperature measured in the experiment grows faster than the prediction by the two models in the initial 100 min for both subcritical and supercritical conditions, which may result from the variation of geometry and heat transfer. Nevertheless, the accurate predictions on the transition from the subcritical to the supercritical condition demonstrate that both COMSOL and Gpyro are capable to predict self-heating ignition of LIBs with a one-step global reaction.

The COMSOL four-step model still predicts a higher temperature for both subcritical (T_{sub}=145°C for β=1, and T_{sub}=142°C for β=1.14) and supercritical (T_{sup}=150°C for β=1, and T_{sup}=147°C for β=1.14) conditions, as shown in Figure 7-7. The temperature at the initial stage is still overestimated (maximum 25°C) compared to the experiments.

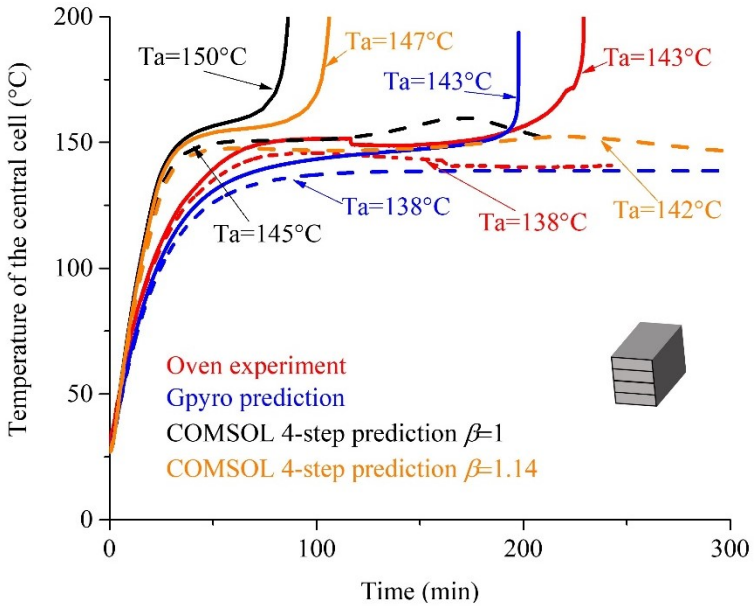

Figure 7-7. The benchmarking results for the COMSOL four-step model against results by the oven experiments and Gpyro for a single prismatic LCO cell for both subcritical condition (dashed curves) and supercritical condition (solid curves). The results for the experiments, Gpyro, and the COMSOL

four-step reaction with β= 1 and 1.14 are presented by curves in red, blue, black, and yellow, respectively.

Table 7-2

The subcritical and supercritical conditions found by the oven experiments and numerical modelling by Gpyro, COMSOL one-step model, COMSOL four-step model with β=1 and 1.14 for the single-cell and the four-cell ensemble.

Type of model	Case 3- single cell comparison			Case 4- four-cell comparison		
	T_{sub} (°C)	T_{sup} (°C)	$T_{a,cr}$ (°C)	T_{sub} (°C)	T_{sup} (°C)	$T_{a,cr}$ (°C)
Oven experiments	147	149	148	138	143	140.5
Gpyro	147	148	148	138	143	140.5
COMSOL one-step	146	147	146.5	138	143	140.5
COMSOL four-step β=1	153	158	155.5	145	150	147.5
COMSOL four-step β=1.14	150	155	152.5	142	147	144.5

Table 7-2 lists experimental results and predictions of the subcritical, supercritical, and calculated critical conditions for case 3 and case 4 by the different models discussed. Overall, Gpyro and the COMSOL one-step model have almost the same prediction as to the experimental results for both single cell and the four-cell ensemble. The critical ambient temperature to trigger self-heating ignition, $T_{a,cr}$, predicted by the COMSOL four-step model is around 7°C (β=1) to 4°C (β=1.14) higher than the experimental results for both single cell and the four-cell ensemble. This difference is acceptable considering the large differences in geometry, size, and improved techniques between the old generation of cylindrical cells presented in Chapter 3 and the prismatic cell in this chapter. Moreover, the decline of $T_{a,cr}$ for the single cell to the four-cell ensemble is accurately predicted for all models, that the experiments showed a 7.5°C of drop and numerical models predict a 6-8°C decline. These results demonstrate that both COMSOL and Gpyro with effective one-step reaction schemes and four-step reaction schemes are capable of predicting the self-heating ignition of LIBs.

7.4 Conclusions

This chapter presents a benchmarking analysis for COMSOL Multiphysics and Gpyro in predicting self-heating ignition of lithium-ion batteries. Four cases with different levels of complexity are analysed considering (1) kinetics at the microscale (pure chemical reactions), (2) heat transfer at mesoscale (pure heat transfer), (3) overall self-heating behaviour at mesoscale (coupled chemical reactions and heat transfer) for a single cell and (4) a four-cell ensemble. For the kinetics at the microscale, the COMSOL one-step model predicts almost the same results as Gpyro, while the COMSOL four-step model predicts a faster temperature increase at the initial stage due to the early-stage reactions. For the heat transfer at mesoscale, the 3-D heat transfer model by COMSOL predicts a faster temperature increase at the initial stage, compared to the results by the 1-D model by Gpyro and COMSOL, which agrees well. For the overall prediction of the self-heating behaviour of LIB at mesoscale, both COMSOL and Gpyro give good predictions of the transition from a subcritical to a supercritical condition, which are also validated against the oven experiments for a single cell and a four-cell ensemble.

Although COMSOL and Gpyro have large differences in their numerical discretization methods, modelling of chemical dynamic and heat transfer, both tools could accurately predict the critical ambient temperature trigger thermal runaway, which is essential for predicting self-heating ignition of LIBs.

Chapter 8. Conclusions

Fire safety for the storage and transport of large-scale LIBs is a major concern to the storage and transport industries with many such fire incidents having been reported in the past two decades, which often resulted in severe damage to property and the environment. However, the understanding of the causes of these types of fires is limited. The research community focusing on battery research has, in the literature, assumed the cause of these fires to short-circuit and has therefore put an emphasis on studying the chemistry of the LIB, in the pursuit of a safer material that would reduce risk. The potential fire hazards resulting from heat transfer have seldomly been discussed for large-scale LIB storage. In this thesis, I explore and investigate the possibility of a cause of fires for LIBs driven by heat transfer, self-heating ignition, which is a fundamental cause of fire when reactants are massively stacked (e.g. around 10 m thick of carbon-rich soil for example[48]).

Three major challenges for the studies of self-heating ignition of LIBs are identified through the review of the literature in Chapter 1, as shown in the diagram in Figure 8-1. The worst cases for self-heating ignition takes place at large scales (storing LIBs at a warehouse-scale), which are difficult to investigate through direct experiments, therefore, is mainly studied by numerical modelling. Modelling real warehouse storage of LIBs involves high complexity of chemistry, geometry, and large sizes, while the state-of-the-art models for LIBs usually focus on one aspect, the chemistry, with little attention to the remaining two. Chapter 2 introduces the theoretical foundations of self-heating ignition and a classical self-heating theory. A general numerical self-heating model is developed using the commercial simulation software COMSOL Multiphysics. A typical LCO type of battery with four-step reaction kinetics from the literature is chosen as an example to analyse the fundamental mechanisms of self-heating

ignition of LIBs. The model developed in Chapter 2 is then modified step by step in Chapter 3 to Chapter 6 to deal with the three major challenges: large geometry size (Chapter 3), complex geometry (Chapter 4), complex geometry in large size (Chapter 5), and potential reactions at low temperature (Chapter 6), as shown in Figure 8-1. The development of these 4 models follows the order of my understanding of this research area, with the increasing complexity of the models from Chapter 3 to Chapter 6. A benchmarking study is conducted in Chapter 7 to compare the different simulation performances by COMSOL and Gpyro for self-heating ignition of LIBs. Chapters 3-7 are the key research contents of the thesis, and their main outcomes are summarized in this section.

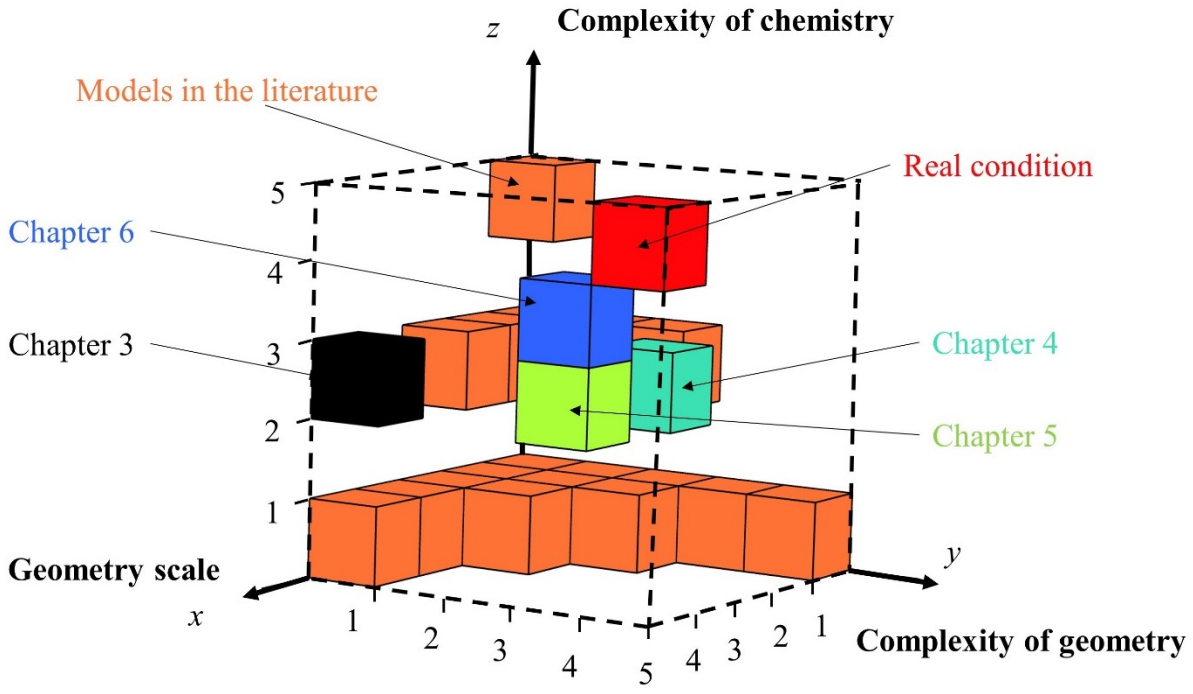

Figure 8-1. The 3-D diagram demonstrates three main challenges involved in modelling the thermal behaviour of large-scale LIB systems (complexity of chemistry, complexity of geometry, and geometry scale) and the state of current models in the literature and models developed in this thesis. Each challenge is divided into five levels according to complexity. The red cube represents the state of real condition for warehouse storage of LIBs. The cubes in orange are the models in the literature, while the black, green, yellow, and blue cubes are models developed in this thesis.

A 3D isotropic and homogeneous (Iso-Hom) model is developed in Chapter 3 to analyse the self-heating behaviour of LIB ensembles in different sizes, from a single cell to a rack with around 2 million cells. Three critical parameters: the critical ambient temperature, $T_{a,cr}$, and onset cell temperature, T_{on}, and onset time, t_{on}, are put forward to analyse the self-heating ignition behaviour of LIBs. The results show that both the critical ambient temperature, $T_{a,cr}$, and onset cell temperature, T_{on}, decrease significantly with the increase of the size of battery ensembles, $T_{a,cr}$ drops from 155 ℃ for a single cell to 85 ℃ for a rack of cells. The model also predicts that the presence of insulations during LIB storage could further decrease the temperature threshold for self-heating ignition ($T_{a,cr}$=60 ℃), and the dominating mechanism of the self-heating ignition of LIBs changes with the size of LIB ensembles. These results are the inspiration of the following studies conducted in Chapters 4-6 to investigate the effects of complex heat transfer during LIB storage and low-temperature reactions.

A 3D isotropic and heterogeneous (Iso-Het) model is developed in Chapter 4 to investigate the effects of complex heat transfer introduced by the packaging and insulation during LIB storage. A case study is conducted for a box with 100 LCO type cylindrical cells in storage. The model predicts that the presence of packaging materials could accelerate self-heating ignition, while the type of materials used for insulation has a negligible influence on the self-heating ignition of the box as long as thermal conductivities of the insulation are the same order of magnitude as that of air. It is predicted that the box with the battery volume ratio χ around 0.51 has the highest tendency to self-ignite. The insulations in the LIB package was found to have crucial impacts on the self-heating behaviour of the LIB storage system should not be omitted for large-scale prediction.

To incorporate the effects of packaging and insulation for large-scale predictions, an anisotropic and homogeneous (Ani-Hom) model is developed in Chapter 5. By transferring the

complex geometry into a modified physics, the Ani-Hom significantly cut down the numerical costs, and its computational efficiency is 10 times higher compared to the Iso-Het model for the box simulation in Chapter 4. The upscaling results by the Ani-Hom model show that the presence of insulations significantly facilitates self-heating ignition for large LIB ensembles. The worst scenario (the rack with χ=0.510) is predicted to self-ignite at an ambient temperature of 45℃, which is 40℃ lower than the prediction by the Iso-Hom model in Chapter 3.

The models developed in Chapters 3-5 are all based on four-step reaction kinetics at around 100℃-200℃. The exothermic reactions at a lower temperature, such as self-discharge might also affect the self-heating ignition behaviour of large LIB ensembles. In Chapter 6, an empirical correlation for self-discharge is developed based on experimental data of a calendaring ageing study from the literature. The potential heat generation by self-discharge is deducted and incorporated in the Ani-Hom model developed in Chapter 5. The results show that self-discharge processes have negligible effects on self-heating ignition of LIB ensembles in small sizes (single cell and box scenarios). However, the heat from self-discharge is predicted to be dominating for the shelf scenario, which significantly facilitates self-heating ignition. The critical ambient temperature of the shelf is predicted to be 20℃, which is 55℃ lower than the results by the model in Chapter 5. The model also predicts that increasing the gaps between cells could be an effective method to lower the risk of self-heating ignition. To simplify the problem, Chapter 6 used an empirical correlation, which might have large uncertainty. It could be beneficial to develop a more fundamental model with higher accuracy in the future to analyse its impacts, which may offer a more general solution for self-heating ignition of LIBs in different types.

A benchmark study is conducted in Chapter 7 to compare the differences of numerical performance by COMSOL Multiphysics and Gpyro for simulating the self-heating ignition of

LIBs. Four cases with different levels of complexity are analysed considering (1) kinetics at the microscale, (2) heat transfer at mesoscale, (3) overall self-heating behaviour at mesoscale for a single cell and (4) a four-cell ensemble. Although COMSOL and Gpyro have large differences in their numerical discretization methods, modelling of chemical dynamic and heat transfer, the results show that both tools could accurately predict the transition from a subcritical to a supercritical condition for the single-cell and the four-cell ensemble against the oven experiment. Therefore, both tools are capable of modelling self-heating ignition of LIBs.

Overall, the numerical models developed in this thesis demonstrate that self-heating ignition can be a potential cause of fires when LIBs are stacked on large scales. The critical ambient temperature for an intensively stacked LIB ensemble could drop to a value close to normal ambient temperature. The potential hazard by self-heating ignition of LIBs should be considered during storage and transport and be included in the safety regulations. Due to the complexity of chemistry and limited experimental data in the literature, the quantitative results predicted in the thesis are based on a specific type of LIB in a specific condition, which may overestimate the real LIB storage condition. However, the methodologies, parameter assessment, and simplification methods developed in this thesis should be able to be applied to other types of LIBs in other conditions. I hope my work can help the battery and fire safety community to better understand the self-heating ignition behaviour of LIBs and prompt an open thread for related research.

References

[1] Q. Wang, P. Ping, X. Zhao, G. Chu, J. Sun, C. Chen, Thermal runaway caused fire and explosion of lithium ion battery, J. Power Sources. 208 (2012) 210–224. https://doi.org/10.1016/j.jpowsour.2012.02.038.

[2] S. Sharma, A.K. Panwar, M.M. Tripathi, Storage technologies for electric vehicles, J. Traffic Transp. Eng. (English Ed. (2020). https://doi.org/10.1016/j.jtte.2020.04.004.

[3] J.N. Barkenbus, Prospects for electric vehicles, Sustain. (2020). https://doi.org/10.3390/su12145813.

[4] E.E. Michaelides, Thermodynamics and energy usage of electric vehicles, Energy Convers. Manag. (2020). https://doi.org/10.1016/j.enconman.2019.112246.

[5] X. Feng, M. Ouyang, X. Liu, L. Lu, Y. Xia, X. He, Thermal runaway mechanism of lithium ion battery for electric vehicles: A review, Energy Storage Mater. 10 (2018) 246–267. https://doi.org/10.1016/j.ensm.2017.05.013.

[6] Y. Yang, S. Bremner, C. Menictas, M. Kay, Battery energy storage system size determination in renewable energy systems: A review, Renew. Sustain. Energy Rev. (2018). https://doi.org/10.1016/j.rser.2018.03.047.

[7] Grand View Research, Lithium-ion Battery Market Worth $87.5 Billion By 2027 | CAGR: 13.0%, (2020). https://www.grandviewresearch.com/press-release/global-lithium-ion-battery-market.

[8] Y. Chen, Y. Kang, Y. Zhao, L. Wang, J. Liu, Y. Li, Z. Liang, X. He, X. Li, N. Tavajohi, B. Li, A review of lithium-ion battery safety concerns: The issues, strategies, and testing standards, J. Energy Chem. (2021). https://doi.org/10.1016/j.jechem.2020.10.017.

[9] Q. Wang, L. Jiang, Y. Yu, J. Sun, Progress of enhancing the safety of lithium ion battery from the electrolyte aspect, Nano Energy. (2019). https://doi.org/10.1016/j.nanoen.2018.10.035.

[10] W. Huang, X. Feng, X. Han, W. Zhang, F. Jiang, Questions and Answers Relating to Lithium-Ion Battery Safety Issues, Cell Reports Phys. Sci. (2021). https://doi.org/10.1016/j.xcrp.2020.100285.

[11] T.D. Hatchard, D.D. MacNeil, A. Basu, J.R. Dahn, Thermal Model of Cylindrical and Prismatic Lithium-Ion Cells, J. Electrochem. Soc. (2001). https://doi.org/10.1149/1.1377592.

[12] B.F. Gray, Spontaneous combustion and self-heating, in: SFPE Handb. Fire Prot. Eng. Fifth Ed., 2016. https://doi.org/10.1007/978-1-4939-2565-0_20.

[13] L. Liu, X. Feng, M. Zhang, L. Lu, X. Han, X. He, M. Ouyang, Comparative study on substitute triggering approaches for internal short circuit in lithium-ion batteries, Appl. Energy. (2020). https://doi.org/10.1016/j.apenergy.2019.114143.

[14] D. Ren, X. Feng, L. Liu, H. Hsu, L. Lu, L. Wang, X. He, M. Ouyang, Investigating the relationship between internal short circuit and thermal runaway of lithium-ion batteries under thermal abuse condition, Energy Storage Mater. (2021). https://doi.org/10.1016/j.ensm.2020.10.020.

[15] M. Chen, S. Lin, W. Song, J. Lv, Z. Feng, Electrical and thermal interplay in lithium-ion battery internal short circuit and safety protection, Int. J. Energy Res. (2020). https://doi.org/10.1002/er.5411.

[16] X. Lai, C. Jin, W. Yi, X. Han, X. Feng, Y. Zheng, M. Ouyang, Mechanism, modeling, detection, and prevention of the internal short circuit in lithium-ion batteries: Recent advances and perspectives, Energy Storage Mater. (2021). https://doi.org/10.1016/j.ensm.2020.11.026.

[17] L. Liu, X. Feng, C. Rahe, W. Li, L. Lu, X. He, D.U. Sauer, M. Ouyang, Internal short circuit evaluation and corresponding failure mode analysis for lithium-ion batteries, J. Energy Chem. (2021). https://doi.org/10.1016/j.jechem.2021.03.025.

[18] W. Xie, X. Liu, R. He, Y. Li, X. Gao, X. Li, Z. Peng, S. Feng, X. Feng, S. Yang, Challenges and opportunities toward fast-charging of lithium-ion batteries, J. Energy Storage. (2020). https://doi.org/10.1016/j.est.2020.101837.

[19] R. Zhao, J. Liu, J. Gu, Simulation and experimental study on lithium ion battery short circuit, Appl. Energy. (2016). https://doi.org/10.1016/j.apenergy.2016.04.016.

[20] S. Yang, W. Wang, C. Lin, W. Shen, Y. Li, Investigation of internal short circuits of lithium-ion batteries under mechanical abusive conditions, Energies. (2019). https://doi.org/10.3390/en12101885.

[21] R. Xiong, R. Yang, Z. Chen, W. Shen, F. Sun, Online Fault Diagnosis of External Short Circuit for Lithium-Ion Battery Pack, IEEE Trans. Ind. Electron. (2020). https://doi.org/10.1109/TIE.2019.2899565.

[22] P. Sun, R. Bisschop, H. Niu, X. Huang, A Review of Battery Fires in Electric Vehicles, 2020. https://doi.org/10.1007/s10694-019-00944-3.

[23] F.H. Gandoman, A. Ahmadi, P. Van den Bossche, J. Van Mierlo, N. Omar, A.E. Nezhad, H. Mavalizadeh, C. Mayet, Status and future perspectives of reliability assessment for electric vehicles, Reliab. Eng. Syst. Saf. (2019). https://doi.org/10.1016/j.ress.2018.11.013.

[24] S. Koch, K.P. Birke, R. Kuhn, Fast thermal runaway detection for lithium-ion cells in large scale traction batteries, Batteries. (2018). https://doi.org/10.3390/batteries4020016.

[25] Federal Aviation Administration, Events with smoke, fire, extreme heat or explosion involving Lithium Batteries, (2020).

[26] R. Cole, MAN HOSPITALISED AFTER BATTERY RECYCLING PLANT EXPLOSION, Resource. (2017).

[27] H. Huo, Y. Xing, M. Pecht, B.J. Züger, N. Khare, A. Vezzini, Safety requirements for transportation of lithium batteries, Energies. (2017). https://doi.org/10.3390/en10060793.

[28] M.D. Farrington, Safety of lithium batteries in transportation, in: J. Power Sources, 2001. https://doi.org/10.1016/S0378-7753(01)00565-1.

[29] L. Bravo Diaz, X. He, Z. Hu, F. Restuccia, M. Marinescu, J.V. Barreras, Y. Patel, G. Offer, G. Rein, Review—Meta-Review of Fire Safety of Lithium-Ion Batteries: Industry Challenges and Research Contributions, J. Electrochem. Soc. (2020). https://doi.org/10.1149/1945-7111/aba8b9.

[30] T.H. Dubaniewicz, J.P. DuCarme, Internal short circuit and accelerated rate calorimetry tests of lithium-ion cells: Considerations for methane-air intrinsic safety and explosion

proof/flameproof protection methods, J. Loss Prev. Process Ind. 43 (2016) 575–584. https://doi.org/10.1016/j.jlp.2016.07.027.

[31] N. Kuganathan, A. Kordatos, A. Chroneos, Li2SnO3 as a Cathode Material for Lithium-ion Batteries: Defects, Lithium Ion Diffusion and Dopants, Sci. Rep. (2018). https://doi.org/10.1038/s41598-018-30554-y.

[32] H. Li, Z. Zhou, Numerical simulation and experimental study of fluid-solid coupling-based air-coupled ultrasonic detection of stomata defect of lithium-ion battery, Sensors (Switzerland). (2019). https://doi.org/10.3390/s19102391.

[33] Y. Wu, S. Saxena, Y. Xing, Y. Wang, C. Li, W.K.C. Yung, M. Pecht, Analysis of manufacturing-induced defects and structural deformations in lithium-ion batteries using computed tomography, Energies. (2018). https://doi.org/10.3390/en11040925.

[34] T.D. Hatchard, D.D. MacNeil, A. Basu, J.R. Dahn, Thermal Model of Cylindrical and Prismatic Lithium-Ion Cells, J. Electrochem. Soc. 148 (2001) A755. https://doi.org/10.1149/1.1377592.

[35] G.H. Kim, A. Pesaran, R. Spotnitz, A three-dimensional thermal abuse model for lithium-ion cells, J. Power Sources. 170 (2007) 476–489. https://doi.org/10.1016/j.jpowsour.2007.04.018.

[36] A.O. Said, C. Lee, X. Liu, Z. Wu, S.I. Stoliarov, Simultaneous measurement of multiple thermal hazards associated with a failure of prismatic lithium ion battery, Proc. Combust. Inst. (2019). https://doi.org/10.1016/j.proci.2018.05.066.

[37] H. Li, H. Chen, G. Zhong, Y. Wang, Q. Wang, Experimental study on thermal runaway risk of 18650 lithium ion battery under side-heating condition, J. Loss Prev. Process Ind. 61 (2019) 122–129. https://doi.org/10.1016/j.jlp.2019.06.012.

[38] Q. Sun, Q. Wang, X. Zhao, J. Sun, Z. Lin, Numerical study on lithium titanate battery thermal response under adiabatic condition, Energy Convers. Manag. 92 (2015) 184–193. https://doi.org/10.1016/j.enconman.2014.12.019.

[39] Z. An, K. Shah, L. Jia, Y. Ma, Modeling and analysis of thermal runaway in Li-ion cell, Appl. Therm. Eng. (2019). https://doi.org/10.1016/j.applthermaleng.2019.113960.

[40] S. Al Hallaj, J.R. Selman, A Novel Thermal Management System for Electric Vehicle Batteries Using Phase-Change Material, J. Electrochem. Soc. 147 (2000) 3231. https://doi.org/10.1149/1.1393888.

[41] S. Panchal, I. Dincer, M. Agelin-Chaab, R. Fraser, M. Fowler, Experimental and theoretical investigations of heat generation rates for a water cooled LiFePO4 battery, Int. J. Heat Mass Transf. 101 (2016) 1093–1102. https://doi.org/10.1016/j.ijheatmasstransfer.2016.05.126.

[42] S. Panchal, M. Mathew, R. Fraser, M. Fowler, Electrochemical thermal modeling and experimental measurements of 18650 cylindrical lithium-ion battery during discharge cycle for an EV, Appl. Therm. Eng. (2018). https://doi.org/10.1016/j.applthermaleng.2018.02.046.

[43] A. Mevawalla, S. Panchal, M.-K. Tran, M. Fowler, R. Fraser, Mathematical Heat Transfer Modeling and Experimental Validation of Lithium-Ion Battery Considering: Tab and Surface Temperature, Separator, Electrolyte Resistance, Anode-Cathode Irreversible and Reversible Heat, Batteries. 6 (2020) 61. https://doi.org/10.3390/batteries6040061.

[44] J. Wang, W. Mei, Z. Cui, W. Shen, Q. Duan, Y. Jin, J. Nie, Y. Tian, Q. Wang, J. Sun, Experimental and numerical study on penetration-induced internal short-circuit of lithium-ion cell, Appl. Therm. Eng. (2020). https://doi.org/10.1016/j.applthermaleng.2020.115082.

[45] B. Wu, V. Yufit, M. Marinescu, G.J. Offer, R.F. Martinez-Botas, N.P. Brandon, Coupled thermal-electrochemical modelling of uneven heat generation in lithium-ion battery packs, J. Power Sources. (2013). https://doi.org/10.1016/j.jpowsour.2013.05.164.

[46] R. Jilte, A. Afzal, S. Panchal, A novel battery thermal management system using nano-enhanced phase change materials, Energy. 219 (2021) 119564. https://doi.org/10.1016/j.energy.2020.119564.

[47] ISO, Fire safety — Vocabulary (ISO 13943:2017), (2017).

[48] F. Restuccia, X. Huang, G. Rein, Self-ignition of natural fuels: Can wildfires of carbon-rich soil start by self-heating?, Fire Saf. J. (2017). https://doi.org/10.1016/j.firesaf.2017.03.052.

[49] P.C. Bowes, Self-heating: evaluating and controlling the hazards, 1984.

[50] L. Cai, R.E. White, An Efficient Electrochemical–Thermal Model for a Lithium-Ion Cell by Using the Proper Orthogonal Decomposition Method, J. Electrochem. Soc. 157 (2010) A1188. https://doi.org/10.1149/1.3486082.

[51] E. Prada, D. Di Domenico, Y. Creff, J. Bernard, V. Sauvant-Moynot, F. Huet, Simplified Electrochemical and Thermal Model of LiFePO 4 -Graphite Li-Ion Batteries for Fast Charge Applications, J. Electrochem. Soc. 159 (2012) A1508–A1519. https://doi.org/10.1149/2.064209jes.

[52] C. Lee, A.O. Said, S.I. Stoliarov, Impact of State of Charge and Cell Arrangement on Thermal Runaway Propagation in Lithium Ion Battery Cell Arrays, Transp. Res. Rec. (2019). https://doi.org/10.1177/0361198119845654.

[53] S. Bilyaz, K.C. Marr, O.A. Ezekoye, Modeling of Thermal Runaway Propagation in a Pouch Cell Stack, Fire Technol. (2020). https://doi.org/10.1007/s10694-020-00970-6.

[54] Z. Hu, G. Rein, Estimation of the Total Number of Battery Cells inside a Large Warehouse, Zenodo. (2018). https://doi.org/10.5281/zenodo.1216153.

[55] P. Huang, Q. Wang, K. Li, P. Ping, J. Sun, The combustion behavior of large scale lithium titanate battery, Sci. Rep. 5 (2015) 1–12. https://doi.org/10.1038/srep07788.

[56] M.S.M. Said, M.Z.M. Tohir, Prediction of lithium-ion battery thermal runaway propagation for large scale applications fire hazard quantification, Processes. (2019). https://doi.org/10.3390/pr7100703.

[57] T. Kim, D. Makwana, A. Adhikaree, J.S. Vagdoda, Y. Lee, Cloud-based battery condition monitoring and fault diagnosis platform for large-scale lithium-ion battery energy storage systems, Energies. (2018). https://doi.org/10.3390/en11010125.

[58] L. Cai, Z. Li, S. Zhang, K. Prenger, M. Naguib, V.G. Pol, Safer lithium-ion battery anode based on Ti3C2Tz MXene with thermal safety mechanistic elucidation, Chem. Eng. J. (2021). https://doi.org/10.1016/j.cej.2021.129387.

[59] J. He, Y. Liao, Q. Hu, Z. Zeng, L. Yi, Y. Wang, H. Lu, M. Pan, Investigation of polyimide as an anode material for lithium-ion battery and its thermal safety behavior, Ionics (Kiel). (2020). https://doi.org/10.1007/s11581-020-03509-5.

[60] P. Peng, F. Jiang, Thermal safety of lithium-ion batteries with various cathode materials: A numerical study, Int. J. Heat Mass Transf. 103 (2016) 1008–1016. https://doi.org/10.1016/j.ijheatmasstransfer.2016.07.088.

[61] T. Ould Ely, D. Kamzabek, D. Chakraborty, Batteries Safety: Recent Progress and Current Challenges, Front. Energy Res. (2019). https://doi.org/10.3389/fenrg.2019.00071.

[62] Z. Hu, X. He, F. Restuccia, H. Yuan, G. Rein, Numerical study of scale effects on self-heating ignition of lithium-ion batteries stored in boxes, shelves and racks, Appl. Therm. Eng. 190 (2021) 116780. https://doi.org/10.1016/j.applthermaleng.2021.116780.

[63] Z. An, L. Jia, L. Wei, C. Dang, Q. Peng, Investigation on lithium-ion battery electrochemical and thermal characteristic based on electrochemical-thermal coupled model, Appl. Therm. Eng. (2018). https://doi.org/10.1016/j.applthermaleng.2018.04.014.

[64] M. Chen, F. Bai, W. Song, J. Lv, S. Lin, Z. Feng, Y. Li, Y. Ding, A multilayer electro-thermal model of pouch battery during normal discharge and internal short circuit process, Appl. Therm. Eng. (2017). https://doi.org/10.1016/j.applthermaleng.2017.03.135.

[65] D. Ren, X. Feng, L. Lu, M. Ouyang, S. Zheng, J. Li, X. He, An electrochemical-thermal coupled overcharge-to-thermal-runaway model for lithium ion battery, J. Power Sources. (2017). https://doi.org/10.1016/j.jpowsour.2017.08.035.

[66] G.H. Kim, A. Pesaran, R. Spotnitz, A three-dimensional thermal abuse model for lithium-ion cells, J. Power Sources. (2007). https://doi.org/10.1016/j.jpowsour.2007.04.018.

[67] C.F. Lopez, J.A. Jeevarajan, P.P. Mukherjee, Characterization of Lithium-Ion Battery Thermal Abuse Behavior Using Experimental and Computational Analysis, J. Electrochem. Soc. (2015). https://doi.org/10.1149/2.0751510jes.

[68] P. Peng, F. Jiang, Thermal behavior analyses of stacked prismatic LiCoO2 lithium-ion batteries during oven tests, Int. J. Heat Mass Transf. (2015). https://doi.org/10.1016/j.ijheatmasstransfer.2015.04.101.

[69] P. Peng, Y. Sun, F. Jiang, Thermal analyses of LiCoO2 lithium-ion battery during oven tests, Heat Mass Transf. Und Stoffuebertragung. (2014). https://doi.org/10.1007/s00231-014-1353-x.

[70] J. Lamb, C.J. Orendorff, L.A.M. Steele, S.W. Spangler, Failure propagation in multi-cell lithium ion batteries, J. Power Sources. 283 (2015) 517–523. https://doi.org/10.1016/j.jpowsour.2014.10.081.

[71] P. Huang, P. Ping, K. Li, H. Chen, Q. Wang, J. Wen, J. Sun, Experimental and modeling analysis of thermal runaway propagation over the large format energy storage battery module with Li4Ti5O12 anode, Appl. Energy. (2016). https://doi.org/10.1016/j.apenergy.2016.08.160.

[72] B.F. Gray, Spontaneous Combustion and Self-Heating, in: SFPE Handb. Fire Prot. Eng., Springer New York, New York, NY, 2016: pp. 604–632. https://doi.org/10.1007/978-1-4939-2565-0_20.

[73] P. Huang, H. Chen, A. Verma, Q. Wang, P. Mukherjee, J. Sun, Non-dimensional analysis of the criticality of Li-ion battery thermal runaway behavior, J. Hazard. Mater. 369 (2019) 268–278. https://doi.org/10.1016/j.jhazmat.2019.01.049.

[74] B. Ditch, The Impact of Thermal Runaway on Sprinkler Protection Recommendations for Warehouse Storage of Cartoned Lithium-Ion Batteries, Fire Technol. (2018). https://doi.org/10.1007/s10694-017-0687-6.

[75] ISO, Fire safety — Vocabulary (ISO 13943:2017), (2017). https://www.iso.org/standard/63321.html.

[76] V. Babrauskas, Ignition Handbook, Principles and applications to fire safety engineering, 2019.

[77] P.H. Thomas, On the thermal conduction equation for self-heating materials with surface cooling, Trans. Faraday Soc. (1958). https://doi.org/10.1039/tf9585400060.

[78] C. Lautenberger, C. Fernandez-Pello, Generalized pyrolysis model for combustible solids, Fire Saf. J. (2009). https://doi.org/10.1016/j.firesaf.2009.03.011.

[79] X. He, F. Restuccia, Y. Zhang, Z. Hu, X. Huang, J. Fang, G. Rein, Experimental Study of Self-heating Ignition of Lithium-Ion Batteries During Storage: Effect of the Number of Cells, Fire Technol. 56 (2020) 2649–2669. https://doi.org/10.1007/s10694-020-01011-y.

[80] X. He, Z. Hu, F. Restuccia, H. Yuan, G. Rein, Computational study of the critical conditions for self-heating ignition of large size Lithium-ion batteries during storage with different states of charge and cathodes (under review), Appl. Therm. Eng. (2021).

[81] H. Yuan, F. Richter, G. Rein, A multi-step reaction scheme to simulate self-heating ignition of coal: Effects of oxygen adsorption and smouldering combustion, in: Proc. Combust. Inst., 2021. https://doi.org/10.1016/j.proci.2020.07.016.

[82] H. Yuan, F. Restuccia, F. Richter, G. Rein, A computational model to simulate self-heating ignition across scales, configurations, and coal origins, Fuel. (2019). https://doi.org/10.1016/j.fuel.2018.09.065.

[83] F. Restuccia, O. Mašek, R.M. Hadden, G. Rein, Quantifying self-heating ignition of biochar as a function of feedstock and the pyrolysis reactor temperature, Fuel. (2019). https://doi.org/10.1016/j.fuel.2018.08.141.

[84] F. Restuccia, N. Ptak, G. Rein, Self-heating behavior and ignition of shale rock, Combust. Flame. (2017). https://doi.org/10.1016/j.combustflame.2016.09.025.

[85] R. Spotnitz, J. Franklin, Abuse behavior of high-power, lithium-ion cells, J. Power Sources. (2003). https://doi.org/10.1016/S0378-7753(02)00488-3.

[86] COMSOL Multiphysics, Comsol Multiphysics Reference Manual: Version 5, Mannal. (2014).

[87] L. Cai, R.E. White, Mathematical modeling of a lithium ion battery with thermal effects in COMSOL Inc. Multiphysics (MP) software, J. Power Sources. 196 (2011) 5985–5989. https://doi.org/10.1016/j.jpowsour.2011.03.017.

[88] A. Melcher, C. Ziebert, M. Rohde, H.J. Seifert, Modeling and simulation of the thermal runaway behavior of cylindrical Li-ion cells-computing of critical parameters, Energies. 9 (2016) 1–19. https://doi.org/10.3390/en9040292.

[89] M. Rossi, T. Wallmersperger, S. Neukamm, K. Padberg-Gehle, Modeling and Simulation of Electrochemical Cells under Applied Voltage, Electrochim. Acta. 258 (2017) 241–254. https://doi.org/10.1016/j.electacta.2017.10.047.

[90] M.E. Lynch, D. Ding, W.M. Harris, J.J. Lombardo, G.J. Nelson, W.K.S. Chiu, M. Liu, Flexible multiphysics simulation of porous electrodes: Conformal to 3D reconstructed microstructures, Nano Energy. 2 (2013) 105–115. https://doi.org/10.1016/j.nanoen.2012.08.002.

[91] M.N. Richard, J.R. Dahn, Accelerating Rate Calorimetry Study on the Thermal Stability of Lithium Intercalated Graphite in Electrolyte. I. Experimental, J. Electrochem. Soc. 146 (1999) 2068–2077. https://doi.org/10.1149/1.1391893.

[92] H. Sun, X. Wang, B. Tossan, R. Dixon, Three-dimensional thermal modeling of a lithium-ion battery pack, J. Power Sources. (2012). https://doi.org/10.1016/j.jpowsour.2012.01.081.

[93] D. Ren, H. Hsu, R. Li, X. Feng, D. Guo, X. Han, L. Lu, X. He, S. Gao, J. Hou, Y. Li, Y. Wang, M. Ouyang, A comparative investigation of aging effects on thermal runaway behavior of lithium-ion batteries, ETransportation. (2019). https://doi.org/10.1016/j.etran.2019.100034.

[94] M.N. Richard, J.R. Dahn, Accelerating Rate Calorimetry Study on the Thermal Stability of Lithium Intercalated Graphite in Electrolyte. II. Modeling the Results and Predicting Differential Scanning Calorimeter Curves, J. Electrochem. Soc. (1999). https://doi.org/10.1149/1.1391894.

[95] D.D. MacNeil, L. Christensen, J. Landucci, J.M. Paulsen, J.R. Dahn, An Autocatalytic Mechanism for the Reaction of Li[sub x]CoO[sub 2] in Electrolyte at Elevated Temperature, J. Electrochem. Soc. (2000). https://doi.org/10.1149/1.1393299.

[96] D.D. MacNeil, J.R. Dann, Test of reaction kinetics using both differential scanning and accelerating rate calorimetries as applied to the reaction of LixCoO2 in non-aqueous electrolyte, J. Phys. Chem. A. 105 (2001) 4430–4439. https://doi.org/10.1021/jp001187j.

[97] D.D. MacNeil, L. Christensen, J. Landucci, J.M. Paulsen, J.R. Dahn, An Autocatalytic Mechanism for the Reaction of Li[sub x]CoO[sub 2] in Electrolyte at Elevated Temperature, J. Electrochem. Soc. 147 (2000) 970. https://doi.org/10.1149/1.1393299.

[98] M.N. Richard, J.R. Dahn, Accelerating Rate Calorimetry Study on the Thermal Stability of Lithium Intercalated Graphite in Electrolyte. II. Modeling the Results and Predicting Differential Scanning Calorimeter Curves, J. Electrochem. Soc. 146 (1999) 2078. https://doi.org/10.1149/1.1391894.

[99] M.N. Richard, J.R. Dahn, Accelerating Rate Calorimetry Study on the Thermal Stability of Lithium Intercalated Graphite in Electrolyte. I. Experimental, J. Electrochem. Soc. (1999). https://doi.org/10.1149/1.1391893.

[100] J.B. Goodenough, K.-S. Park, The Li-ion rechargeable battery: a perspective., J. Am. Chem. Soc. 135 (2013) 1167–76. https://doi.org/10.1021/ja3091438.

[101] P. Lyu, X. Liu, J. Qu, J. Zhao, Y. Huo, Z. Qu, Z. Rao, Recent advances of thermal safety of lithium ion battery for energy storage, Energy Storage Mater. (2020). https://doi.org/10.1016/j.ensm.2020.06.042.

[102] X. Zhu, Z. Wang, H. Wang, C. Wang, Review of Thermal Runaway and Safety Management for Lithium-ion Traction Batteries in Electric Vehicles, Jixie Gongcheng Xuebao/Journal Mech. Eng. (2020). https://doi.org/10.3901/JME.2020.14.091.

[103] Y. Peng, X. Zhou, Y. Hu, X. Ju, B. Liao, L. Yang, A new exploration of the fire behaviors of large format lithium ion battery, J. Therm. Anal. Calorim. (2020). https://doi.org/10.1007/s10973-019-08459-3.

[104] B. Ditch, D. Zeng, Fire Hazard of Lithium-ion Battery Energy Storage Systems: 1. Module to Rack-scale Fire Tests, Fire Technol. (2020). https://doi.org/10.1007/s10694-020-01041-6.

[105] Y. Liu, P. Sun, H. Niu, X. Huang, G. Rein, Propensity to self-heating ignition of open-circuit pouch lithium-ion battery pile on a hot boundary, Fire Saf. J. (2020) 103081. https://doi.org/10.1016/j.firesaf.2020.103081.

[106] N. Bal, Uncertainty and complexity in pyrolysis modelling, The University of Edinburgh, 2012.

[107] C.L. Beyler, Ignition Handbook, Fire Technol. (2004). https://doi.org/10.1023/b:fire.0000026981.83829.a5.

[108] H. Huo, Y. Xing, M. Pecht, B.J. Züger, N. Khare, A. Vezzini, Safety requirements for transportation of lithium batteries, 2017. https://doi.org/10.3390/en10060793.

[109] DHL, 2019 Lithium Battery Guidance Document, Revision 1, (2019).

[110] B. Diouf, R. Pode, Potential of lithium-ion batteries in renewable energy, Renew. Energy. 76 (2015) 375–380. https://doi.org/10.1016/j.renene.2014.11.058.

[111] A. Ahmad, Z.A. Khan, M. Alam, Y. Rafat, R.C. Chabaan, I. Khan, A. Bharadwaj, A Bibliographical Review of Electrical Vehicles (xEVs) Standards, SAE Int. J. Altern. Powertrains. (2018). https://doi.org/10.4271/08-07-01-0005.

[112] R. Cole, MAN HOSPITALISED AFTER BATTERY RECYCLING PLANT EXPLOSION, Resource. (2017). https://resource.co/article/man-hospitalised-after-battery-recycling-plant-explosion-11871.

[113] Nanfang Metropolis Daily, Fire broke out in Zhongshan Tianmao Battery Factory, neighborhoods were evacuated overnight, Nanfang Metrop. Dly. (2013). http://www.zhev.com.cn/news/show-1387157495.html.

[114] J.N. Carras, B.C. Young, Self-heating of coal and related materials: Models, application and test methods, Prog. Energy Combust. Sci. 20 (1994) 1–15. https://doi.org/10.1016/0360-1285(94)90004-3.

[115] DHL, 2019 Lithium Battery Guidance Document, Revision 1, (2019). http://www.dhl-usa.com/content/dam/downloads/g0/express/shipping/Lithium_batteries/Lithium_battery_guidance_document.pdf.

[116] H. Huo, Y. Xing, M. Pecht, B.J. Züger, N. Khare, A. Vezzini, Safety Requirements for Transportation of Lithium Batteries, Energies. 10 (2017) 793. https://doi.org/10.3390/en10060793.

[117] J.H. Whitelaw, Conduction heat transfer, Int. J. Heat Mass Transf. (1967). https://doi.org/10.1016/0017-9310(67)90078-6.

[118] S.A. Al-Ajlan, Measurements of thermal properties of insulation materials by using transient plane source technique, Appl. Therm. Eng. (2006). https://doi.org/10.1016/j.applthermaleng.2006.04.006.

[119] C. Jin, Y. Sun, H. Wang, X. Lai, S. Wang, S. Chen, X. Rui, Y. Zheng, X. Feng, H. Wang, M. Ouyang, Model and experiments to investigate thermal runaway characterization of lithium-ion batteries induced by external heating method, J. Power Sources. (2021). https://doi.org/10.1016/j.jpowsour.2021.230065.

[120] A.O. Said, A. Garber, Y. Peng, S.I. Stoliarov, Experimental Investigation of Suppression of 18650 Lithium Ion Cell Array Fires with Water Mist, Fire Technol. (2021). https://doi.org/10.1007/s10694-021-01151-9.

[121] K. Yu, X. Yang, Y. Cheng, C. Li, Thermal analysis and two-directional air flow thermal management for lithium-ion battery pack, J. Power Sources. (2014). https://doi.org/10.1016/j.jpowsour.2014.07.086.

[122] J.M. Yuk, H.K. Seo, J.W. Choi, J.Y. Lee, Anisotropic lithiation onset in silicon nanoparticle anode revealed by in situ graphene liquid cell electron microscopy, ACS Nano. (2014). https://doi.org/10.1021/nn502779n.

[123] Q. Zhang, Y. Cui, E. Wang, Anisotropic lithium insertion behavior in silicon nanowires: Binding energy, diffusion barrier, and strain effect, J. Phys. Chem. C. (2011). https://doi.org/10.1021/jp1115977.

[124] Z. Hu, X. He, F. Restuccia, G. Rein, Numerical Study of Self-Heating Ignition of a Box of Lithium-Ion Batteries During Storage, Fire Technol. 56 (2020) 2603–2621. https://doi.org/10.1007/s10694-020-00998-8.

[125] J.S. Gnanaraj, E. Zinigrad, L. Asraf, H.E. Gottlieb, M. Sprecher, D. Aurbach, M. Schmidt, The use of accelerating rate calorimetry (ARC) for the study of the thermal reactions of Li-ion battery electrolyte solutions, in: J. Power Sources, 2003. https://doi.org/10.1016/S0378-7753(03)00255-6.

[126] Q. Wang, P. Ping, X. Zhao, G. Chu, J. Sun, C. Chen, Thermal runaway caused fire and explosion of lithium ion battery, J. Power Sources. 208 (2012) 210–224. https://doi.org/10.1016/j.jpowsour.2012.02.038.

[127] C. Geisbauer, K. Wöhrl, C. Mittmann, H.-G. Schweiger, Review—Review of Safety Aspects of Calendar Aged Lithium Ion Batteries, J. Electrochem. Soc. 167 (2020) 090523. https://doi.org/10.1149/1945-7111/ab89bf.

[128] M. Broussely, S. Herreyre, P. Biensan, P. Kasztejna, K. Nechev, R.J. Staniewicz, Aging mechanism in Li ion cells and calendar life predictions, J. Power Sources. 97–98 (2001) 13–21. https://doi.org/10.1016/S0378-7753(01)00722-4.

[129] H. Albert, Self-Discharge Losses in Lithium-Ion Cells, (n.d.) 19–24.

[130] R. YAZAMI, Y. REYNIER, Mechanism of self-discharge in graphite–lithium anode, Electrochim. Acta. 47 (2002) 1217–1223. https://doi.org/10.1016/S0013-4686(01)00827-1.

[131] H. Wenzl, A. Haubrock, H.P. Beck, Degradation of lithium ion batteries under complex conditions of use, Zeitschrift Fur Phys. Chemie. 227 (2013) 57–71. https://doi.org/10.1524/zpch.2012.0170.

[132] J. Ye, H. Chen, Q. Wang, P. Huang, J. Sun, S. Lo, Thermal behavior and failure mechanism of lithium ion cells during overcharge under adiabatic conditions, Appl. Energy. 182 (2016) 464–474. https://doi.org/10.1016/j.apenergy.2016.08.124.

[133] E. Sarasketa-Zabala, I. Gandiaga, L.M. Rodriguez-Martinez, I. Villarreal, Calendar ageing analysis of a LiFePO4/graphite cell with dynamic model validations: Towards realistic lifetime predictions, J. Power Sources. 272 (2014) 45–57. https://doi.org/10.1016/j.jpowsour.2014.08.051.

[134] E. Redondo-Iglesias, P. Venet, S. Pelissier, Global Model for Self-Discharge and Capacity Fade in Lithium-Ion Batteries Based on the Generalized Eyring Relationship, IEEE Trans. Veh. Technol. 67 (2018) 104–113. https://doi.org/10.1109/TVT.2017.2751218.

[135] X. Han, L. Lu, Y. Zheng, X. Feng, Z. Li, J. Li, M. Ouyang, A review on the key issues of the lithium ion battery degradation among the whole life cycle, ETransportation. 1 (2019). https://doi.org/10.1016/j.etran.2019.100005.

[136] W.M. Seong, K.Y. Park, M.H. Lee, S. Moon, K. Oh, H. Park, S. Lee, K. Kang, Abnormal self-discharge in lithium-ion batteries, Energy Environ. Sci. 11 (2018) 970–978. https://doi.org/10.1039/c8ee00186c.

[137] I. Zilberman, S. Ludwig, A. Jossen, Cell-to-cell variation of calendar aging and reversible self-discharge in 18650 nickel-rich, silicon–graphite lithium-ion cells, J. Energy Storage. 26 (2019) 100900. https://doi.org/10.1016/j.est.2019.100900.

[138] I. Zilberman, J. Sturm, A. Jossen, Reversible self-discharge and calendar aging of 18650 nickel-rich, silicon-graphite lithium-ion cells, J. Power Sources. 425 (2019) 217–226. https://doi.org/10.1016/j.jpowsour.2019.03.109.

[139] M. Dubarry, N. Qin, P. Brooker, Calendar aging of commercial Li-ion cells of different chemistries – A review, Curr. Opin. Electrochem. 9 (2018) 106–113. https://doi.org/10.1016/j.coelec.2018.05.023.

[140] P. Keil, S.F. Schuster, J. Wilhelm, J. Travi, A. Hauser, R.C. Karl, A. Jossen, Calendar Aging of Lithium-Ion Batteries, J. Electrochem. Soc. 163 (2016) A1872–A1880. https://doi.org/10.1149/2.0411609jes.

[141] M. Naumann, M. Schimpe, P. Keil, H.C. Hesse, A. Jossen, Analysis and modeling of calendar aging of a commercial LiFePO4/graphite cell, J. Energy Storage. 17 (2018) 153–169. https://doi.org/10.1016/j.est.2018.01.019.

[142] A. Barré, B. Deguilhem, S. Grolleau, M. Gérard, F. Suard, D. Riu, A review on lithium-ion battery ageing mechanisms and estimations for automotive applications, J. Power Sources. (2013). https://doi.org/10.1016/j.jpowsour.2013.05.040.

[143] T. Utsunomiya, O. Hatozaki, N. Yoshimoto, M. Egashira, M. Morita, Self-discharge behavior and its temperature dependence of carbon electrodes in lithium-ion batteries, J. Power Sources. 196 (2011) 8598–8603. https://doi.org/10.1016/j.jpowsour.2011.05.066.

[144] S. Byun, J. Park, W.A. Appiah, M.H. Ryou, Y.M. Lee, The effects of humidity on the self-discharge properties of Li(Ni1/3Co1/3Mn1/3)O2/graphite and LiCoO2/graphite lithium-ion batteries during storage, RSC Adv. 7 (2017) 10915–10921. https://doi.org/10.1039/c6ra28516c.

[145] P. Keil, S.F. Schuster, J. Wilhelm, J. Travi, A. Hauser, R.C. Karl, A. Jossen, Calendar Aging of Lithium-Ion Batteries, J. Electrochem. Soc. (2016). https://doi.org/10.1149/2.0411609jes.

[146] K. Liu, T.R. Ashwin, X. Hu, M. Lucu, W.D. Widanage, An evaluation study of different modelling techniques for calendar ageing prediction of lithium-ion batteries, Renew. Sustain. Energy Rev. 131 (2020). https://doi.org/10.1016/j.rser.2020.110017.

[147] P. Keil, S.F. Schuster, J. Wilhelm, J. Travi, A. Hauser, R.C. Karl, A. Jossen, Calendar aging of lithium-ion batteries i. impact of the graphite anode on capacity fade, J. Electrochem. Soc. (2016). https://doi.org/10.1149/2.0411609jes.

[148] F. Restuccia, N. Fernandez-Anez, G. Rein, Experimental measurement of particle size effects on the self-heating ignition of biomass piles: Homogeneous samples of dust and pellets, Fuel. (2019). https://doi.org/10.1016/j.fuel.2019.115838.

[149] A. Bar-Ilan, G. Rein, D. C.walther, A.C. Fernandez-Pello, J.L. Torero, D.L. Urban, The effect of buoyancy on opposed smoldering, Combust. Sci. Technol. (2004). https://doi.org/10.1080/00102200490514822.